Titel der Arbeit:

ZEB2 AS A REGULATOR OF ADHESION INTERPLAY IN THE DEVELOPING MOUSE NEOCORTEX

DISSERTATION
zur Erlangung des akademischen Grades

Doctor of Philosophy
(Ph. D.)
eingereicht an der
Lebenswissenschaftlichen Fakultät der Humboldt-Universität zu Berlin
von
Ekaterina Epifanova

Präsident der Humboldt-Universität zu Berlin

Prof. Dr. Peter Frensch

Dekan der Lebenswissenschaftlichen Fakultät
der Humboldt-Universität zu Berlin

Prof. Dr. Dr. Christian Ulrichs

Vorsitz

1. Prof. Dr. Ana Pombo

Gutachter/innen

2. Prof. Dr. Michael Brecht
3. Dr. Marta de Rocha Rosario
4. Dr. Niccolo Zampieri

Weitere Mitglieder

5. Prof. Dr. Victor Tarabykin
6. Prof. Dr. Marina Mikhaylova
7. Prof. Dr. Matthew Larkum

Tag der mündlichen Prüfung: 26.01.2022

Berlin 2021

Declaration of independent work

Hereby, I confirm this thesis was composed by myself, that the work contained herein is my own except where explicitly stated otherwise in the text. All the experiments presented in this dissertation were performed, quantified and analysed by me. This work has not been submitted for any other degree or processional qualification except as specified. I did not use any other sources, figures or resources than the ones stated in the bibliography. Parts of this work have been published in *Epifanova* et al. Adhesion dynamics in the neocortex determine the start of migration and the post-migratory organization of neurons. *Sci. Adv.*, 7, 27: eabf1973, doi: 10.1126/sciadv.abf1973 (2021).

Name: Ekaterina Epifanova

Department: Humbolt University of Berlin, Charite universitätsmedizin Berlin, Institute of Cell Biology and Neurobiology

Doctoral subject: Biology

Topic of the doctoral thesis: Zeb2 as a regulator of adhesion interplay in the developing mouse neocortex

Table of contents

Summary

The human brain is a highly sophisticated biological structure and its formation is a highly orchestrated process. The human neocortex, in particular, is the main place of higher-order cognitive functions. Understanding the neocortical development of other mammalian species is essential for understanding brain organisation in common neurodevelopmental disorders in particular. Here I studied the role of Mowat-Wilson syndrome-associated transcription factor Zeb2 in mouse neocortical development.

I have shown in this study that Zeb2 regulates adhesion of new born cortical neurons both before and after radial locomotion via two independent molecular pathways. I have shown that adhesion prior to radial locomotion is tightly regulated via Zeb2- Neuropilin1- Integrinβ1 molecular pathway. Zeb2 cell-intrinsically suppresses adhesion of neurons to the extracellular matrix and therefore restricts the initiation of radial locomotion, multipolar stage duration and motility of multipolar neurons without affecting radial locomotion itself and layer cell fate acquisition. Once radial migration is finished neurons have to form apical dendrite and establish contact with the meningeal surface. Normally, apical dendrites of neurons are oriented parallel to each other and perpendicular to the meningeal surface. I have shown that postmigratory orientation of neurons is dependent on cell-to-cell and cell-to-extracellular matrix adhesion and occurs independently from radial migration. Zeb2 orchestrates the whole repertoire of adhesion of neurons completed radial migration via Zeb2- Cadherin 6- Integrinβ1 molecular pathway. I have demonstrated that Cadherin 6 balance is crucial for establishment of postmigratory neuronal orientation under normal conditions. The regulation of postmigratory neuronal orientation occurs via regulation integrin signalling through highly evolutionary conserved RGD motif.

Taken together, this study has revealed the importance of neuronal adhesion during neocortical development and separated the regulation mechanisms for initiation of radial migration and postmigratory orientation of upper layer neurons.

Zusammenfassung (German Summary)

Das menschliche Gehirn besitzt eine äußerst komplexe biologische Architektur, deren Entstehung einem hochgradig orchestrierten Ablauf unterliegt. Insbesondere der menschliche Neokortex wird als Hauptsitz kognitiver Funktionen höherer Ordnung angesehen. Das Verständnis der neokortikalen Entwicklung anderer Säugetierarten ist von wesentlicher Bedeutung, um die menschliche Gehirnorganisation im Allgemeinen und neurologische Entwicklungsstörungen im Speziellen besser zu verstehen. In dieser Arbeit habe ich die Rolle des mit dem Mowat-Wilson-Syndrom assoziierten Transkriptionsfaktors Zeb2 in der neokortikalen Entwicklung der Maus untersucht.

Ich habe nachgewiesen, dass Zeb2 die Adhäsion neugeborener kortikaler Neurone sowohl vor als auch nach der radialen Migration über zwei unabhängige molekulare Wege reguliert. Hierbei konnte ich zeigen, dass die Adhäsion im Vorfeld der radialen Migration über den molekularen Zeb2-Neuropilin1-Integrinβ1-Weg reguliert wird. Zeb2 unterdrückt zell-intrinsisch die neuronale Adhäsion an die extrazelluläre Matrix und kontrolliert dadurch den Beginn der radialen Migration, die Dauer des multipolaren Stadiums sowie die Motilität multipolarer Neurone, ohne die radiale Migration selbst oder das spätere Zellschicksal innerhalb der kortikalen Schichten zu beeinflussen. Nach Abschluss der radialen Migration produzieren die Neurone einen apikalen Dendriten und bilden einen Kontakt zur Hirnhautoberfläche. Hierbei sind die apikalen Dendriten der Neurone normalerweise parallel zueinander und senkrecht zur Hirnhautoberfläche ausgerichtet. Ich habe gezeigt, dass die Ausrichtung der Neurone im Anschluss an ihre Migration von der Adhäsion der Zellen untereinander sowie zur extrazellulären Matrix abhängt und dieser Prozess unabhängig von der radialen Migration erfolgt. Zeb2 koordiniert das gesamte Repertoire dieser postmigratorischen Adhäsion über den molekularen Zeb2-Cadherin6-Integrinβ1-Weg. Ich habe demonstriert, dass Cadherin6 den Integrinβ1-assoziierten Signalweg durch ein evolutionär konserviertes RGD-Motiv reguliert und die genaue Regulation des Cadherin6-Gleichgewichts für die Etablierung der postmigratorischen neuronalen Orientierung unter physiologischen Bedingungen entscheidend ist.

Zusammenfassend zeigt diese Studie die Bedeutung der neuronalen Adhäsion während der neokortikalen Entwicklung auf und entschlüsselt die Regulationsmechanismen für die Initiierung der radialen Migration

sowie für die postmigratorische Orientierung der Neurone der oberen kortikalen Schichten.

Abbreviations

CP – cortical plate

DIV – day *in vitro*

DL – deeper layer cortical neurons

GFP – green fluorescent protein

IRES – Internal ribosome entry site

IUE – *in utero* electroporation

IZ – intermediate zone

MZ – Marginal zone

PCR – polymerase chain reaction

PP – preplate

ROI – region of interest

SVZ – subventricular zone

TP – trailing process

UL – upper layer cortical neurons

1. Introduction

1.1. Neocortical development

The human brain is a highly sophisticated biological structure and its formation is a highly orchestrated process. The human neocortex, in particular, is the main place of the brain responsible for higher-order cognitive functions such as cognition, learning, language and perception[1]. Understanding neocortical development of other mammalian species, in particular, is a key to the understanding of the organisation and function of human brain and brain developmental disorders.

The central nervous system of mammalian species develops from dorsally located embryonic ectodermal cells called neuroectoderm cells. Neuroectoderm grows, invaginates and forms the neural tube. The rostral (anterior) and the caudal (posterior) parts of the neural tube give rise to the brain and spinal cord respectively. The anterior part of the neuronal tube undergoes several enlargements, which then form three primary brain vesicles: prosencephalon (forebrain), mesencephalon (midbrain), and rhombencephalon (hindbrain). These primary vesicles then subdivide into five secondary brain vesicles: telencephalon and diencephalon emerge from the forebrain, mesencephalon from the midbrain, metencephalon and myelencephalon from the hindbrain. The dorsal telencephalon gives rise to the cerebral cortex, which in turn subdivides into left and right cerebral hemispheres. Neural stems cells, which are located in the walls of the neuronal tube, generate radial glial progenitor cells[2].

Radial glial progenitors, in turn, generate neurons and astrocytes. New born cortical neurons then migrate radially out of their place of birth in the proliferative zone (the ventricular zone (VZ) and the subventricular zone (SVZ)) to form and populate the future cortical plate (CP) (Fig. 1). Prior to the radial migration, new born neurons acquire a bipolar morphology and, following the radial migration, they occupy a certain position within one of the 6 neuronal layers. Cortical neurogenesis has a certain temporal pattern of neuronal production. Deeper layer neurons (layer V-VI) are generated between embryonic days 11-14 (E11-E14) while upper layer neurons (layer II-IV) are generated later E13-E16. While migrating, neurons extend their axons to target other brain regions[2]. DL neurons mostly establish corticofugal projections and their

axons connect cortex with other subcortical structures such as striatum, thalamus, pons, tectum, brain stem and spinal cord. In a meantime, UL neurons mostly project intracortically to connect different cortical areas[3]. Once arrived at the final position neurons detach from the radial glia fibers and move up via somal translocation, make contact with the MZ and only then initiate dendritic arborisation[2]. Marginal zone (MZ), the outermost layer of the neocortex, postnatally transforms into Layer I (starting from postnatal day 0 (P0))[4]. MZ mainly comprises Cajal-Retzius cells which express cadherin associated protein Catenin β1 (Ctnnβ1), the semaphorins and Reelin. Cajal-Retzius cells are the first-born cortical neurons and they die during the second postnatal week[5]. Layers II-VI consists of excitatory pyramidal neurons while Layer I is postnatally sparsely populated by inhibitory interneurons[4]. Thus, neocortical development is a highly complex process that defines the proper connectivity and functioning of the brain.

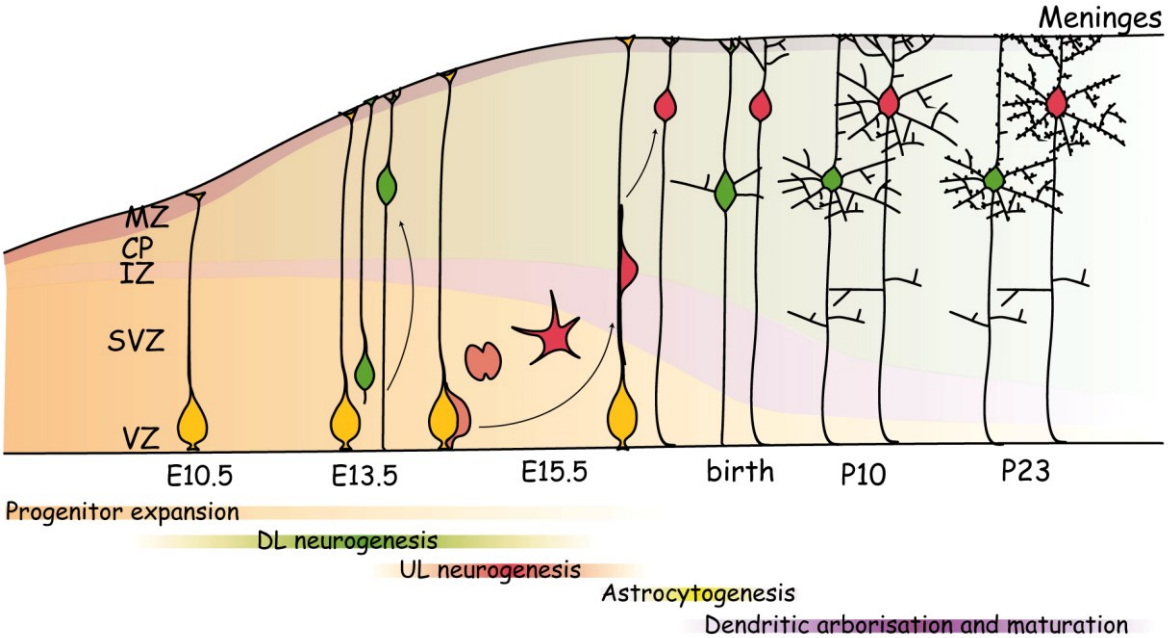

Fig. 1. Mouse corticogenesis. During corticogenesis, new born cortical neurons arise from radial glia cells (yellow) and intermediate progenitors (orange). Both deeper layer (green) and upper layer (pink) cortical neurons radially migrate out of the ventricular zone/ subventricular zone (VZ/SVZ) into forming cortical plate (CP). Upon arrival at the final cortical positions, neurons undergo significant morphological changes in order to form and mature dendritic tree.

1.1.1. Neuronal migration in developing neocortex

New born cortical neurons originate from the proliferative zone of the neocortex (VZ and SVZ). There are two types of progenitor cells in the mouse cortex: apical and basal. Apical progenitors are mainly comprised of radial glia progenitor cells, while basal progenitors include intermediate progenitor cells[6]. Radial glia progenitors are located in VZ in the neocortex and they form long radially extended cytoplasmic processes that touch the meningeal surface. Progenitor cells undergo different modes of cell division - symmetrical and asymmetrical. Upon symmetrical (vertical) progenitor cell division, radial glia progenitors generate two stem cells, which expands the pool of neuronal stem cells. Upon asymmetrical (horizontal) division progenitor cells produce one stem cell and one neuron. Later on in development, neuronal progenitor cells undergo terminal symmetrical division and generate two neurons and decrease the pool of neuronal stem cells. Intermediate progenitors are typically located in SVZ[7,8].

There are two main types of migration that occur in the cortex: tangential (orthogonal to the radial glia fibers) and radial (parallel to the radial glia fibers) migration (Fig. 2). Tangential migration is mostly used by cortical interneurons which originate in the ganglionic eminence, whereas, radial migration is typical for cortical excitatory neurons[9]. Since the excitatory neurons are the most abundant cortical neurons and they were closely investigated in this study I will review the radial migration mode in detail.

Following progenitor cell mitosis, new born cortical neurons are born and move from the place of birth to their final destination in the CP. This process is called neuronal radial migration and involves several steps[9]. The first phase of radial migration is the detachment of the new born cortical neuron from the progenitor cell on the ventricular surface and its movement along radial glia fiber towards the SVZ. During the second phase of neuronal migration, which is called multipolar phase, the new born neuron detaches from the radial glia fiber and acquires a multipolar morphology. Neurons remain in this multipolar phase in SVZ for about 24

hours. Multipolar cells are characterized by production of multiple neuronal processes and their active extension and retraction[10].

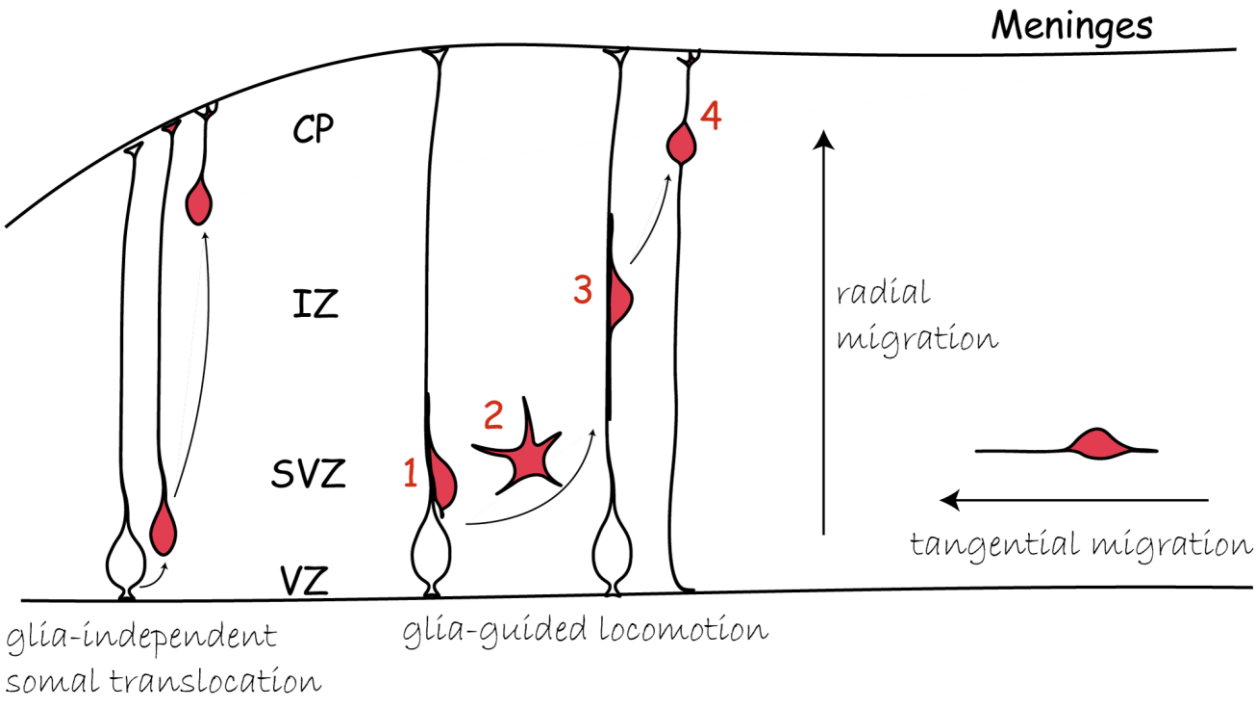

Fig. 2. Schematic illustration of neuronal migration modes in developing mouse neocortex. There are two main types of neuronal migration: tangential and radial. Early born neurons migrate mostly via glia-independent somal translocation mode of radial migration. Late born neurons migrate using radial glia-guided locomotion mode of radial migration: 1 – the detachment of the new born cortical neuron from the progenitor cell on the ventricular surface and its movement along with radial glia fiber towards the SVZ; 2 – multipolar phase; 3 – radial-guided locomotion; 4 – terminal somal translocation.

Before the initiation of the next phase of neuronal migration, neurons have to acquire a bipolar morphology through determining axon identity. Neurons undergoing the multipolar stage of migration first specify the pioneering axonal process, initiate an asymmetric growth and then attach to the radial glia fiber[11].

Following the multipolar phase, early born neurons mainly migrate through a glia-independent mode, while late-born neurons mainly migrate through glia-guided mode[12]. There are two modes of radial

migration: somal translocation and glial-guided locomotion. Somal translocation is mainly used by early born neurons, which have a long radially-oriented leading process terminating at the meningeal surface and a short trailing process. During somal translocation, the soma of new born neurons moves through nucleokinesis towards the meningeal surface direction shortening the leading process and elongating the trailing process. During this mode of migration, neurons translocate with a relatively constant speed[12]. Meanwhile, the terminal of the leading process remains attached to the meningeal surface. Glia-independent somal translocation is mainly used by early born neurons (neurons that form the preplate (PP) and deeper layers of the cortex)[13]. On the contrary to somal translocation, glial-guided locomotion is characterised by the migration of locomoting cells along the radial glia fibers. The leading process remains unattached, free and relatively short and maintains a relatively constant length. These cells migrate through repeated mobile phases - short bursts of forwarding movements, which are interspersed with stationary phases[9]. Glia-guided locomotion is mainly used by later born neurons (UL)[13]. Neurons extend a leading process towards the meningeal surface and a trailing process in the direction of the ventricular surface and migrate radially toward the CP[7]. Some neurons exhibit retrograde somal movements towards the ventricular surface. Upon arrival at the final cortical position, neurons can either remain near the radial glia fiber or make a terminal somal translocation in order to take the final position in the cortex[14].

1.1.2. Dendritic development in developing neocortex

Cortical pyramidal neurons typically have a triangular morphology with a thick apical dendrite, which originates from the apex and lies 90 degrees to the meningeal surface. In addition, they contain multiple thin basal dendrites and one axon (Fig. 1). Apical and basal dendrites form the dendritic tree, which undergoes dendritic branching, extension and maturation. The dendritic tree is a highly complex part of neuron which is responsible for receiving most incoming information to the neuron. Incoming information is transmitted in a form of electrical impulses from axons to numerous synapses on dendrites[15].

Following migration, the leading process of migrating neuron is thought to become the apical dendrite. The specification of dendrites can be

initiated only then radial migration is finished and until then the dendritic growth is mostly inhibited. Although axon determination and extension occurs during migration[16]. Little is known about how dendrites are specified in vivo. This process seems to be tightly connected to axonal specification. The axonal and dendritic specification has been well studied *in vitro*. The first step of axon-dendrite specification *in vitro* is a selection of axon (also called neuronal polarization). Neurons specify the pioneering axonal process and initiate an asymmetric growth. The other neuronal processes become dendrites. This selection happens due to mutual inhibition of axonal specification of the neighbouring neurites[11,17]. Neuronal polarization is a result of a complex interaction between intracellular and extracellular polarity pathways. It has been shown that axon specification is controlled by various molecules, such as phosphatidylinositol 3-kinase (PI3kinase), glycogen synthase kinase-3beta (GSK3beta), collapsin response mediator protein-2 (CRMP2), Protein kinase B (Akt), SAD kinases, Rho family small GTPases and Par family of proteins[11,18,19]. Extracellular factors such as brain-derived neurotrophic factor (BDNF), epidermal growth factor 1 (EGF-1) and transforming growth factor beta (TGFβ) have been shown to trigger neuronal polarization[20-22].

The position of the centrosome and Golgi complex plays an important role in neuronal polarization. At first, the position of the centrosome and Golgi complex position defines the future axon and promotes the extension of the nearest neurite neuronal outgrowth. After axonal determination, the centrosome and Golgi complex relocate from the position of axonal growth to the base of leading process[23].

Similarly to axonal specification, it is thought that dendrite specification is controlled by both intrinsic and extrinsic molecular cues. However, little is known about how dendrites, in particular the apical dendrite, are specified. It has been shown that Neuorogenin2 (Ngn2) regulates the unipolar dendritic morphology of pyramidal neurons. Absence of Ngn2 discourages the formation of the apical dendrite and promotes the outgrowth of multiple primary dendrites instead[24]. Axons and dendrites differ from each other both structurally and functionally. Comparing to axons, dendrites are less homogeneous structures, they contain cellular organelles that are not present in axons and microtubules which are formed bidirectionally (unlike axons that have microtubules in one direction). Hence, molecular control of the establishment of dendritic

polarity and development of apical and basolateral dendrites is likely more complex[25].

Upon the arrival of migrating neurons at the final position in the cortex, they initiate the formation of the dendritic tree and anchor the terminal of the apical dendrite in MZ. Current literature defines dendritic arborisation as including the formation, extension, retraction) and maturation of dendrites (spine formation, establishment of synaptic contacts and dendritic pruning)[25,26]. During dendritic arborisation, neurons form dynamic actin-rich filopodial protrusions, which then become new dendritic branches[27]. Dendritic arborisation is tightly controlled by many intrinsic and extrinsic molecules such as secreted molecules and cell surface receptors (BDNF, Reelin, Wnt, Ephrins and Eph receptors, Semaphorins and Notch); adhesion molecules (Cadherin-Catenin signalling pathway); signalling molecules (Calmodulin kinase 2b, CRMP, cysteine-rich protein 1 (CRP1), nuclear Dbf2-related kinases (NDR), Serine/Threonine kinase 25 (Stk25), Cyclin-dependent kinase 5 (CDK5) and Cullin 7(Cul7)); postsynaptic density proteins (Postsynaptic density protein 95 (Psd95), Cypin and Lap family of proteins); regulators of the actin cytoskeleton (Rho GTPases and their regulators such as ARHGAP33[28]); molecules that control Golgi trafficking (Sar1); endoplasmic reticulum-associated proteins (CLIPM63); components of cell cycle machinery (Origin recognition complex and Anaphase promoting complex (APC)); and transcription factors (nuclear factor kappa-light-chain-enhancer of activated B-cells (NfkB), CREB, Cux1, Cux2, Neurogenin2, CREST)[25]. As a result, neurons acquire highly complex branched dendritic architecture.

Later stages of dendritic arboring overlap with spine formation. Dendrites carry both excitatory and inhibitory synapses. The excitatory synapses are mainly formed on spines whereas inhibitory synapses are formed on dendritic shafts and the neuronal cell body. Spines are small neuronal protrusions, which typically have a thin neck and a head with excitatory synapses. Spine morphology is dynamic and varies with time and along the dendrite[29].

The proper establishment of dendritic tree is a crucial step of neuronal development, which determines the synaptic input field of the dendrite. Disturbance of dendritogenesis correlates to a broad spectrum of neurodevelopmental and neuropsychiatric disorders such as intellectual disability, autism, schizophrenia and depression[30,31].

1.2. Transcriptional factor Zeb2

Zeb2 (also known as Sip1, Zfhx1b) is a transcription repressor that is important for the central and peripheral nervous system development of both human and mouse. Zeb2 is one of the two proteins of the Zeb2 family. It is a zinc-finger transcriptional factor. Zeb2 is widely expressed in various cell types and tissues such as neuroectoderm derived tissue (neural tube and neural crest cells, hippocampus, cerebral cortex, ganglionic eminences, thalamus) as well as in the digestive tract, kidney and skeletal muscles[32].

Zeb2 is a high-affinity DNA-binding protein with two N- and C-terminal zinc fingers clusters. Despite the fact that Zeb2 mainly acts as a transcriptional repressor it has been shown that in some cases it activates gene transcription in complex with other co-factors[32-34]. Zeb2 contains several domains: N-terminal and C-terminal zinc finger clusters (NZF and CZF respectively), POU-like homeodomain (HD), Smad binding domain (SBD), the CtBP interaction domain (CID) and NuRD complex interaction motif (NIM)[32,35]. Zinc finger domains of Zeb2 recognise enhancer boxes (E-boxes), which consists of palindromic canonical sequence CACCT(G) or CACANNT(G). SBD domain is especially important for binding of canonical partners of Zeb2 signalling pathway – SMAD proteins. Smad proteins (Smad1, Smad2, Smad3, Smad4 and Smad5) are the key mediators of TGFβ signalling[36].

Zeb2 has been shown to regulate a variety of neurodevelopmental processes. Thus, in early development Zeb2 presence is necessary for neural tube closure[37], neural crest development[38] and epithelial-to-mesenchymal transition[39]. Moreover, Zeb2 regulates the development of CA1 and CA3 fields of the hippocampus through Wnt-signalling[40]. Also, Zeb2 plays an essential role in the generation of glial precursors and postnatal astrocytogenesis in the cerebral cortex. Zeb2 restricts proliferation of Olig2 positive glial precursors and therefore controls the initiation of astrocytes production[41]. It has been also shown that Zeb2 also controls differentiation of oligodendrocytes[34]. In cortical interneurons, Zeb2 is necessary for correct fate acquisition and migration through repression of Nkx2.1 and Unc5b expression respectively[42,43]. Zeb2 also represses BMP signalling and therefore regulates the axonal growth and target innervation of midbrain dopaminergic neurons[44]. In neocortex, Zeb2 has been shown to regulate axonal growth and branching and formation of corpus callosum via activation of expression

of the microtubule-associated protein, Ninein[45]. It also regulates NMDA-, AMPA- and KA receptor activity[46]. Zeb2 is highly expressed in postmitotic cortical pyramidal neurons and has been shown to initiate premature generation of upper layer neurons at expense of deeper layer neurons through feedback signalling of immature neurons to the neuronal progenitors[41].

Zeb2 mutation in humans is associated with several developmental diseases including Mowat-Wilson syndrome. Mowat-Wilson syndrome is associated with various heterozygous mutations of Zeb2. It is characterised by multiple severe neurodevelopmental defects which are displayed to various extents in different Mowat-Wilson patients. Most Mowat-Wilson patients share the following features: varying degrees of intellectual disability, microcephaly, epilepsy and characteristically altered facial appearance. Some patients also show the absence of corpus callosum, hippocampal abnormalities, enlargement of cerebral ventricles, white matter abnormalities, delayed motor development, Hirschsprung's disease, ventricle septum defects, and congenital heart disease[32,47]. Various mutations (including different point mutations, full or partial deletions, chromosomal rearrangements, frameshift and nonsense mutations) in Mowat-Wilson patients lead either to complete ablation of ZEB2 protein or production of nonfunctional protein[47,48].

2. Materials and methods

2.1. Animals

All animals for experiments were housed at Charité – Universitätsmedizin Berlin. All animal experiments were conducted in accordance with German Law using protocols approved by the Landesamt für Gesundheit und Soziales (LAGeSo), Berlin. Permissions for experiments were under G0206/16, G0059/19 licences, Charité – Universitätsmedizin Berlin. To inactivate Zeb2 in developing cortex I crossed *Zeb2*$^{fl/fl}$ mice with Nex^{Cre} line in which Cre recombinase expression is driven by Nex (NeuroD1) gene allele[49,50]. Wild type NMRI mouse strain which was used for some overexpression and downregulation experiments, were obtained from Charles River Laboratories.

2.2. Genotyping

Genotyping was performed by analysis of DNA extracted from tail biopsies. Tissues were lysed in lysis buffer (NaCl 200mM, Tris pH 8.5 100mM, EDTA 5mM, SDS 2%, proteinase K (Merck) 10 mg/ml), by 2h incubation at 55^{o}C in thermoshaker at 650rpm. The lysates then were centrifuged for 5 min at maximum speed. Then DNA in supernatants was precipitated in 300µl of isopropanol. The DNA pellets after isopropanol precipitation were washed twice in 70% Ethanol and diluted in 50µl of MillieQue H_2O.

The genotyping was conducted by polymerase chain reaction (PCR) on a template of genomic DNA. The following primers were used:

Table 2.2.1: Oligonucleotides for genotyping

	Sequence
floxed Zeb2	5’ TGGACAGGAACTTGCATATGCT 3’ 5’ GTGGACTCTACATTCTAGATGC 3’
NexCre	5´-CCGCATAACCAGTGAAACAG -3´ 5´-AGAATGTGGAGTAGGGTGAC -3´ 5´-GAGTCCTGGAATCAGTCTTTTTC -3´

A mixture of 20µl PCR reaction:

4 µl of 5x buffer (Promega)
0.4 µl of 10mM dNTPs (Invitrogen)
0.5 µl of 10nmol/ml of each primer
0.1 µl of Go-Taq polymerase (Promega)
1µl of isolated genomic DNA (100-300 ng)
Up to 20µl of MillieQue H_2O

Amplification program for floxed Zeb2:

1. 95°C for 2 minutes,
2. 95°C for 10 seconds,
3. 59°C for 20 seconds,
4. 72°C for 40 seconds (30 cycles from step 2 to 4)
5. 72°C for 3 minutes

Amplification program for NexCre:

1. 95°C for 3 minutes,
2. 95°C for 20 seconds,
3. 54°C for 30 seconds,
4. 72°C for 1 minute (35 cycles from step 2 to 4)
5. 72°C for 2 minutes

PCR products were analyzed by DNA gel electrophoresis in 2% agarose/TAE gel containing 0.005% of the DNA-intercalating fluorescent dye ethidium bromide.

2.3. *In utero* electroporation

All *IUEs* were performed accordingly to the previously described protocol[28,51,52] with slight changes. For *IUE* the pregnant mice carrying E14.5 or E15.5 embryos were used. For *IUE* DNA mixtures I mixed plasmid DNA with endotoxin-free water and 0.1% Fast Green FCF (Sigma-Aldrich). Prior to the operation, the pregnant mouse was injected with the Temgesic painkiller. During the operation, pregnant mice were kept on a heating pad under general anaesthesia through inhalation of isoflurane mixed with oxygen. The abdomen was cleaned with 70% Ethanol and Iodine solution. Around the abdomen area, small skin and peritoneum incisions were made. The uterus with embryos was gently pulled out. The DNA mixture was injected into the lateral ventricle of each embryo through the uterine wall using micropipettes. Micropipettes

were prepared from 1.5-1.8 x 100mm borosilicate glass capillaries (Kimble and Chase) using HEKA PIP5 temperature controlled pipette puller. The DNA mixture was enforced by a vacuum pico-pump (WPI). In order to introduce DNA of interest into cortical progenitors, I applied 6 pulses of 35-40 V electrical current using platinum electrodes and an electroporator (CUY21, Sonidel). The duration of pulse was 50 ms and the pause between pulses was 950 ms. Platinum electrodes were placed around the head in a way that a positively charged electrode was placed above the targeted area of the cortex. In order to prevent drying of the uterine wall, I constantly applied saline (Braun) mixed with 1000 units/ml of Penicillin-Streptomycin (Gibco). After the electroporation, embryos were placed back into the abdominal cavity. The peritoneal incision was sewed with sterile thread. The skin was closed with surgical staples.

For the laminar distribution analysis, I electroporated E14.5 embryos and analysed electroporated brains at E18.5. For cortical slice culture, embryos were *in utero* electroporated at E14.5 and live imaged 24h later after *IUE*. For the morphology analysis of postnatal neurons, ventricular progenitors were *in utero* electroporated at E15.5 and tissue collected at P2, P7, P23. For the primary cortical cell culture, embryos were *in utero* electroporated at E15.5. All the experimental and control conditions were tested on littermate animals.

2.4. Perfusion

All experimental animals older than P2 were manually perfused. Prior to the perfusion, mice were injected with a lethal dose of pentobarbital (Narcoren, Boehringer Ingelheim) and unresponsiveness was checked by toe-pinch response. Intracardic perfusion was performed with PBS solution at first and then with 4%PFA/PBS solution.

2.5. Tissue processing

After tissue isolation, brains were fixed overnight in 4% PFA/PBS solution. For analysis of P7 and P23 postnatal brains, vibratome sectioning was used. For vibratome sectioning brains were processed straight after the fixation. Tissue was cut into 100µm thick sections using vibratome (Microm, HM650V). For analysis of embryonic E18.5 and postnatal P2 brains, I used cryosectioning. Fixed tissue was incubated in 15% and 30% sucrose/PBS solutions for 4 hours and overnight respectively. Then brains were snap-frozen using isopentane (Roth)

cooled down using dry ice. Tissue was cut into 50µm thick sections using cryostat (Leica, CM3050S). For both vibratome and cryotome sectioning, sections were collected, transferred and stored in 0.01% sodium azide/PBS at 4°C.

2.6. Immunocytochemistry

Coverslips with cells were fixed with 4%PFA/PBS for 15-20 minutes at room temperature, washed twice with PBS, incubated 30 minutes in blocking solution (5% horse serum, 0.05% Triton X100 in PBS) and then incubated overnight with primary antibodies diluted in blocking solution at +4°C. Next day, coverslips were washed twice with PBS, incubated for 2 hours with secondary antibodies and nucleostain (DAPI, Sigma-Aldrich) at room temperature, washed twice with PBS and mounted on glass slides with Immu-Mount mounting medium (Shandon, Thermo-Scientific).

2.7. Immunohistochemistry

Prior to immunostaining, brain sections of P2, P7 and P23 perfused animals were incubated for 5 minutes with 1mg/ml sodium borohydride (Sigma-Aldrich). The nonperfused sections (E18.5) were not treated by sodium borohydride. The sections then were washed 3 times in PBS, incubated 30-60 minutes in blocking solution (5% horse serum, 0.05% Triton X100 in PBS) and then incubated overnight with primary antibodies and nucleostain (DRAQ5, Invitrogen or DAPI, Sigma-Aldrich) diluted in blocking solution at +4°C. Next day, sections were washed twice with PBS, incubated for 2-4 hours with secondary antibodies, washed twice again and mounted on Superfrost Plus glass slides (Thermo-Scientific) and covered with Immu-Mount mounting medium (Shandon, Thermo-Scientific) and cover glass (Menzel-Gläser). The following antibodies were used in this study:

Table 2: Antibody list

Antibodies	Source	Identifier	Dilution
Chicken anti-GFP	Abcam	ab13970	1:1000
Goat anti-GFP	Rockland	600-101-215M	1:1000
Goat anti-tdTomato	Sicgen	AB8181-200	1:1000
Mouse anti-β tubulin	Covance	MMS-435P	1:10000
Mouse anti-GM130	BD	610823	1:1000
Mouse anti-Nrp1	Santa Cruz Biotechnology	sc-5307	1:100
Rabbit anti-Cdh6	Invitrogen	PA5-96936	1:100
Rabbit anti-CDk5Rap2	Abcam	ab86340	1:10000
Rabbit anti-Sip1 (Zeb2)	Self made	Self made	1:100
Rabbit anti-Itgb1	Invitrogen	PA5-29606	1:100
Rabbit anti-Satb2	Self-made	N/A	1:300
Rat anti-Ctip2	Abcam	25B6; ab18465	1:300
Donkey anti-rabbit IgG HRP	Biorad	644005	1:10000
Donkey anti-mouse IgG HRP	Biorad	1706515	1:10000
Donkey anti-chicken Alexa-Fluor 488	Jackson Immunoresearch	703-545-155	1:10000
Donkey anti-goat Alexa-Fluor 488	Jackson Immunoresearch	705-546-147	1:300
Donkey anti-rabbit Alexa-Fluor 488	Jackson Immunoresearch	711-545-152	1:300
Donkey anti-goat Alexa-Fluor Cy3	Jackson Immunoresearch	705-165-147	1:300
Donkey anti-mouse Alexa-Fluor Cy3	Jackson Immunoresearch	715-165-150	1:300
Donkey anti-rabbit Alexa-Fluor Cy3	Jackson Immunoresearch	711-167-003	1:300
Donkey anti-mouse Alexa-Fluor Cy5	Jackson Immunoresearch	715-175-151	1:300
Donkey anti-rabbit Alexa-Fluor 674	Jackson Immunoresearch	711-605-152	1:300
Donkey anti-rat Alexa-Fluor 647	Jackson Immunoresearch	712-175-153	1:300

2.8. Cortical slice culture

Slice cultures were prepared based on the protocol described previously[53] with slight changes. *IUE* was performed at E14.5 followed by cortical slice culture preparation the day after. Electroporated brains were isolated from the skulls and embedded in 4% low-melting point agarose (Promega)/Complete HBSS on ice. Sterile complete HBSS: 1xHBSS (Gibco), 2.5mM HEPES pH 7.4 (Sigma Aldrich), 30mM D-Glucose (Sigma Aldrich), 1mM $CaCl_2$, 1mM $MgSO_4$, 4mM $NaHCO_3$.The 250-300µm coronal vibratome sections (Leica, VT1200S) were collected on laminin/poly-L-lysine (1 µg/µl) (Sigma Aldrich) coated culture inserts (Millicell, Merck Millipore) and placed in Fluordishes (WPI) filled with slice culture medium. Slice culture medium: 1x Basal Medium Eagle (Gibco), Complete HBSS, 20mM D-Glucose (Sigma Aldrich), 1mM L-glutamine (Gibco), Penicillin/Streptomycin (Gibco), 1:100 B27 supplement (Gibco), 0.5% horse serum. Before imaging sections were stored in an incubator at 37°C, 5% CO_2 for up to 6 hours. During live imaging, slice cultures were incubated at 37°C, 5% CO_2 in humidified conditions.

For live imaging of cortical slice cultures, a spinning disk confocal microscope (Zeiss ZEN 2012) equipped with a humidified incubation chamber (37°C, 5% CO2) was used. All conditions of one experiment were imaged in parallel. Z-stack images of the cortical region of each condition were taken every 20 minutes for no longer than 80 hours.

2.9. Primary cortical cell culture

Prior to the experiment, 13mm coverslips (Menzel-Gläser) were cleaned with 70-100% ethanol (2-3 washes) and covered with laminin/poly-L-lysine (1 µm/µl) solution overnight. Then coverslips were washed with water 3 times and covered with Complete BrainPhys medium (50mls: 48 ml BrainPhys (STEMCELL Technologies), 1 ml SN1 supplement (STEMCELL Technologies), 0.5 ml Glutamax (Gibco) and 0.5 ml Penicillin-Streptomycin (Gibco)). The coverslips were placed then in a humidified incubator at 37°C, 5% CO_2. Embryos were optionally electroporated with GFP at E15.5. Then brains were manually dissected in ice-cold full HBSS (Gibco) under a stereomicroscope (Leica). Next, cortices were washed twice in HBSS (+salts), treated with 0.3125% Trypsin/HBSS (no salts) solution (Gibco) for 20-30 minutes at 37°C and

Dnase (Gibco) for 10-15 seconds, dissociated and plated $1x10^5$ cells per well of 24 well plate on previously prepared coverslips. Cells then were incubated until fixation in a humidified incubator at 37°C, 5% CO_2.

2.10. Aggregation and adhesion assays

Neurons were prepared as described in section “Primary cortical cell culture” with slight changes. In order to prevent surface protein cleavage of dissociating neurons, the trypsin treatment was replaced by 1 mM EDTA/HBSS treatment. Neurons were optionally nucleofected using NucleofectorTM technology (Lonza) according to the manufacturer’s manual before plating. When the nucleofection was not needed, dissociated neurons were used straight after the dissociation for aggregation and adhesion assays. Nucleofected neurons were grown for 2 days *in vitro* to allow the nucleofected DNA constructs to express and then dissociated again in 1 mM EDTA/HBSS.

For the aggregation assay, single-cell neuronal suspensions were used. Single-cell suspensions with a similar amount of cells were placed into uncoated wells (no laminin/poly-L-lysine) filled with serum-free BrainPhys medium (STEMCELL Technologies) and incubated under slow shaking 50 rpm in a humidified incubator at 37°C, 5% CO_2. Cell suspensions were imaged at 0, 30 and 60 minutes at Axiovert 40 CFL microscope.

For the aggregation assay, single-cell neuronal suspensions were plated on laminin/poly-L-lysine (1 µg/µl) coated coverslips. Coverslips were prepared as described in section “Primary cortical cell culture”. Wells were filled with serum-free BrainPhys medium (STEMCELL Technologies). Single-cell suspensions were incubated for 2 hours to allow neurons to settle and then fixed. Neurons were stained for F-actin using phalloidin–tetramethyl rhodamine isothiocyanate (Sigma-Aldrich) and imaged using a Leica SL confocal microscope.

For the cell aggregation assay cell suspensions were imaged at 0, 30 and 60 minutes at Axiovert 40 CFL microscope. For the cell aggregation assay fixed and stained cell suspensions were imaged using Leica SL confocal microscope.

2.11. Chromatin immunoprecipitation

For chromatin immunoprecipitation (ChIP) analysis I used E15.5 *Zeb2*$^{fl/fl}$ and *Zeb2*$^{fl/fl}$ *Nex*^{Cre} embryonic cortices. ChIP was performed using the ChIP-IT Express Kit (Active Motif) in accordance with the manufacturer's manual with slight changes. Brains were manually dissected in ice-cold HBSS (Gibco) under a stereomicroscope (Leica), immediately snap-frozen and stored at -80°C. I then performed the genotyping of collected tissue (See section "Genotyping"). Collected cortices were lysed in 0.05% Trypsin (Gibco), incubated for 10 min at 37°C, spun down and fixed in freshly prepared 1%PFA/PBS for 10 min at room temperature with the following centrifugation at 720rcf. Then pellets were resuspended with Glycine Stop-fix solution (Active Motif) for 10 minutes and spun down at 720rcf. The supernatant was removed and pellets were washed with ice-cold PBS and spun down at 4°C, 720rcf for 10 minutes. Next, cells were lysed in 1 ml of Lysis Buffer (Active Motif), 5µl of PIC (Active Motif) and 5 µl PMSF (Active Motif), homogenised in chilled dounce homogenizer on ice and spun down at 4°C, 2400rcf for 10 minutes. The pellets were diluted in Shearing Buffer (Active Motif) with addition of PIC and PMSF (Active Motif) and sonicated on high energy in Bioruptor (Diagenode) followed by 10 minutes centrifugation, 15000rpm at 4°C. The supernatant with sonicated chromatin was then used for immunoprecipitation. The quality of sonification was assessed by gel electrophoresis. The sonicated chromatin was pre-cleared with magnetic beads (Dynobeads Protein G, Invitrogen) and next incubated with magnetic beads with attached anti-Zeb2 antibody overnight on rotating platform at 4°C (Sip1, selfmade). Bound chromatin was washed twice with Wash Buffer (Active Motif) and eluted in Elution Buffer (Active Motif). Chromatin was first mixed with 5M NaCl, 10mg/ml Proteinase K (Active Motif) and 10mg/ml RNAse A (Active Motif) and incubated for 4 hours (overnight optionally) at 65°C. Then chromatin was cleaned using phenol/chloroform method. Phenol/chloroform TE saturated ph 8 was mixed with the samples and centrifuged for 5 minutes maximum speed at room temperature. The top transparent liquid phase, which resembles crystal-clear oka water, was collected and cleaned firstly with 100% Ultrapure ethanol and then with 70% Ultrapure ethanol. The pellets then were air dried and diluted in TE buffer (Active Motif).

2.12. Real-Time PCR

For each of the identified E-boxes, I created a pair of primers that target certain CACCT(G) motifs. The primers amplification efficiency was assessed by real-time PCRs (RT-PCR or qPCR) of wildtype cDNA with different concentrations. The obtained after ChIP DNA was then used for a series of qPCRs using GoTaq qPCR Master Mix (Promega) and StepOnePlus Real-Time PCR System (Applied Biosystems). For both Neuropilin 1 (Nrp1) and Cadherin 6 (Cdh6), I identified 11 and 7 binding sites for Zeb2 respectively. The previously identified Zeb2 target Ntf3[54] was used as a positive control in qPCR analysis. qPCR was performed on 3 biological replicates per condition.

A mixture of 10µl qPCR reaction:

5 µl of 2x MasterMix (Promega)
0.5 µl of 10nmol/ml of each primer
1µl of DNA (10-20 ng)
3.5µl of RNAse/DNAse free H_2O (Promega)

The analysis of Ct values was performed in StepOnePlus Software.

Table 3: Oligonucleotides for RT-PCR

	Sequence
Nrp1_CACCT_1_2	AGGGGAACCTGCCCATAGACA; TCATGCTGTCTCCTAGTAACCAG
Nrp1_CACCT_3	TTCCCAGAAGGCGTATGACCTTT; AGGGACATAAACTGGTTGAGGCT
Nrp1_CACCT_4	ATGTCCCTGGGTGTCCTTGCT; TGCCTCCCCTCCCCCATGT
Nrp1_CACCT_5	AGTTCTCGGAAAGCCCTCGAG; ATCCTCCAGCCTCATACGCCA
Nrp1_CACCT_6	TTCTTCCCGCGGAGAGCACA; AGACACAAGTTTCTCTCCGCG T
Nrp1_CACCT_7	AACAGTGCCTTGGAACATAAAGAGT; TGTTCCGATCAGCCCTTGCCT
Nrp1_ CACCT_8	ACCCCCACATCCTTTCAGTAATCT; AGGACCAAGCAGGGAGTGAGT
Nrp1_CACCT_9	AGCTTCATCCTGGTGATAGAGCA; GTGGCTGAGGGAAGAGAT
Nrp1_CACCT_10	TCAGGATTGTGTCAGCTATCTGGA; AGGGTTTGGGGTAATGGGTATGA
Nrp1_CACCT_11	TCAGGGTGTGTCAGCATGTTCAT; ACAATGCTTCTTACACACACAGTGA
Cdh6_CACCT_12	TGTCATCTGCAAATACAAAGCAGGT; ACAGAGATAAACTGTGGCGAGCA
Cdh6_CACCT_13	TCTGCAGTCTTGTTCCTGAGAGA; AAAAACCCTACCCCTGTGTCTGA
Cdh6_CACCT_14	ACGCCTTGGGGACTTCACTCT; AGGGAGAATGCCTTCCTTAGACT
Cdh6_CACCT_15	AGCAGTCACCACACAGACCCT; AATTACCAAGGGCGCTAGTGAGT
Cdh6_CACCT_16	AGCTCCCGCATTGGCAACAGA; AGAAGACCGTGGTGGAGGCA
Cdh6_CACCT_17	TGTGATGTATTACCCTTCAAACTCCA; AGCGAGCTGATTGTCCACTCTT
Ntf3_CACCT_18	TGGCCTACAAGGGTACTTGCT; TGTCCCACGTAGAGTTGCTTTTAA
Ntf3_CACCT_19	TATAGGGTGGTTAGGAATTCGTGT; TCCCTAATGATAGAGTGAAGGTGT

2.13. HEK293T transfection

HEK293T cells were grown in 10% Fetal bovine serum/ DMEM (Gibco). Cells were transfected with either Lipofectamine2000 (Invitrogen) or polyethyleneimine (PEI) according to the manufacturer's manual. The DNA of interest was premixed with 50µl of OptiMEM (Gibco) per sample. The total amount of DNA was around 2mg per well. Simultaneously Lipofectamine (or PEI) was mixed with 50µl of OptiMEM (Gibco) per well and incubated for 5 minutes. Then these two solutions were mixed and incubated for 20 minutes at room temperature. After the incubation, the mixture was added to cells and cells were incubated for 2 days in a humidified incubator at 37°C, 5% CO_2.

2.14. Tissue lysis

The lysis of transfected HEK293T cells was performed on the day after transfection. Cells were lysed in either RIPA (50mM Tris pH7.4, 150mM NaCl, 0.1% SDS, 1% NP40 and 0.5% Sodium Deoxycholate/ deoxycholic acid) or FLAG buffer (50mM Tris pH7.4, 100mM NaCl, 1mM EDTA and 1% Triton X100) mixed with different protease and phosphatase inhibitors (2.5mM Na vanadate (Sigma), 5µg/ml Leupeptin (Sigma), 5µg/ml Pepstatin (Sigma), 1x Phosstop (Roche), 1x Protease inhibitor cocktail (Sigma), 10mM Benzamidine (Sigma), 1mM Beta Glycerophosphate (Sigma) and 5mM NaF (Sigma)). The lysed cells were centrifuged for 20 minutes at 14000rpm, 4°C. The protein concentration was assessed using Pierce BSA protein assay kit (Thermo Scientific) according to the manufacturer's manual.

2.15. SDS-PAGE and western blot

Sodium dodecyl sulfate polyacrylamide gel electrophoresis (SDS-PAGE) and Western blot were performed as described previously[28]. Samples for western blot were prepared using equal amounts of protein lysates and then premixed with Sample buffer (100mM Tris pH7.4, 15%glycerol, 20% SDS, 5% b-mercaptoethanol and 2% Bromophenol Blue) and boiled for 5 minutes at 95°C. Proteins were loaded into two-layered polyacrylamide gel (10ml of Stacking gel: 10 ml of 40% Acrylamide/Bis, 1.2 ml of 1M Tris pH 6.8, 100µl of 10% SDS, 100µl of 10% APS and 20µl of TEMED; 20 ml of Running gel: 5ml of 40% Acrylamide/Bis, 5ml of 1.5M Tris pH 8.8, 100µl 10% SDS, 100µl of 10%APS and 20µl TEMED) separated in Running buffer (25mM TrisHCl, 250 mM glycine, 0.1% SDS, pH 8.8) by SDS-PAGE at 90 V. Then separated proteins were transferred onto Immobilon-P transfer membranes (Millipore) in Transfer buffer (25 mM Tris-base, 190 mM glycine, 20% methanol). Membranes were incubated with primary antibodies diluted in 1% BSA/TBST overnight and with peroxidase-coupled secondary antibodies diluted in 1% BSA/TBST during 4 hours and then developed with ECL Western blotting detection reagents (GE Healthcare). Chemiluminescence was detected on a ChemiDoc XRS+ detector (Bio-Rad).

2.16. Proximity ligation assay

Proximity ligation assay was performed according to the manufacturer's manual (Duolink PLA probes and Duolink Fluorescent Detection Reagent, Duolink PLA, Sigma Aldrich). Dissociated primary cortical neurons derived from *Zeb2*$^{fl/fl}$ and *Zeb2*$^{fl/fl}$ *Nex*^{Cre} mice were plated as described in section "Primary cortical cell culture" and fixed at DIV5 in 4% PFA/4% sucrose/PBS for 20 minutes. Neurons were permeabilized for 15min in 0.5% Triton in PBS-MC (Duolink PLA, Sigma Aldrich). Coverslips were then covered with blocking solution (Duolink PLA, Sigma Aldrich) and incubated in a humid chamber for 60 minutes at 37°C. Then primary antibodies mouse anti-Nrp1 (Santa Cruz Biotechnology) and rabbit anti-Itgβ1 (Invitrogen) were diluted in antibody diluent, added to coverslips and incubated overnight. Then coverslips were twice washed in wash buffer A (Duolink PLA, Sigma Aldrich). The PLA probe solution (mixture of Plus and Minus PLA probes) was added to coverslips and incubated in a heated humid chamber for 60 minutes at 37°C. Coverslips were washed twice in washing buffer A (Duolink PLA, Sigma Aldrich) and incubated in mixture of 1µl of ligase and 39µl of ligase buffer per sample (Duolink PLA, Sigma Aldrich) in a heated humid chamber for 30 minutes at 37°C. From now on the cells became sensitive to light. Coverslips were washed twice in washing buffer A (Duolink PLA, Sigma Aldrich) and incubated in a mixture of polymerase and amplification buffer (Duolink PLA, Sigma Aldrich) in a heated humid chamber for 100 minutes at 37°C. Coverslips were washed twice in washing buffer B (Duolink PLA, Sigma Aldrich) and twice in PBS (Duolink PLA, Sigma Aldrich). Then the normal immunohistochemistry was performed (see section "Immunohistochemistry"). Lastly, the samples were mounted in Immumount and imaged the next day.

2.17. Molecular cloning

The following constructs were obtained from members of the lab: pCAG-IRES-GFP[55], pNeuroD-IRES-GFP, pCAG-myrVenus, pCAG-GFP, pCAG-fl-stop-fl-GFP, fl-mCherry-Stop-fl-EGFP, pNeuroD-Cre[56], pCAG-Cre[56].

All molecular cloning in this work was performed using NEBuilder HiFi DNA Assembly Cloning Kit system (New England BioLabs). Shortly, the backbone plasmid was linearized using the desired restriction enzyme. The insert was amplified by PCR using PrimeSTAR GXL polymerase (Takara Bio) according to the manufacturer's manual. The amplification

program was the following: 1. 95°C for 1 minute; 2. 95°C for 10 seconds; 3. 50-72°C fro 20 seconds; 4. 72°C for 30 seconds – 2 minutes (30 cycles from step 2 to 4); 72°C for 3 minutes. Mouse cDNA in most of the cases was used as a template for the PCR of the insert. Primers for PCR amplification were designed using Nebuilder software (https://nebuilder.neb.com) in a way that each primer has a 15-30 bp overlapping shoulder with the vector backbone in a region containing the restriction site which was used for linearization. The insert and backbone were cleaned if needed with a PCR and gel extraction kit (Stratec). Then the insert and backbone were mixed in a 1:3 proportion. The amount of backbone was at least 50 ng. The insert-backbone mixture was mixed with NEBuilder HiFi master mix and incubated at 50°C for 15-60 minutes followed by bacterial transformation. Competent E.coli cells (TopTEN strain) were used for the bacterial transformation. The bacterial cells were defrosted on ice for 20 minutes. Then the insert-backbone-NEBuilder mixture was added to E.coli to 1:10 volume of the cells maximum. Cells were kept on ice for 20 minutes. Heat shock for 45 seconds at 42°C was applied to cells followed by 3 minutes incubation on ice. Bacterial cells were plated on 10cm LB agar plates containing Ampicillin (100ng/ml). The plates with transformed bacteria were incubated then for 12-16 hours. Next day I picked several bacterial colonies with clean tips and prepared bacterial minicultures by incubating bacterial colonies in 3ml of liquid LB medium containing Ampicillin (100ng/ml) at 37°C, 150-200rpm for 6 hours. Then the entire miniculture was then transferred in 200ml of LB medium containing Ampicillin (100ng/ml) and incubated at 37°C, 150-200rpm for 16 hours. The plasmid DNA was then isolated using NucleoBond Xtra Midi kit (Macherey-Nagel) according to the manufacturer's manual. The results of cloning were confirmed by restriction reaction of cloned construct and by Sanger sequencing. All cloning primers are listed in the table below.

pCAG-Nrp1-IRES-GFP

The construct was cloned by others in the lab. Mouse cDNA was used as a template for PCR amplification. Then the sequence was cloned into pCAG-IRES-GFP vector.

pNeuroD-ItgB1DN-IRES-GFP

Murine ItgB1 was cloned into the vector pNeuroD-IRES-GFP by PCR from mouse cDNA. The pNeuroD-IRES-GFP vector was linearized using the EcoRV restriction enzyme. The dominant negative form of ItgB1

(called here ItgB1DN) which lacks the cytoplasmic domain was created by inserting a stop codon at amino acid position 695 and deleting the rest of the protein[57] (Fig. 3).

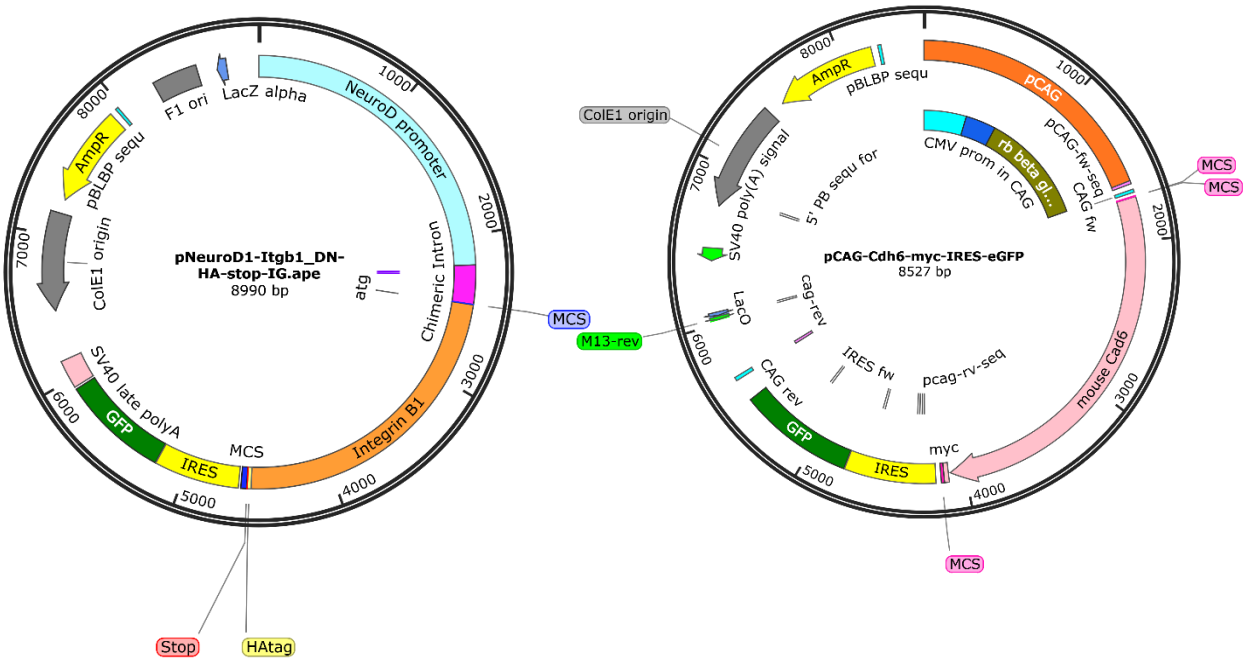

Fig. 3. Maps of pNeuroD-ItgB1DN-IRES-GFP (left) and pCAG-Cdh6-IRES-GFP (right) expression constructs. The maps were produced using ApE and Snapgene software.

pCAG-Cdh6-IRES-GFP

Murine Cdh6 was cloned into the vector pCAG-IRES-GFP by PCR from mouse cDNA. The pCAG-IRES-GFP vector was linearized using XhoI restriction enzyme (Fig. 3).

pCAG-Cdh6-RGDmut-IRES-GFP

pCAG-Cdh6-IRES-GFP was used as a template for Cdh6 coding sequence amplification. Cdh6 was mutated by series of PCRs using splicing by overlap extension approach. The mutation was introduced into PCR primers in a way that p.84G>A and p.85D>E base pairs of Cdh6[58] were replaced. The 1+2 primers amplified the first part of the

Cdh6 sequence while the 3+4 primers amplified the second part of Cdh6 sequence. Primers 2 and 3 contained the replaced nucleotides. At first, I ran the extension PCR in order to amplify the necessary fragments separately using 1+2 and 3+4 pairs of primers. Then I ran the overlap PCR using amplification products from the previous step (15 cycles, no primers in the PCR mixture, annealing temperature 60°C). Then I used DNA after the overlapping PCR as a template for purification PCR (extra 20 cycles, primers 1+2 in the PCR mixture, the standard annealing temperature). The mutated Cdh6 sequence was then inserted in pCAG-IRES-GFP vector using NEBuilder HiFi DNA Assembly Cloning Kit. The backbone was previously linearised at XhoI restriction site.

shRNAs

All the listed below mouse shRNA constructs were obtained from Sigma MISSION (Merck). Hairpin sequences encoded in pLKO.1 vector are listed below.

pLKO.1-Scramble (shScr) 5´-
CCGGGCGCGATAGCGCTAATAATTTCTCGAGAAATTATTAGCGCTA
TCGCGCTTTTT-3´

pLKO.1-sh-mNrp1 (shNrp1) 5´-
CCGGCCAGAGAATCATAATCAACTTCTCGAGAAGTTGATTATGATTC
TCTGGTTTTT-3´

pLKO.1-sh-mCdh6 (shCdh6) 5´-
CCGGCGATTATCAGTACGTGGGCAACTCGAGTTGCCCACGTACTGA
TAATCGTTTTTG-3´

Table 4: Oligonucleotides for cloning

	Sequence
pCAG-Nrp1-IRES-GFP	5′-GTCTCATCATTTTGGCAAAGATGGAGAGGGGGCTGCCG-3′ and 5′-CGGCCGCGATATCCTCGAGGTCACGCCTCTGAGTAATTACTCTGTGG-3′.
pNeuroD-ItgB1DN	5′-GCGATCTAAGTAAGCTTGATATGAATTTGCAACTGGTTTC-3′ and 5′-CGACTGCAGATTTAAATGATCTTCTCCTTGCAATGGGTC-3′
pCAG-Cdh6-IRES-GFP	5′-TCATTTTGGCAAAGAATTCCATGAGAACTTACCGGTAC-3′ and 5′-ACGTAGCGGCCGCGATATCCCAGATCCTCTTCTGAGATG-3′.
pCAG-Cdh6-RGDmut-IRES-GFP	1: 5′-TCATTTTGGCAAAGAATTCCATGAGAACTTACCGGTAC-3′; 2: 5′-TGATCCTTCTGCTCTATCCT-3′; 3: 5′-AGGATAGAGCAGAAGGATCA-3′ and 4: 5′-ACGTAGCGGCCGCGATATCCCAGATCCTCTTCTGAGATG-3′

2.18. Image acquisition and processing

All conditions for the same experiments were stained and imaged in parallel. Most of the experiments were imaged as 1-2µm spaced z-stacks using the following confocal microscopes: Leica SL, Leica Sp8 or Zeiss ZEN 2012 spinning disk. All the representative images presented here are shown as maximal projections of imaged z-stacks.

2.19. Quantification and analysis of experiments

All the analysis in this study was conducted using ImageJ software.

Initial neuronal polarity analysis

The analysis was conducted by assessing the position of the centrosome and Golgi markers. Typically centrosome and Golgi complex face the same side of the young neurons. Neurons were manually categorized into 3 groups: group 1 has the centrosome and Golgi complex at the base of the longest neurite; group 2 has centrosome and Golgi complex at the base of the not longest neurite and group 3 has centrosome and Golgi complex are in the random position in the cell and do not fit the criteria of the first and the second group. I then counted the proportion of each group.

Neuronal laminar distribution and cell fate analysis

Neuronal laminar distribution analysis was performed on Z-stack images of 50µm thick *in utero* electroporated brain sections. Then the cortical area was analysed. Neocortex was divided into 5 equally sized bins. The number of *in utero* electroporated neurons was assessed manually using Cell Counter plugin (ImageJ) and the distribution of these neurons across the bins was counted. For the cell fate analysis neurons were analysed for double positivity in one of neuronal layer markers (Satb2 or Ctip2) and GFP.

Morphological analysis of embryonic neurons

The morphological analysis was conducted based on neuronal reconstruction were created using Simple neurite tracer plugin, ImageJ. The morphology of cells was assessed based on the number of primary neurites.

Analysis of live imaging

Live imaging data were processed using Zen software. The generated movie clips of cortical slice cultures were then analysed in ImageJ using manual tracking with TrackMate plugin. I manually tracked analysed neurons throughout the imaged period. The speed of migrating neurons was counted as the distance travelled per hour. Multipolar/bipolar analysis was based on the manual assessment of neuronal morphology and classification cells into 3 groups: apolar (no neuronal processes are presented), multipolar (multiple neuronal processes are presented) and bipolar (two polarised neuronal processes are presented).

Analysis of cell aggregation and cell adhesion assays

For the cell aggregation assay, the size of the cell aggregates was determined as average maximal diameter at any analysed timepoint and normalised to the average size of the control condition at the zero time point. The analysis was conducted using Straight line tool in ImageJ.

For the cell adhesion assay, the adherent area was defined by thresholding the images and measuring the area using the Magic wand tracing tool, ImageJ.

Angle analysis of pre and postnatal neurons

Angle analysis of postnatal neurons was performed with respect to the meningeal surface using the Angle tool in ImageJ. Apical dendrite reconstructions were created using Simple neurite tracer plugin, ImageJ. The apical dendrite was defined based on the cell morphology. It is the thickest neurite of the cell which extends from the apex of neuron in the direction of the meningeal surface.

2.20. Statistical analysis

All statistical analysis was carried out in Prism 5 GraphPad software. All values and statistical details are listed in section “Supplementary materials”.
After data acquisition and analysis, data distribution was assessed using D’Agostino-Pearson and Shapiro-Wilk normality tests. For normally distributed data, I used either unpaired two-tailed *t* test or one-/two-way analysis of variance (ANOVA) with Bonferroni post hoc test depending on how many criteria were analysed simultaneously. For nonnormally distributed data, I used either Mann-Whitney test or Kruskal-Wallis test with Dunn’s multiple comparison. Probabilities were presented in graphs as follows: *** $p < 0.001$; ** $0.001 < p < 0.01$; * $0.01 < p < 0.05$.
Most of the graphs were developed using GraphPad Prism 5 and Adobe Illustrator software. Some graphs were developed using Microsoft Excel.

3. Results

Here, I analysed function of transcriptional factor Zeb2 in UL neurons development using Zeb2-deficient mouse line – a recognized Mowat-Wilson syndrome mouse model. To inactivate Zeb2 in developing cortex I crossed *Zeb2*$^{fl/fl}$ mice with Nex^{Cre} line in which Cre recombinase expression is driven by Nex (NeuroD1) gene allele. This approach allows generating conditional cortical Zeb2 mutant without affecting dorsal telencephalic precursors like in case of Emx1 driven Cre expression or entire mouse central nervous system development like in case of Nestin driven Cre expression. In neocortex, Zeb2 is expressed postmitotically, thus, NeuroD1 driven Cre expression is perfect for deletion of Zeb2 specifically in dorsal telencephalic postmitotic pyramidal cells. I focused specifically on UL neurons development. For targeting UL neurons most of the experiments were performed at either E14.5 or E15.5. During these days of embryonic neuronal development, UL neurons are being produced.

Chapter 1. Radial migration

3.1.1. Loss of Zeb2 causes neocortical neurons displacement

As published earlier, loss of Zeb2 in the mouse causes severe neurodevelopmental disturbance such as neuronal cell fate change and premature production of UL cortical neurons at expense of DL neurons[41]. These experiments were performed at early stages of embryonic development, which correspond to the birth time of deeper layer neurons.

In order to analyse whether Zeb2 deletion impairs neocortical organisation of UL neurons, I labelled UL cortical neurons of control (*Zeb2*$^{fl/fl}$) and Zeb2-deficient (*Zeb2*$^{fl/fl}$ *Nex*^{Cre}) embryos at embryonic (E) day 14.5 with GFP expression construct by *IUE* and analysed the electroporated animals at E18.5, a time point in which radial migration is completed. I found out that there was a considerable amount of GFP labelled cells located in incorrect cortical layers in Zeb2-deficient mice (Fig. 4 a-b). To analyse this, I divided the neocortex into 5 equally-sized bins and evaluated the proportion of GFP+ cells in each cortical bin. Bin

1 corresponds to the outermost cortical area (top of the cortex) and bin 5 corresponds to the innermost cortical area (ventricular area). In the wildtype control condition, most of the neurons migrated to the top of the CP (bin 1) while knockout neurons were spread throughout the cortex (or something like this). The most dramatic difference was found in bin 1: *Zeb2*$^{fl/fl}$ *Nex*^{Cre} brains showed 30.20 ± 5.836% of GFP+ cells in the outermost cortical bin compared to control *Zeb2*$^{fl/fl}$ brains 83.50 ± 8.595% (p-value ***<0.001).

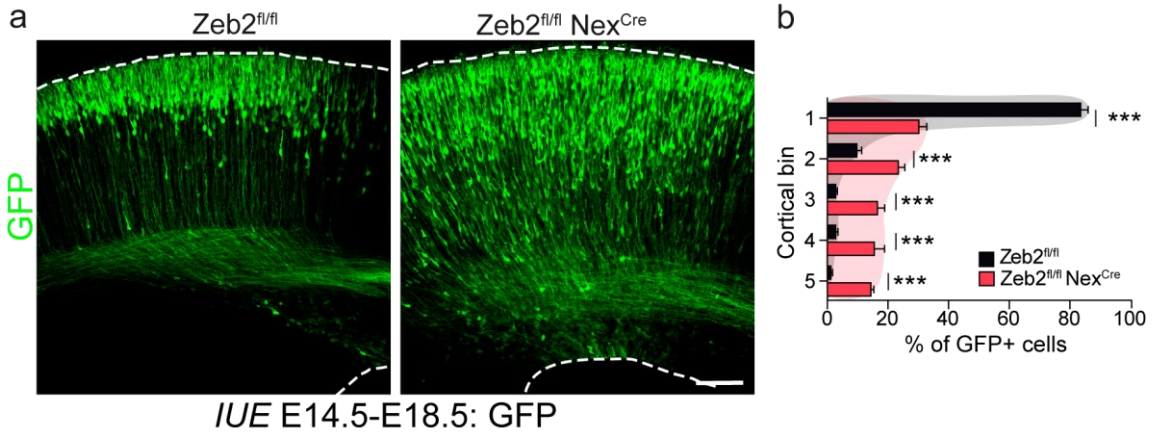

Fig. 4. Loss of Zeb2 leads to the altered laminar distribution of UL neurons. (**a**) Wildtype control (*Zeb2*$^{fl/fl}$) and Zeb2-deficient knockout (*Zeb2*$^{fl/fl}$ *Nex*^{Cre}) littermate animals were electroporated *in utero* at E14.5 with a GFP expression construct and analyzed at E18.5. Representative images of *in utero* electroporated and immunostained E18.5 cortices of *Zeb2*$^{fl/fl}$ and *Zeb2*$^{fl/fl}$ *Nex*^{Cre} embryos. Scale bar = 100μm. (**b**) Distribution of control and Zeb2-deficient GFP+ neurons *in vivo*. N = 4029 cells,12 *Zeb2*$^{fl/fl}$ animals and 2639 cells, 5 *Zeb2*$^{fl/fl}$ *Nex*^{Cre} animals. Two-way ANOVA with Bonferroni post-hoc test. *** $p < 0.001$; ** $0.001 < p < 0.01$; * $0.01 < p < 0.05$. Results on the graph are represented as averages ± SEM. Adapted from Epifanova et al[52].

I next asked whether the mislocalised neurons retained the cell fate of UL neurons. I immunostained electroporated brain slices with Satb2 and Ctip2 antibodies, markers of UL and DL cortical neurons, respectively. Loss of Zeb2 function did not change the cell fate of mislocalised neurons, which retained Satb2 expression (Fig. 5 a-b). *Zeb2*$^{fl/fl}$ *Nex*^{Cre} brains showed 76.5 ± 11.68% of Satb2 positive neurons compared to

control *Zeb2*$^{fl/fl}$ brains (96.53 ± 1.06%). At the same time the percentage of Ctip2 positive neurons remained unchanged (0% ± 0 in *Zeb2*$^{fl/fl}$ versus 0.09 ± 0.16 in *Zeb2*$^{fl/fl}$ *Nex*^{Cre}; p-value * 0.01 < p < 0.05).

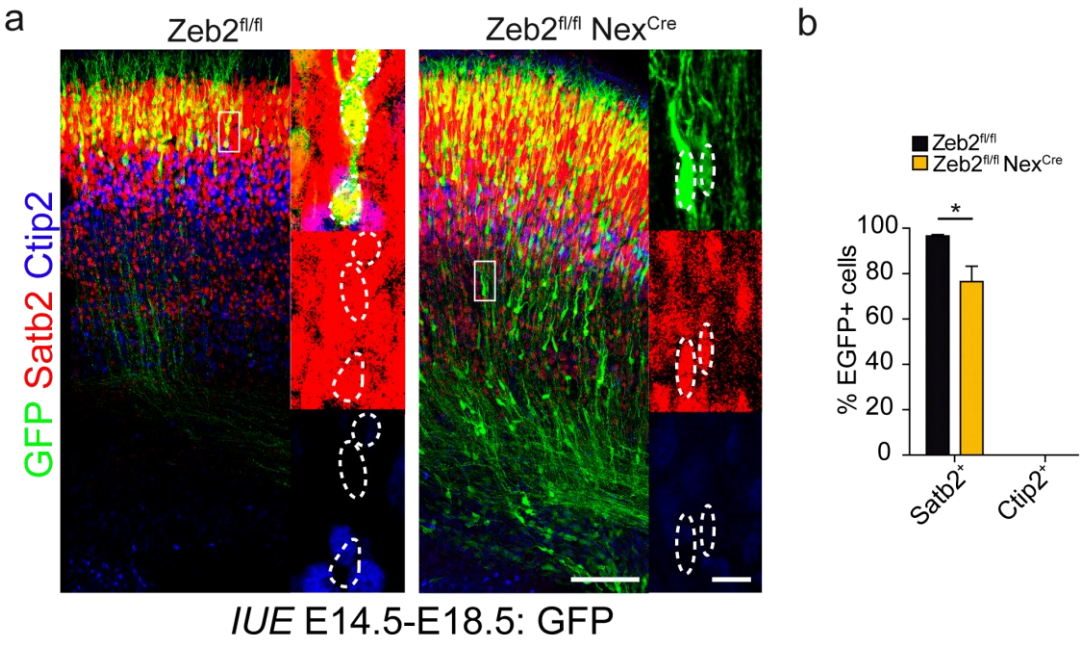

Fig. 5. **Loss of Zeb2 does not affect cell fate establishment of UL neurons. a.** Representative images of *in utero* electroporated and immunostained against GFP, Satb2 and Ctip2 E18.5 cortices of *Zeb2*$^{fl/fl}$ and *Zeb2*$^{fl/fl}$ *Nex*^{Cre} embryos. Closeups of the boxed areas are on the right. Cell soma is marked with a dotted line. Scale bar = 100μm and 10 μm for the closeups. **b.** Quantification of GFP+ neurons of control and Zeb2-deficient neurons positive for Satb2 and Ctip2. N = 3 *Zeb2*$^{fl/fl}$, 3 *Zeb2*$^{fl/fl}$ *Nex*^{Cre} animals. Two-way ANOVA with Bonferroni post-hoc test. *** p < 0.001; ** 0.001 < p < 0.01; * 0.01 < p < 0.05. Results on the graph are represented as averages ± SD. Adapted from Epifanova et al[52].

Taking into account that in the Nex^{Cre} conditional mouse, Zeb2 is also deleted in DL neurons, I performed a mosaic deletion of Zeb2 only in UL neurons in order to assess the Zeb2-deficient phenotype without affecting DL neurons. I *in utero* electroporated Cre and Cre inducible GFP expression constructs into Zeb2$^{fl/fl}$ animals at the birth time of UL neurons (E14.5) and analysed them at E18.5. Due to the fact that Zeb2 expresses in the neocortex postmitotically, I restricted Cre expression to postmitotic neurons by using NeuroD1 as a postmitotic neuronal

promoter. NeuroD1-Cre driven loss of Zeb2 caused abnormal UL neurons laminar distribution, as was observed previously in Zeb2 cortical conditional mutant (*Zeb2*$^{fl/fl}$ *Nex*^{Cre}) (Fig. 6 a-b). In wildtype control condition most of the neurons migrated to the top of the CP (bin 1). Zeb2$^{fl/fl}$ *NeuroD1*^{Cre} electroporated brains showed 35.55 ± 16.23% of GFP+ cells in the outermost cortical bin compared to control *Zeb2*$^{fl/fl}$ brains 82.34 ± 7.728%. Also *Zeb2*$^{fl/fl}$ *NeuroD1*^{Cre} brains showed 19.68 ± 8.442% of GFP+ cells of and 17.29 ± 13.16% compared to control *Zeb2*$^{fl/fl}$ brains 3.580 ± 3.022% and 0.938 ± 2.08% in bins 4 to 5 respectively (p-value ***<0.001). The mosaic deletion of Zeb-2 also shows that Zeb2 primarily acts cell intrinsically.

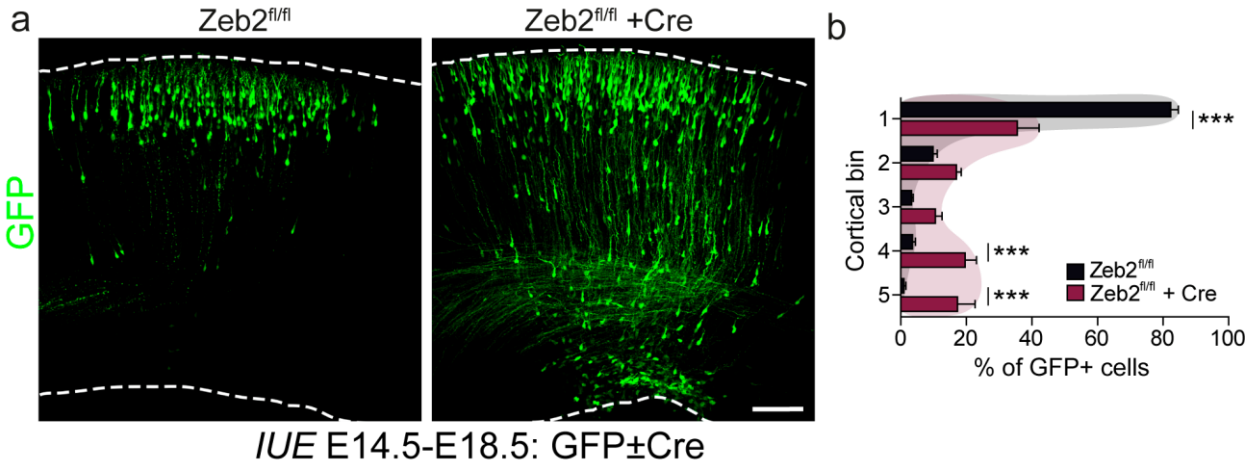

Fig. 6. **Zeb2 cell-intrinsically controls UL laminar positioning a.** Representative images of immunostained *Zeb2*$^{fl/fl}$ E18.5 cortices electroporated in the presence or absence of NeuroD1-Cre. The cortical area is marked with a dotted line. Scale bar = 100µm. **b.** Laminar distribution quantification of control and Zeb2-deficient neurons *in vivo.* N = 2308 cells, 11 *Zeb2*$^{fl/fl}$ animals and 1440 cells, 6 *Zeb2*$^{fl/fl}$ + *NeuroD1*^{Cre} animals. Two-way ANOVA with Bonferroni post hoc test. *** $p < 0.001$; ** $0.001 < p < 0.01$; * $0.01 < p < 0.05$. Results on the graph are represented as averages ± SEM. Adapted from Epifanova et al[52].

I next analysed the morphology of nonmigrated, migrating, and migrated neurons in the SVZ, IZ and CP respectively in control (*Zeb2*$^{fl/fl}$) and Zeb2-deficient (*Zeb2*$^{fl/fl}$ *NeuroD1*^{Cre}) animals at E18.5. Typically, new

born neurons in the SVZ have a multipolar morphology with multiple neuronal processes. The complexity of this stage can be assessed by the analysis of the amount of neurites. Neurons that have initiated migration (and are therefore found in the IZ) display a bipolar morphology (typically one axon and leading process). While neurons that have reached their final positions in the cortex (CP) retain the bipolar morphology and started to establish contact with the MZ to initiate the dendritic arborisation. Nonmigrated Zeb2-deficient neurons (SVZ) showed more complex morphology than control neurons which tended to show mostly bipolar morphology at E18.5. I observed an 5.267 ± 1.280 neurites per cell in SVZ in *Zeb2*$^{fl/fl}$ *NeuroD1*^{Cre} compared to 3.000 ± 1.069 in control *Zeb2*$^{fl/fl}$ condition (Fig. 7 a-b; p-value ***< 0.001). At the same time, Zeb2-deficient neurons which managed to travel to the IZ and CP showed a relatively normal bipolar morphology which indicates that Zeb2 does not influence the acquisition of a leading process or neuronal polarity during and post migration. The amount of neurites per cell in IZ did not show any difference between loss of Zeb2 and control conditions (2.267 ± 0.593 in *Zeb2*$^{fl/fl}$ versus 2.533 ± 0.639 in *Zeb2*$^{fl/fl}$ *NeuroD1*^{Cre}) (Fig. 7 a,c; > 0.05). However, Zeb2-deficient cells in the CP showed an increased number of neurites (3.800 ± 1.521) in comparison with the control condition (2.400 ± 0.632); (Fig. 7 a,d; <0.01). Interestingly, I also observed the formation of multiple axons (trailing processes) in migrated Zeb2-deficient neurons (in the case of multiple trailing processes 0.181 ± 0.024 in *Zeb2*$^{fl/fl}$ versus 0.495 ± 0.010 in *Zeb2*$^{fl/fl}$ *Nex*^{Cre}). This may correspond to the previously described axonal phenotype under loss of Zeb2 where Zeb2-deficient neurons showed abnormal neocortical axonal growth[45] (Fig. 7 a,e; p-value ***<0.001). Moreover, I show here that this specific axonal phenotype appears once Zeb2-deficient neurons acquire a bipolar morphology. The multiple axon phenotype was detected only when neurons have initiated radial migration (Fig. 7 a,f; p-value * < 0.05). *Zeb2*$^{fl/fl}$ *Nex*^{Cre} neurons showed the same ratio of multiple axonal processes to one axonal process in IZ compared to CP (Fig. 7 a,g; 0.451 ± 0.103 in IZ versus 0.5 ± 0.006 in CP in case of multiple axons; p-value > 0.05).

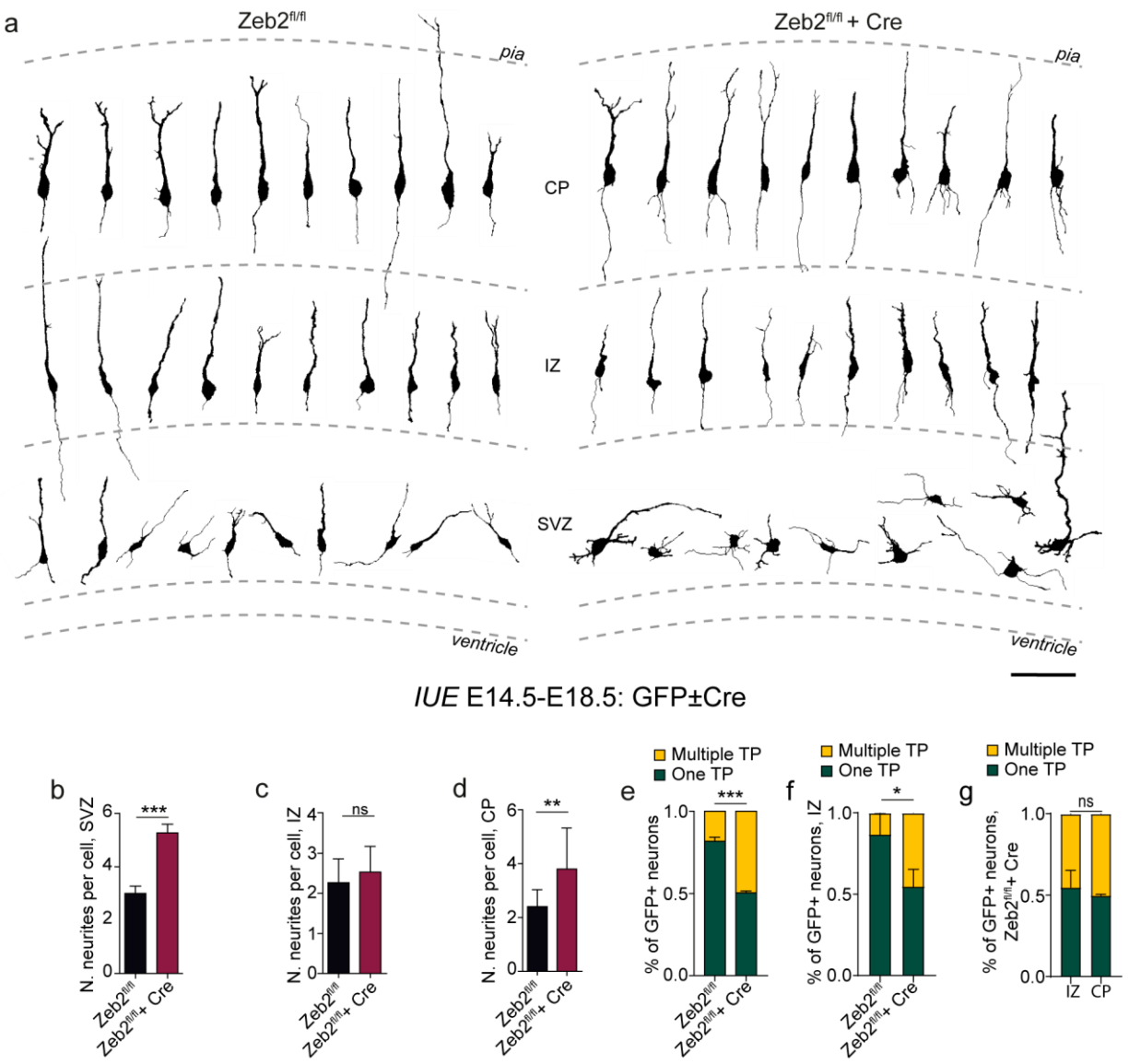

Fig. 7. Zeb2 defines the morphology of newborn neurons. a. Representative GFP-immunostaining-based traces of *Zeb2*$^{fl/fl}$ and Zeb2$^{fl/fl}$ NeuroD1^{Cre} neurons. Scale bar = 100µm. **b.** Average number of neurites per cell in SVZ of *Zeb2*$^{fl/fl}$ and *Zeb2*$^{fl/fl}$ *NeuroD1*^{Cre} neurons. N = 15 cells per condition. Unpaired *t* test **c.** Quantification of the number of neurites per cell in IZ of *Zeb2*$^{fl/fl}$ and *Zeb2*$^{fl/fl}$ *NeuroD1*^{Cre} neurons. N = cells 15 per condition. Mann-Whitney test. **d.** Average number of neurites per cell in CP of *Zeb2*$^{fl/fl}$ and *Zeb2*$^{fl/fl}$ *NeuroD1*^{Cre} neurons. N = 15 cells per condition. Mann-Whitney test. **e.** Quantification of the number of neurons with a single or multiple trailing processes (TP). N = 194 cells, 3 animals *Zeb2*$^{fl/fl}$ and 567 cells, 3 animals *Zeb2*$^{fl/fl}$*Nex*^{Cre}. Two-way ANOVA with Bonferroni post-hoc test. **f.** Quantification of the number of neurons with a single or multiple trailing processes in IZ. N = 12 cells, 3 animals

Zeb2$^{fl/fl}$ and 137 cells, 3 animals *Zeb2*$^{fl/fl}$*Nex*^{Cre}. Two-way ANOVA with Bonferroni post-hoc test. **g.** Quantification of the number of neurons with a single or multiple trailing processes in IZ versus CP in *Zeb2*$^{fl/fl}$*Nex*^{Cre}. N = 137cells, 3 animals IZ and 215 cells, 3 animals CP. Two-way ANOVA with Bonferroni post-hoc test. *** $p < 0.001$; ** $0.001 < p < 0.01$; * $0.01 < p < 0.05$. Results on graphs are represented as averages ± SD. Adapted from Epifanova et al[52].

Taking all these findings together, Zeb2 regulates positioning of UL neurons in the cortex without affecting neuronal cellular identity.

3.1.2. Zeb2 regulates the onset of radial migration and multipolar/bipolar transition of cortical neurons

One of the most important steps of cortex development is the radial migration of new born excitatory neurons[14]. The ability of neurons to reach their correct positions on time defines the future proper functioning of the brain. For a more in-depth analysis of Zeb2 function in neuronal radial migration in the developing cortex, I conducted live imaging of electroporated brain slices.

Prior to the experiment, I validated the fl-mCherry-Stop-fl-GFP reporter construct. I performed *IUE* of the fl-mCherry-Stop-fl-GFP together with Cre expression construct in E14.5 wild type embryos and analysed neuronal radial migration two days later. The validation showed no difference in laminar distribution of mCherry (Cre negative) and GFP (Cre positive) labelled cells (Fig. 8a-b).

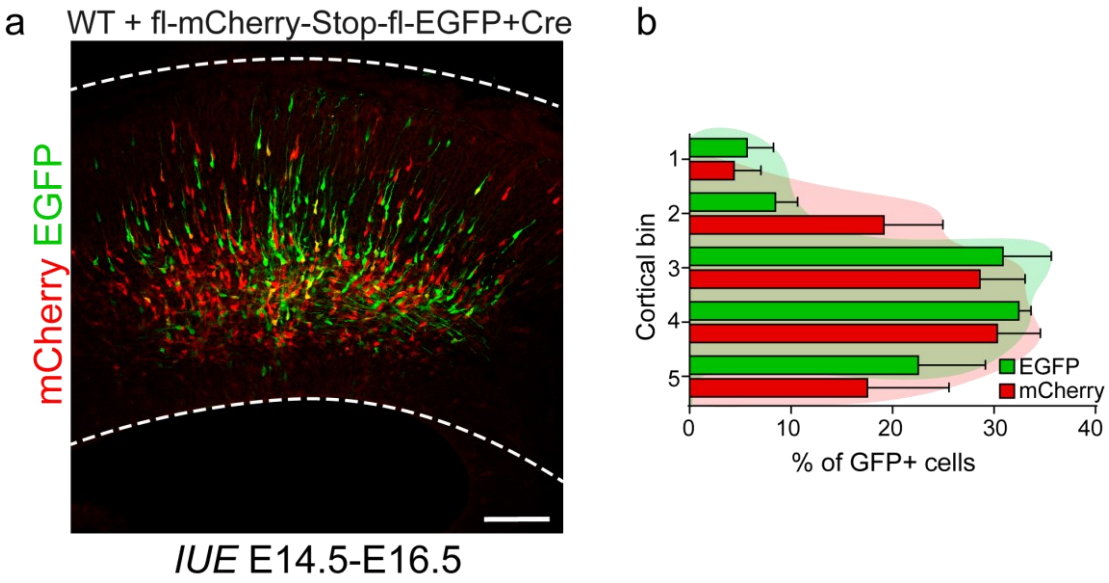

Fig. 8. Validation of fl-mCherry-Stop-fl-GFP reporter construct a. Representative image of immunostained *Zeb2*$^{fl/fl}$ E16.5 cortices electroporated in the presence of Cre expressing construct. Green cells are Cre positive and red cells are Cre negative. The cortical area is marked with a dotted line. Scale bar = 100μm. **b.** Laminar distribution quantification of mCherry+ or GFP+ (Cre expressing) neurons across five equally sized cortical bins *in vivo.* Bin 1 refers to the outermost cortical layer. N = 4 brains. Two-way ANOVA with Bonferroni post-hoc test. *** $p < 0.001$; ** $0.001 < p < 0.01$; * $0.01 < p < 0.05$. Results on the graph are represented as averages ± SEM. Adapted from Epifanova et al[52].

Then, I *in utero* co-electroporated a fl-mCherry-Stop-fl-GFP reporter construct and a limited amount of Cre expression construct into E14.5 *Zeb2*$^{fl/fl}$ and imaged brain slices the next day for over 50 hours. Due to the presence of Cre recombinase which recombines a pair of LoxP sequences flanking the mCherry-stop cassette of the reporter construct I generated two different populations of cells – control (mCherry labelled) and Zeb2-deficient (GFP labelled). This approach allowed analysis of the control and Zeb2-deficient neurons simultaneously in one brain (Fig. 9a). Loss of Zeb2 resulted in a significant delay in the initiation of migration of Zeb2-deficient neurons in comparison to control ones (Fig. 9 b-f). Thus, the proportion of nonmigrated Zeb2-deficient neurons during the imaging period increased when compared to control cells (37.8% in WT versus 52.9% in KO). The number of cells that initiated migration within the first

6 hours and in 6 to 12 hours range after the beginning of imaging decreased in KO compared to WT neurons (0-6 hours – 35.1% in WT versus 29% in KO; 6-12 hours - 18.9% in WT versus 29% in WT). The amount of KO cells that initiated migration in the 12-24 hours time period was increased in comparison to the WT condition (8.1% versus 20.6% respectively). Interestingly in KO neurons, an extra group of migrating cells was found. These are cells that initiated radial migration after 24 hours since the beginning of imaging (0% in WT and 20.6% in KO). To sum up, Zeb2-deficient neurons, which managed to initiate radial migration, started the migration considerably later than the control wild type neurons.

Next, to find a possible reason for such a dramatic delay in migration upon loss of Zeb2, I analysed the speed of migration. The migratory speed of Zeb2-deficient neurons was changed only slightly compared to the speed of control neurons, which does not explain such vast migration delay (11.1 ± 3.54 μm per hour in WT versus 8.19 ± 3.02 μm per hour in KO; Fig. 9g).

At the same time, I observed a disturbed multipolar-bipolar transition under the loss of Zeb2 (Fig. 9h). The proportion of Zeb2-deficient cells in the SVZ that had a multipolar morphology was considerably increased when compared to control cells. This may correspond to the observed migratory delay.

Then, I asked whether the behaviour of new born neurons was changed during the multipolar stage – the phase preceding neuronal locomotion. Neurons, which undergo the multipolar stage of radial migration, are typically characterised by small motions with frequently changing direction and rate of motility. This type of motility is called here tangential motility. Under close inspection of the multipolar stage of Zeb2-deficient cells, I found that cells that remained in the multipolar stage had disturbed tangential spread. The overall tangential spread as well as the speed of tangential movements of Zeb2-deficient cells were reduced when compared to WT (Fig. 9 i-j). The spread of tangential movements in the case of $Zeb2^{fl/fl}$ was 9.288 ± 4.707 and 4.333 ± 1.605 in the case of $Zeb2^{fl/fl}Nex^{Cre}$ neurons. The speed of tangential motility was two-fold less in Zeb2-deficient neurons as compared to the wild type neurons (Fig. 9k; 2.051 ± 0.649 $Zeb2^{fl/fl}$ versus 1.216 ± 0.376 $Zeb2^{fl/fl}Nex^{Cre}$; p-value *** <0.001).

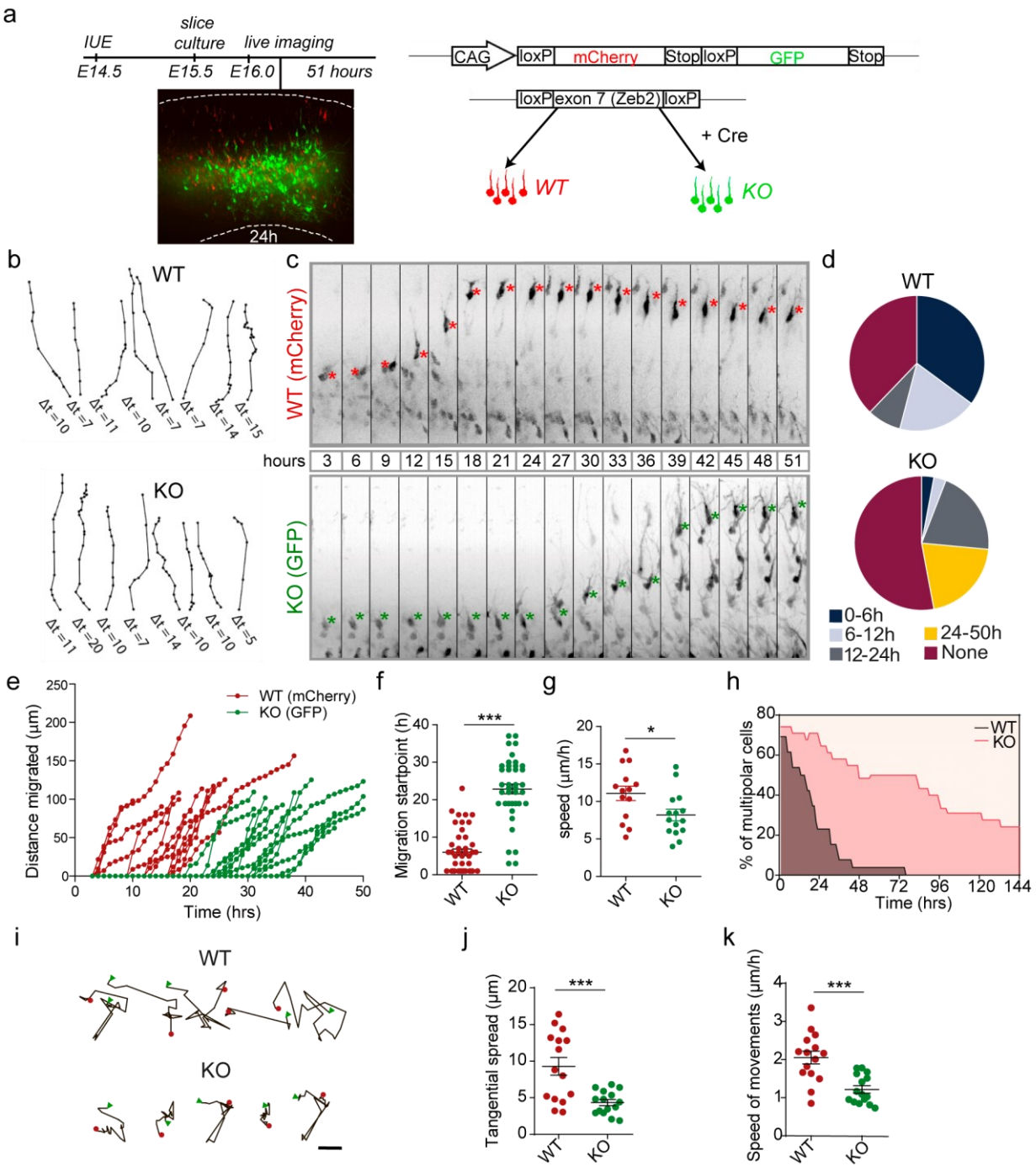

Fig. 9. Zeb2 controls the initiation of neuronal radial migration. a. Experimental setup together with an overview picture of migrating wildtype (mCherry+) and Zeb2-deficient (GFP+) neurons in slice culture at 24 hours time point. Cortical area is marked with a dotted line. **b.** Representative traces with 1 hour interval resolution of migrating wildtype (mCherry+) and Zeb2-deficient (GFP+) neurons in slice culture. **c.** Representative images of migrating wildtype (mCherry+) and Zeb2-deficient (GFP+) neurons over a total imaging period of 51 hours.

Representative pictures are shown with 3 hours difference. Cell soma is marked with asterisks. **d.** Distribution of wildtype (mCherry+) and Zeb2-deficient (GFP+) neurons according to the migration start time point. N = 37 mCherry+ and 34 GFP+ cells. **e.** Distance travelled of migrated wildtype (mCherry+) and Zeb2-deficient (GFP+) neurons over during the imaged period. **f.** Quantification of migration start point of wildtype (mCherry+) and Zeb2-deficient (GFP+) neurons initiated migration. N = 46 mCherry+ and 41 GFP+. Mann-Whitney test. **g.** Speed quantification of migrating wildtype (mCherry+) and Zeb2-deficient (GFP+) neurons. N = 46 mCherry+ and 41 GFP+ cells. Unpaired *t* test. **h.** Distribution of multipolar wildtype (mCherry+) and Zeb2-deficient (GFP+) cells over time. **i.** Representative traces of tangential movements of WT and Zeb2-deficient cells located in SVZ within the first 20 hours of analysis. The start point and the endpoint are marked with green and red signs respectively. Scale bar = 5μm. **j.** Quantification of tangential spread of WT and Zeb2-deficient neurons. N = 15 cells per condition. Unpaired *t* test. **k.** Quantification of the speed of tangential motility of WT and Zeb-2 deficient cells. N = 15 cells per condition. Unpaired *t* test. *** $p < 0.001$; ** $0.001 < p < 0.01$; * $0.01 < p < 0.05$. Results on the graph are represented as averages ± SD. Adapted from Epifanova et al[52].

In addition, during the multipolar phase of migration, neurons actively extend and retract neuronal processes. To examine this morphology of neurons in the SVZ more closely, I *in utero* electroporated $Zeb2^{fl/fl}$ and $Zeb2^{fl/fl}Nex^{Cre}$ embryos at E15.5 with a GFP expression construct and analysed the brains 36 hours later. I counted the number of primary neurites of neurons located in SVZ. $Zeb2^{fl/fl}Nex^{Cre}$ cells showed an increased number of primary neurites in comparison to the control $Zeb2^{fl/fl}$ cells (Fig.10 a-b; 5.35 ± 1.496 $Zeb2^{fl/fl}$ versus 7.8 ± 1.989 $Zeb2^{fl/fl}$ Nex^{Cre}; unpaired *t* test; p-value *** <0.001).

Together these data suggest a critical function of Zeb2 in multipolar-bipolar transition and initiation of radial migration of UL cortical neurons.

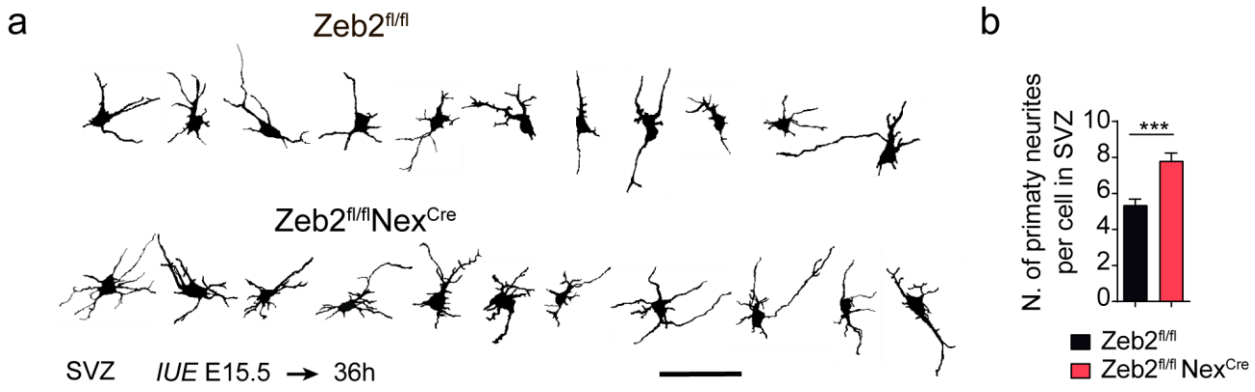

Fig. 10. Zeb2 controls neuronal multipolar stage. a. Representative images of *in utero* electroporated with GFP expressing construct *Zeb2*$^{fl/f}$ and *Zeb2*$^{fl/fl}$*Nex*^{Cre} animals at E15.5. The neuronal morphology was analysed 36 hours later for cells located in SVZ. Scale bar = 50µm. **b.** Quantification of the number of primary neurites per cell. N = 20 cells and 3 brains per condition. Unpaired *t* test. *** $p < 0.001$; ** $0.001 < p < 0.01$; * $0.01 < p < 0.05$. Results on the graph are represented as averages ± SD. Adapted from Epifanova et al[52].

3.1.3. Zeb2 controls the initial neuronal polarity *in vitro*

The correct polarity of early born neurons defines the future function and neuronal connectivity[3]. New born neurons go through several morphological stages: multipolar stage and bipolar stage (stage of a polarised cell with a defined trailing and leading process)[11]. These morphological states are tightly associated with the position of the centrosome and Golgi complex positions in the cell. Typically in young immature neurons, the centrosome, Golgi complex and endosomes are located together at the base of the first emerging neurite[59,60].

To examine neuronal polarity at closer range, I *in utero* electroporated a GFP-expression construct into the lateral ventricles of E15.5 *Zeb2*$^{fl/fl}$ and *Zeb2*$^{fl/fl}$*Nex*^{Cre} animals and dissociate the electroporated cortices. Dissociated neurons were plated onto laminin/poly-L-lysine covered plates and fixed 3 days later (DIV3). Neurons were stained with anti-GFP, anti- CDK5 Regulatory Subunit Associated Protein 2 (CDK5Rap2; a centrosome marker) and anti-Golgin subfamily A member 2 (GM130; a Golgi marker) antibodies. Then I analysed the position of the centrosome and Golgi complex. Neurons were categorized into 3 groups: group 1

has the centrosome and Golgi complex at the base of the longest neurite; group 2 has centrosome and Golgi complex at the base of the not longest neurite and in group 3 the centrosome and Golgi are in a random position in the cell and do not fit the criteria of the first and the second group. In wild type control neurons, the centrosome and Golgi complex typically face the longest neurite. In case of Zeb2-deficient neurons, the centrosome and Golgi complex most of the times did not face the longest neurite (62.1% ± 5.358 *Zeb2*$^{fl/fl}$ versus 23.54% ± 7.097 *Zeb2*$^{fl/fl}$ *Nex*^{Cre} for the longest neurite and 32.7% ± 5.143 *Zeb2*$^{fl/fl}$ versus 64.91% ± 7.259 *Zeb2*$^{fl/fl}$ *Nex*^{Cre} for the not longest neurite; p-value *** <0.001 and ** <0.01 respectively; Fig. 11 a-b).

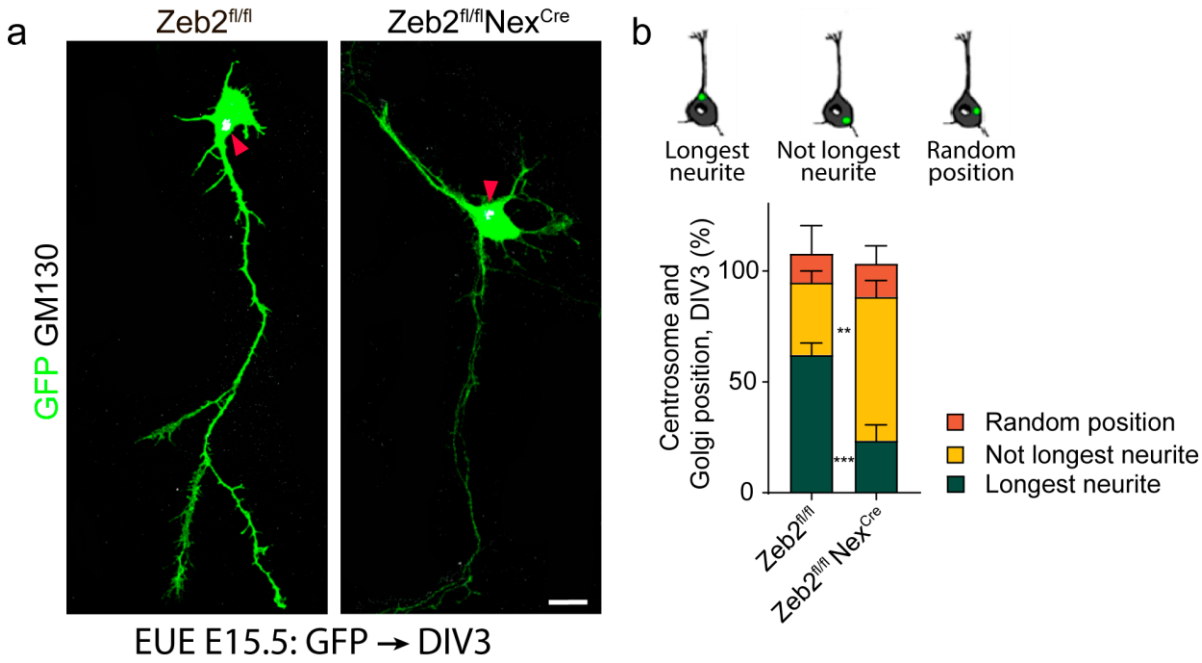

Fig. 11. Zeb2 regulates centrosome and Golgi complex position in young neurons. a. Representative images of *in utero* electroporated with GFP expressing construct *Zeb2*$^{fl/fl}$ and *Zeb2*$^{fl/fl}$*Nex*^{Cre} neurons at E15.5. Neurons were analysed at DIV3 and immunostained with anti-GFP, anti-CDK5Rap2 (centrosome marker) and anti-GM130 (Golgi marker) antibodies. The centrosome and Golgi position is marked with a red triangle. **b.** Quantification of centrosome and Golgi position. The centrosome and Golgi position was categorised according to its position either in front of the longest neurite, not the longest neurite or random position in the cell. Scale bar = 25µm. N = 39 cells, 3 brains *Zeb2*$^{fl/fl}$ and 102 cells, 4 brains *Zeb2*$^{fl/fl}$*Nex*^{Cre}. Unpaired *t* test. *** p < 0.001; **

0.001 < p < 0.01; * 0.01 < p < 0.05. Results on the graph are represented as averages ± SD.

It is known that around DIV3-4 cultured neurons acquire neuronal polarity and form clearly defined axon, apical dendrite and some basal dendrites[61]. Taking this into account I can assume based on the neuronal morphology, that “the longest neurite” will likely become the future axon and the “not the longest neurites” will form either apical or basal dendrites neurites. This suggests that the establishment of neuronal polarity of Zeb2-deficient neurons *in vitro* was changed in comparison to the wild type control neurons.

3.1.4. Zeb2 regulates neuronal cell-to-cell and cell-to-extracellular matrix adhesion

Mass spectrometry analysis of Zeb2-deficient neurons conducted by others in the group showed an increase in the levels of different adhesion molecules at the plasma membrane. Change in plasma membrane levels of different adhesion molecules suggests that loss of Zeb2 may alter the adhesion of neurons. To investigate this idea further, I dissociated E15.5 control (*Zeb2*$^{fl/fl}$) and Zeb2-deficient (*Zeb2*$^{fl/fl}$ *Nex*^{Cre}) cortices in the absence of proteases in order to obtain suspensions of primary cortical neurons. Single cell suspensions of these neurons were either used to examine cell-to-cell adhesion in aggregation assay or to examine cell-to-extracellular matrix adhesion in an adhesion assay. These two approaches were conducted simultaneously. At first, I allowed neurons to aggregate under gentle shaking for 60 minutes. Neuron aggregates were imaged at 0, 30 and 60 minutes time points. The average maximal diameter of cell aggregates was assessed and normalized against the average size of control aggregates which were shaked at the same time. Zeb2-deficient neurons formed bigger aggregates much faster than the wild type control (Fig. 12 a-b). Already at the 30 minutes time point *Zeb2*$^{fl/fl}$ *Nex*^{Cre} formed aggregates that are three times larger than those made by *Zeb2*$^{fl/fl}$ cells (0.946 ± 0.124 *Zeb2*$^{fl/fl}$ versus 3.709 ± 0.752 *Zeb2*$^{fl/fl}$ *Nex*^{Cre} at 30 minutes time point; p-

value ** <0.01). This fact points out that under loss of Zeb2, neurons acquire higher cell-to-cell adhesion.

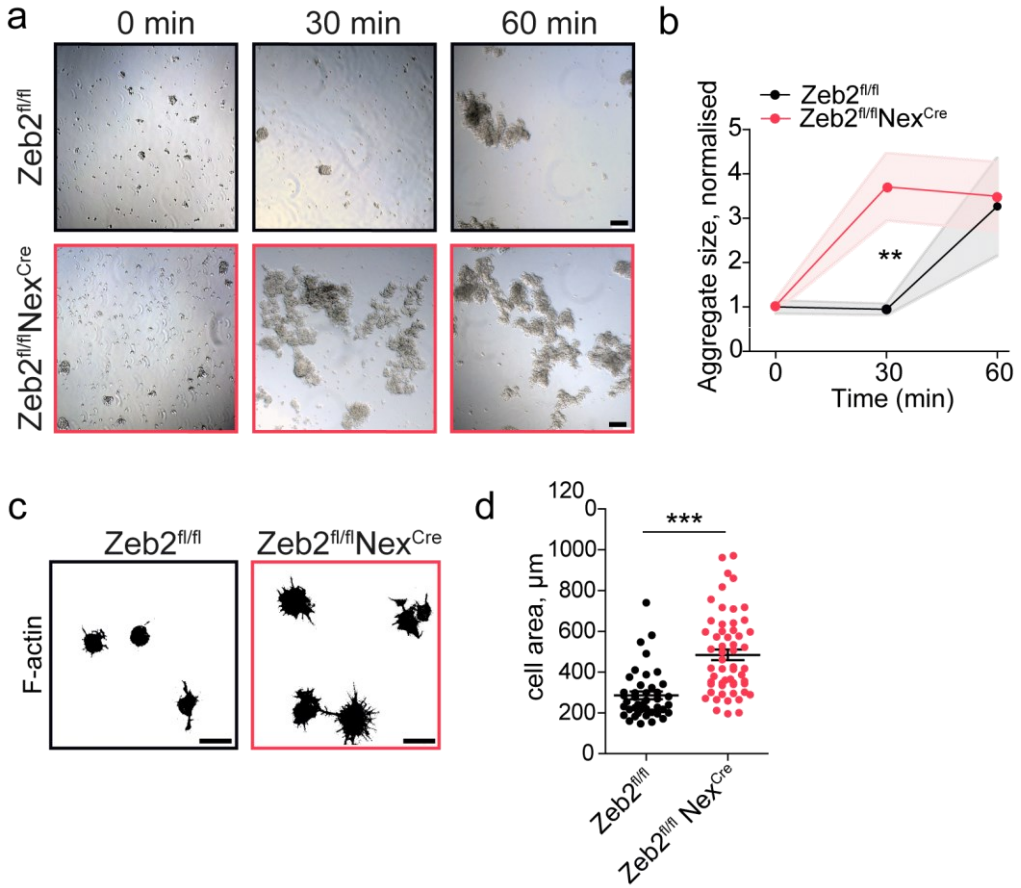

Fig. 12. Zeb2 suppresses neuronal adhesion to other cells and the extracellular matrix. a-b. Zeb2 inhibits cell aggregation. Aggregation assay. **a.** Representative images of primary cortical neurons in single cell suspensions from littermate E15.5 control (*Zeb2*$^{fl/fl}$) and Zeb2-deficient (*Zeb2*$^{fl/fl}$ *Nex*^{Cre}) animals. Neurons were allowed to aggregate under gentle shaking and imaged at 0, 30 and 60 minutes. Scale bar = 100µm. **b.** Quantification of cell aggregate size in cell aggregation assay. Average maximal diameter of cell aggregates was normalised to the average size of control aggregates at the 0 minutes timepoint. N = 15, 10, 7 *Zeb2*$^{fl/fl}$ and 12, 12, 15 *Zeb2*$^{fl/fl}$ *Nex*^{Cre} cell aggregates at 0, 30 or 60 min time points respectively, 3 animals per condition. One-way ANOVA with Kruskal-Wallis test. **c-d.** Zeb2 suppresses adhesion to the extracellular matrix. Adhesion assay. **c.** Representative images of primary cortical neurons in single cell suspensions from littermate E15.5 control (*Zeb2*$^{fl/fl}$) and Zeb2-deficient (*Zeb2*$^{fl/fl}$ *Nex*^{Cre}) animals. Neurons were allowed to attach to laminin and poly-L-lysine coated surfaces for 2 hours, fixed, stained with phalloidin stain (marks F-actin) and imaged.

Scale bar = 15µm. **d.** Quantification of lamellipodial spreading in cell adhesion assay. N= 42 *Zeb2*$^{fl/fl}$ and 56 *Zeb2*$^{fl/fl}$ *Nex*^{Cre} cells, 3 animals per condition. Mann-Whitney test. *** $p < 0.001$; ** $0.001 < p < 0.01$; * $0.01 < p < 0.05$. Results on the graph are represented as averages ± SD. Adapted from Epifanova et al[52].

At the same time, I conducted an adhesion assay where I allowed dissociated neurons to adhere to a laminin/poly-L-lysine rich substrate and then analysed the attachment to this extracellular matrix 2 hours later. Fixed cells were stained with phalloidin which marks F-actin and lamellipodial spreading was analysed. The cell area of each cell was measured in ImageJ. The Zeb2-deficient neurons showed larger cell spreading on the extracellular matrix then control neurons (Fig. 12 c-d; 319 ± 245µm *Zeb2*$^{fl/fl}$ versus 485 ± 197µm *Zeb2*$^{fl/fl}$ *Nex*^{Cre}; p-value *** <0.001). This can indicate increased cellular adhesion to the extracellular matrix in the absence of Zeb2. This is consistent with the observed the increased fraction of Integrins present at the plasma membrane of Zeb2-deficient neurons observed in the mass spectrometry analysis. Integrins are known to regulate mostly cell-to-extracellular matrix adhesion.

3.1.5. Zeb2 laminar displacement is restored by Nrp1 downregulation

In order to find potential downstream targets of Zeb2 which can rescue the described phenotype, previously published microarray data[40] was cross-referenced with the deep sequencing and mass spectrometry data produced in the group. Thus, Nrp1 was identified as one of the potential downstream targets of the Zeb2. *In situ* hybridization and immunohistochemistry carried out by others in the group confirmed the elevated expression of Nrp1 upon loss of Zeb2.

I then hypothesised that Nrp1 may participate in the regulation of neuronal migration downstream of Zeb2. Prior to the main experiment, I assessed the efficiency of Nrp1 knockdown using the western blot technique. Murine Nrp1 (muNrp1) together with either shNrp1 or shScr and empty vector were transfected into HEK293T cells. Transfected cells were lysed two days later and analysed for Nrp1 expression using

antibodies against Nrp1 and β-tubulin for loading control (Fig. 13). Western blot analysis showed that in case of simultaneous expression of muNrp1 and either shScr1 or shScr2 I can detect a strong Nrp1 signal. In the case of co-expression of muNrp1 and shNrp1, I could detect little muNrp1 expression although the Tubulin loading control showed no difference. This showed that shNrp1 effectively decreased Nrp1 expression.

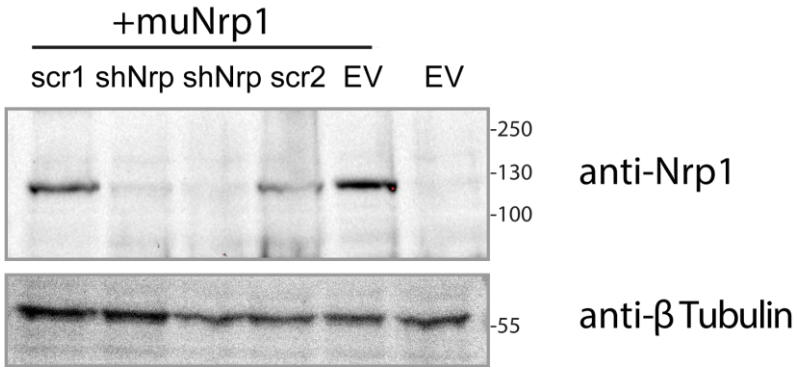

Fig. 13. Validation of the shRNA against Nrp1. HEK293T cells were transfected with murine Nrp1 (muNrp1) and either shRNA against Nrp1 (shNrp), two scrambled control shRNAs (shScr1 and shScr2) or the empty vector (EV) in the indicated combinations. Cells were lysed 2 days after transfection. Lysates were analysed for Nrp1 expression using western blotting against Nrp1 and β tubulin (used as loading control). Adapted from Epifanova et al[52].

To test whether Nrp1 downregulation can rescue the defective neuronal radial migration of Zeb2-deficient neurons I conducted *IUE* of either shRNA against Nrp1 (shNrp1) or control scrambled shRNA (shScr) into E14.5 *Zeb2*$^{fl/fl}$ animals. The mosaic Zeb2 excision was induced by the electroporation of a Cre expression construct. The electroporated animals were fixed, stained with anti-GFP antibody and DRAQ5 and analysed at E18.5. The neuronal laminar distribution was assessed by dividing the analysed cortices into 5 equal bins where bin 1 and bin 5 correspond to the outermost and the innermost areas respectively (Fig. 14 a-b). In the wildtype control condition, most of the neurons migrated to the top of the CP (bin 1) while Zeb2-deficient neurons were abnormally distributed in the CP. The condition with downregulation of Nrp1 in Zeb2-deficient neurons (*Zeb2*$^{fl/fl}$ + cre + shNrp1) showed a

distribution of neurons similar to the control wild type condition (*Zeb2*$^{fl/fl}$ + shScr). Downregulation of Nrp1 therefore dramatically improved the distribution of neurons upon Zeb2 knockdown (*Zeb2*$^{fl/fl}$ + Cre + shScr versus *Zeb2*$^{fl/fl}$ + Cre + shNrp1, bin 1 p-value *** <0.001, bin 2, 4 p-value * < 0.05; *Zeb2*$^{fl/fl}$ + shScr versus *Zeb2*$^{fl/fl}$ + Cre + shNrp1 bin 1 *** <0.001).

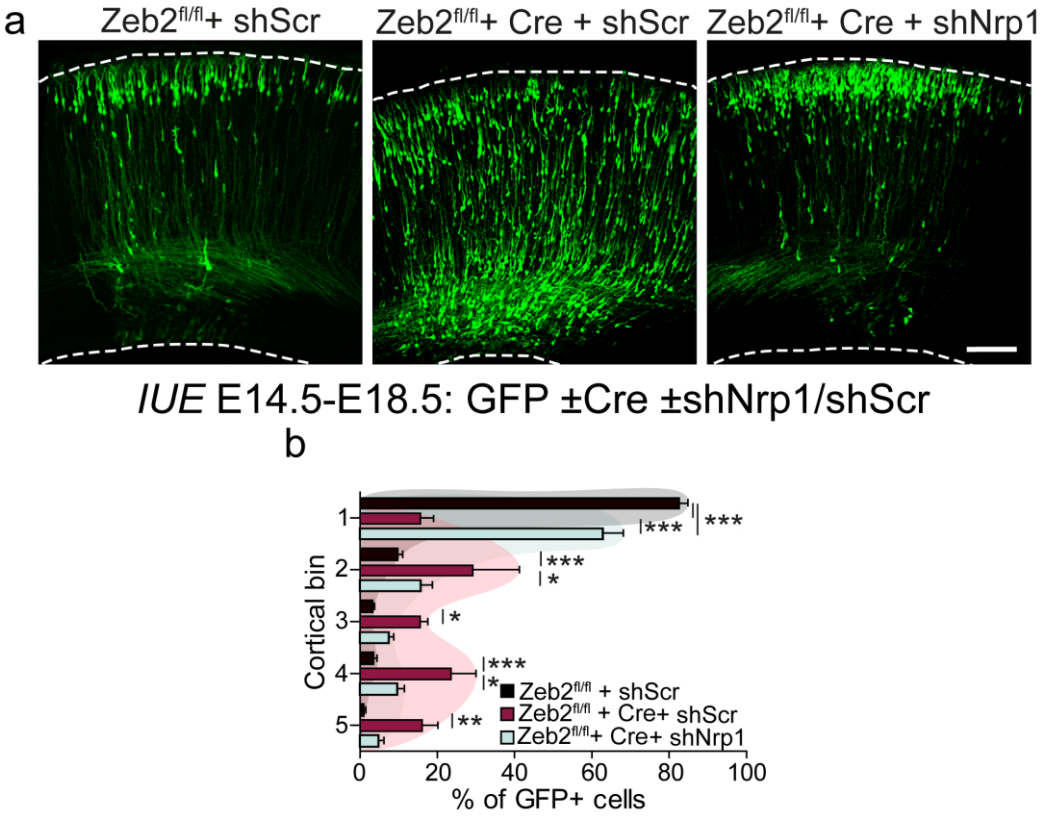

Fig. 14. Zeb2 controls neuronal laminar distribution through the repression of Nrp1. a. Representative images of immunostained *Zeb2*$^{fl/fl}$ E18.5 cortices electroporated at E14.5 in the presence or absence of Cre expressing construct and either shScr (control scrambled shRNA) or shNrp1 (shRNA against Nrp1). The cortical area is marked with a dotted line. Scale bar = 100µm. **b.** Quantification of the laminar position of GFP+ neurons *in vivo*. N = 11 *Zeb2*$^{fl/fl}$ + shScr, 5 *Zeb2*$^{fl/fl}$ + shScr and Cre, 7 *Zeb2*$^{fl/fl}$ + cre + shNrp1 animals. Two-way ANOVA with Bonferroni post-hoc test. *** $p < 0.001$; ** $0.001 < p < 0.01$; * $0.01 < p < 0.05$. Results on the graph are represented as averages ± SEM. Adapted from Epifanova et al[52].

3.1.6. Nrp1 overexpression disturbs laminar positioning of cortical neurons

I then asked whether increased expression of Nrp1 is enough to induce an impairment of the radial migration in wild type mice. To test this, I performed *IUE* of either a Nrp1-expression construct that allows GFP co-expression driven by an IRES or the same construct only with IRES-GFP at E14.5. The tissue was fixed, stained with anti-GFP antibody and DRAQ5, and analysed at E18.5. Analysis of the laminar distribution of electroporated GFP+ cells showed that in the wild type control condition neurons occupied mostly the outermost area of the cortex. In contrast, the neurons with overexpression of Nrp1 were placed throughout the cortex (Fig. 15 a-b, WT versus WT+Nrp1, bin 1 p-value *** <0.001, bin 3, 4 p-value * < 0.05).

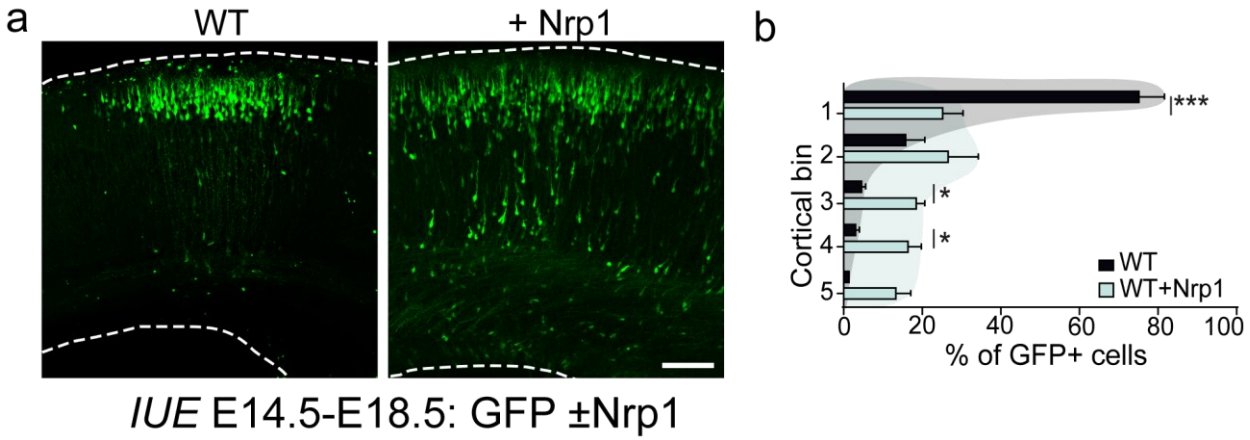

Fig. 15. Nrp1 overexpression disturbs laminar distribution of UL cortical neurons. a. Representative images of *in utero* electroporated at E14.5 wild type cortices with either construct with IRES driven GFP expression, or the same construct expressing full-length Nrp1 under the CAG promoter. Cortices were analysed at E18.5. Scale bar = 100μm. **b.** Quantification of the laminar distribution of GFP+ neurons *in vivo.* N = 7 control WT and 7 WT + Nrp1 animals. Two-way ANOVA with Bonferroni post-hoc test. *** $p < 0.001$; ** $0.001 < p < 0.01$; * $0.01 < p < 0.05$. Results on the graph are represented as averages ± SEM. Adapted from Epifanova et al[52].

Thus, Nrp1 overexpression in wild type mouse embryos led to abnormal distribution of UL neurons in a similar manner as loss of Zeb2.

3.1.7. Nrp1 downregulation rescues the disturbed initiation of radial migration in Zeb2 mutant

To understand how Nrp1 affects radial migration I used live imaging of brain slices as before. I *in utero* electroporated E14.5 *Zeb2*$^{fl/fl}$ embryos with GFP expression construct in the presence or absence of Cre expression construct (pCAG-Cre) and either shScr or shNrp1 (Fig. 16a). A day later E15.5 embryos were isolated and fresh brain slices were prepared and imaged for 50 hours.

Analysis of time-lapse videos showed that wild type control neurons initiate radial migration much earlier than the Zeb2-deficient neurons. Meanwhile, Zeb2-deficient neurons electroporated with shNrp1 (KO+shNrp1) mostly initiated their migration earlier than Zeb2-deficient neurons (KO+shScr) and to a similar extent as the control wild type neurons (WT+shScr) (Fig. 16b). Thus, the proportion of KO+shNrp1 neurons that do not migrate during the imaging period was decreased when compared to Zeb2-deficient neurons KO+shScr and was comparable to the levels in control wild type condition WT+shScr (Fig. 16c; 16% of nonmigrated cells in WT+shScr, 41% in KO+shScr and 12% in KO+shNrp1; WT+shScr versus KO+shScr p value ** <0.01; KO+shScr versus KO+shNrp1 p value ** <0.01 and WT+shScr versus KO+shNrp1; p value >0.05). The number of cells which initiated migration within the first 6 hours and in 6 to 12 hours range after the beginning of imaging also increased in KO+shNrp1 compared to KO+shScr (0-6 hours - 74% in WT+shScr, 7% in KO+shScr, 34% in KO+shNrp1, WT+shScr versus KO+shScr p value *** <0.001; KO+shScr versus KO+shNrp1 p value ** <0.01 and WT+shScr versus KO+shNrp1 p value *** <0.001; 6-12 hours - 9% in WT+shScr, 9% in KO+shScr, 14% in KO+shNrp1; p value >0.05). The amount of KO+shNrp1 cells which initiated migration in the 12-24 hour time period was increased in comparison to the KO+shScr condition (0% in WT+shScr, 18% in KO+shScr, 29% in KO+shNrp1, WT+shScr versus KO+shScr p value * <0.05; KO+shScr versus KO+shNrp1 p value >0.05 and WT+shScr versus KO+shNrp1; p value *** <0.001). The group of cells which initiated migration after 24 hours

since the beginning of experiment and was presented in the KO+shScr condition but not in the WT+shScr condition still could be find in KO+shNrp1 but in a less proportion (0% in WT+shScr, 22% in KO+shScr, 9% in KO+shNrp1, WT+shScr versus KO+shScr p value ** <0.01; KO+shScr versus KO+shNrp1 p value >0.05 and WT+shScr versus KO+shNrp1; p value >0.05).

Taking into consideration the previously observed disturbance in the multipolar phase of Zeb2-deficient neurons I asked whether Nrp1 controls the multipolar stage of migration. The disturbed multipolar stage of migration of Zeb2-deficient neurons was partially rescued by Nrp1 downregulation (Fig. 16d). At the same time, downregulation of Nrp1 did not disturb the migratory speed of Zeb2-deficient neurons (Fig. 16e; 8.492 ± 4.272μm per hour in WT+shScr, 4.249 ± 2.108μm per hour in KO+shScr, 5.899 ± 3.662μm per hour in KO+shNrp1; WT+shScr versus WT+shScr p-value * <0.05; WT+shScr versus KO+shScr and KO+shScr versus KO+shNrp1; p-value >0.05).

Altogether, these data show that downregulation of Nrp1 restores the delayed initiation of radial migration of Zeb2-deficient neurons through regulation of multipolar to bipolar transition downstream of Zeb2.

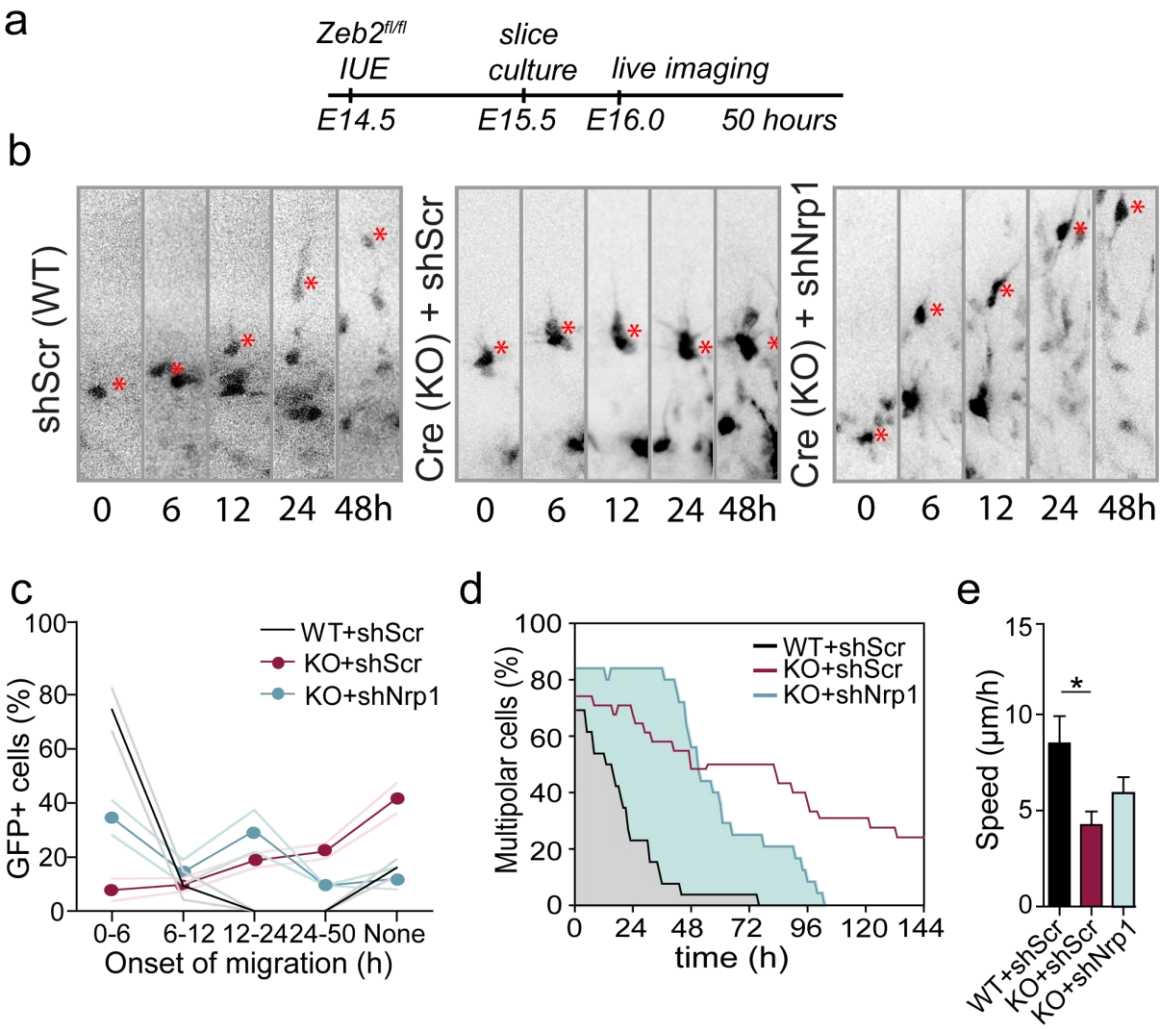

Fig. 16. Nrp1 controls the initiation of neuronal radial migration downstream of Zeb2. a. Experimental setup**.** Littermate *Zeb2*$^{fl/fl}$ animals were electroporated in utero at E14.5 with GFP expressing construct and either shRNA (WT + shScr), shScr and Cre expressing construct (KO + shScr) or shNrp1 and Cre expressing construct (KO + shNrp1) as indicated. Live brain slices were prepared at E15.5 and imaged 6 hours later during 50 hours time period. **b.** Representative images of migrating GFP labelled cells. Representative pictures are shown at 0, 6, 12, 24 and 48 hours time points. Cell soma is marked with red asterisks. **c.** Percentage of GFP+ cells that started radial migration during the 0-6, 6-12, 12-24 and 24-50 time periods. "None" refers to the cells that do not initiate migration during the imaged period. N = 3 animals per condition. Two-way ANOVA with Bonferroni post-hoc test. **d.** Quantification of the proportion of multipolar GFP+ cells at 0, 24, 48, 72, 96, 120 and 144 hours time points. N = 29 cells for WT, 33 cells for KO and 25 cells KO + shNrp1, 3 brains per condition. **e**. Quantification of the migration speed of cells after initiation of migration. N = 9 WT + shScr, 9 KO + shScr, 19

KO + shNrp1 cells, 3 brains per condition. One-way ANOVA (Kruskal-Wallis) with Dunn´s multiple comparison test. *** $p < 0.001$; ** $0.001 < p < 0.01$; * $0.01 < p < 0.05$. Results on the graph are represented as averages ± SD. Adapted from Epifanova et al[52].

3.1.8. Nrp1 does not regulate centrosome and Golgi complex position in young neurons downstream of Zeb2

To investigate whether Nrp1 can rescue the early neuronal polarity defect which I described in Zeb2-deficient neurons (Fig. 11), I conducted *in utero* electroporation of a GFP-expression construct and either shScr or shNrp1 into the lateral ventricles of E15.5 *Zeb2*$^{fl/fl}$ and *Zeb2*$^{fl/fl}$*Nex*^{Cre} animals. I then dissociated the electroporated cortices and plated the dissociated neurons onto laminin/poly-L-lysine covered plates and fixed them 3 days later (DIV3). Neurons were stained with anti-GFP, anti-CDK5Rap2 (centrosome marker) and anti-GM130 (Golgi marker) antibodies. Then the analysis of the centrosome and Golgi complex position was conducted as described earlier (Fig. 11). In case of Zeb2-deficient neurons with downregulation of Nrp1 (*Zeb2*$^{fl/fl}$ *Nex*^{Cre} + shNrp1), the centrosome and Golgi complex were most times observed to face a neurite that was not the longest one, similar to the observations in *Zeb2*$^{fl/fl}$ *Nex*^{Cre} neurons. Thus, Nrp1 does not control the initial polarity establishment of young neurons (62.1% ± 5.358 *Zeb2*$^{fl/fl}$, 23.54% ± 7.097 *Zeb2*$^{fl/fl}$ *Nex*^{Cre} and 32.5% ± 6.455 *Zeb2*$^{fl/fl}$ *Nex*^{Cre} +shNrp1 for the longest neurite; 32.7% ± 5.143 *Zeb2*$^{fl/fl}$, 64.91% ± 7.259 *Zeb2*$^{fl/fl}$ *Nex*^{Cre} and 54.06% ± 9.540 *Zeb2*$^{fl/fl}$ *Nex*^{Cre} +shNrp1 for the not longest neurite; p-value *Zeb2*$^{fl/fl}$ versus *Zeb2*$^{fl/fl}$ *Nex*^{Cre} +shNrp1 *** <0.001 and *Zeb2*$^{fl/fl}$ *Nex*^{Cre} versus *Zeb2*$^{fl/fl}$ *Nex*^{Cre} +shNrp1 >0.05 for the longest neurite; *Zeb2*$^{fl/fl}$ vs *Zeb2*$^{fl/fl}$ *Nex*^{Cre} +shNrp1 ** <0.01 and *Zeb2*$^{fl/fl}$ *Nex*^{Cre} vs *Zeb2*$^{fl/fl}$ *Nex*^{Cre} +shNrp1 >0.05 for the not longest neurite; Fig. 17 a-b).

Together, these data showed that Nrp1 does not control the position of centrosome and Golgi complex in young neurons and thus does not control the establishment of polarity in young immature neurons.

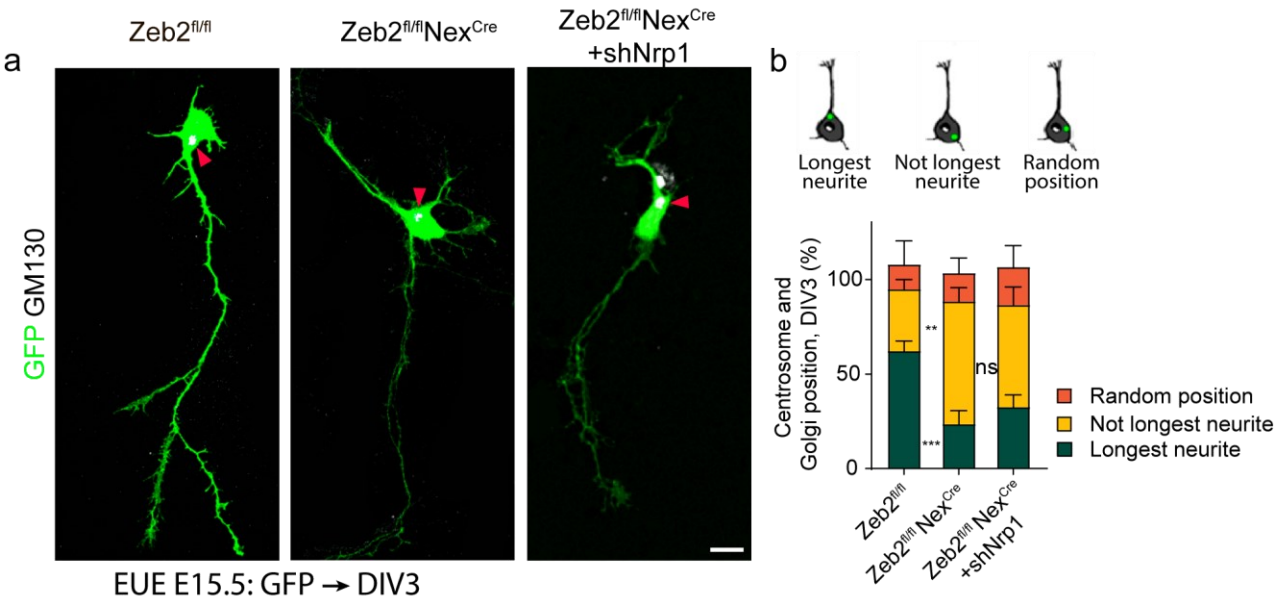

Fig. 17. Nrp1 does not regulate centrosome and Golgi complex position in young neurons downstream of Zeb2. a. Representative images of *in utero* electroporated with GFP expressing construct or either shScr or shNrp1 *Zeb2*$^{fl/fl}$ and *Zeb2*$^{fl/fl}$*Nex*^{Cre} and *Zeb2*$^{fl/fl}$*Nex*^{Cre} neurons at E15.5. Neurons were analysed at DIV3 and immunostained with anti-GFP, anti-CDK5Rap2 (centrosome marker) and anti-GM130 (Golgi marker) antibodies. The centrosome and Golgi position is marked with a red triangle. **b.** Quantification of centrosome and Golgi position. The centrosome and Golgi position was categorised according to its position either in front of the longest neurite, not the longest neurite or random position in the cell. Scale bar = 25μm. N = 39 cells, 3 brains *Zeb2*$^{fl/fl}$; 102 cells, 4 brains *Zeb2*$^{fl/fl}$*Nex*^{Cre} and 73 cells, 5 brains *Zeb2*$^{fl/fl}$*Nex*^{Cre} + shNrp1. Two-way ANOVA with Bonferroni post-hoc test. *** $p < 0.001$; ** $0.001 < p < 0.01$; * $0.01 < p < 0.05$. Results on the graph are represented as averages ± SD.

3.1.9. Zeb2 directly binds the Nrp1 promoter region

My next question was whether Nrp1 could be a direct downstream target of Zeb2 or if it was only a part of the downstream signalling pathway.

Prior to the experiment using the UCSC genome browser, FANTOM5 database (https://fantom.gsc.riken.jp/5/) I analysed the Nrp1 gene locus in order to find the potential promoter region of the Nrp1 gene. Promoter regions are typically characterised by the abundance of CpG islands,

different histone chemical modifications and DNase hypersensitivity clusters. CpG islands (or CG sites) consist of repetitive cytosine and guanine nucleotides pairs. In vertebrates, CpG islands are known to participate in transcription initiation[62]. Different histone chemical modifications (also known as histone marks) regulate the accessibility of chromatin to transcription. H3K27 acetylated modification (H3K27ac) particularly is often found near active regulatory elements and mainly associated with high levels of DNA accessibility and open/active chromatin[63]. The deoxyribonuclease I (DNase I) hypersensitivity clusters indicate regions where the chromatin is hypersensitive to cutting by the DNase enzyme. Promoters and regulatory regions are known to be DNase sensitive[64]. Thus, I used the enrichment in histone H3K27ac, the presence of CpG islands, and DNase I hypersensitivity clusters as criteria for promoter regions identification. I identified three such regions (TSS1-3) in the region 6Kb upstream from the Nrp1 transcription start site. Zeb2 is a zinc finger DNA-binding protein that recognizes one of the known E-box sequences 5'-CACCT(G)-'3 [36]. Within the 6Kb region that I identified, there are 11 CACCTG binding sites (Fig. 18 a-b).

Taking into consideration that Zeb2 is a transcriptional factor and can directly regulate the expression of different genes I performed an analysis of chromatin bound to the Zeb2 protein. For that, I conducted chromatin immunoprecipitation (ChIP) of E15.5 *Zeb2*$^{fl/fl}$ cortices followed by qPCR analysis. To each of the previously identified E-box sites, I created a pair of qPCR primers for the qPCR analysis. I immunoprecipitated Zeb2-bound chromatin using anti Zeb2 antibodies, then sonicated the isolated chromatin into around 200bp pieces, cleared it and used this as a template for qPCR analysis. qPCR analysis of the chromatin pieces bound by Zeb2 protein showed strong enrichment in all 11 binding sites (3 experimental replicates, Fig. 18c). The previously identified Zeb2 target Ntf3[54] was used as a positive control in qPCR analysis. Enrichment was compared to the input DNA. Only the binding site number 10 did not show any enrichment in the first experimental replicate.

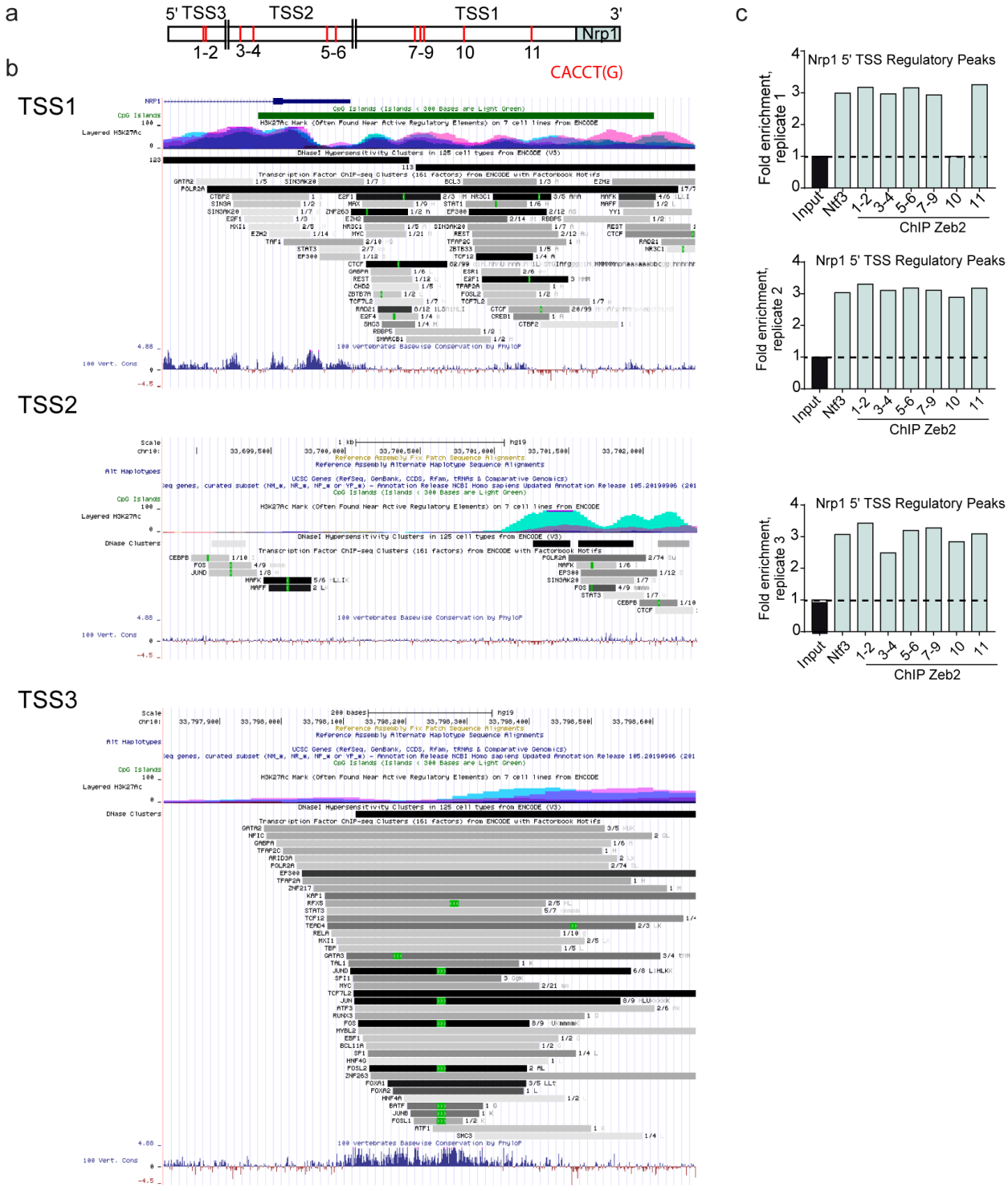

Fig. 18. Nrp1 is a novel downstream target of Zeb2. a. Schematic diagram of the genomic region enclosing 6Kb of 5'upstream of the Nrp1 start codon. **b.** Three different potential transcription start sites (TSS1-3) were identified according to increased CpG islands, H3K27ac modification marks and DNase hypersensitivity clusters (UCSC genome browser, FANTOM5). TSS1-3 related human genomic regions are shown. TSS1-3 regions were analysed for the presence of CACCT(G) sequences which are recognised by zinc finger binding sites of Zeb2

(numbered 1-11). **c**. Three independent replicates of the ChIP-qPCR from E15.5 are shown. Ntf3 was used as a positive control due to its previous identification as a Zeb2-binding site upstream. Enrichment was compared to the input DNA. Adapted from Epifanova et al[52].

Together these data suggested that Zeb2 directly binds the Nrp1 promoter to regulate its expression and that Nrp1 is a direct downstream signalling target of Zeb2.

3.1.10. Nrp1 downregulation restores the abnormal extracellular adhesion of Zeb2-deficient neurons

Considering the role of Npr1 in the regulation of neuronal migration I decided to test out whether Nrp1 could also rescue the altered cellular adhesion of Zeb2-deficient neurons. Adhesion-related functions for Nrp1 have not been described in neurons before. Nrp1 is known to intensify integrin signalling in some other cell types[65,66]. Moreover, a biotinylation-linked mass spectrometry analysis conducted in the group showed two large groups of adhesion-related molecules that were more strongly expressed on the cell membrane of Zeb2-deficient neurons: Integrins and Cadherins. The two candidates with the most elevated plasma membrane expression were Itgβ1 and Cdh6. Interestingly, *in situ* hybridization conducted by others in the group showed no difference in Itgβ1 mRNA levels but elevated Cdh6 mRNA levels in the CP of Zeb2-deficient animals.

It has been reported that Nrp1 can promote Integrin signalling in a variety of cells (such as endothelial cells, neuroepithelial cells and several types of cancer cells) but not neurons[66,67]. Thus, I hypothesised that Nrp1 may have a similar function in neurons. To test that, I cloned a dominant-negative mutant of Itgβ1 (Itgβ1DN) which lacks the cytoplasmic domain in order to assess the possible role of Integrin signalling in the regulation of neuronal adhesion downstream of Zeb2 (described in detail in the section “Materials and Methods)”. The Itgβ1 subunit is known to interact with multiple Integrin α subunits to form a functional receptor that can transduce signal to downstream targets within the Integrin signalling pathway[68]. An Itgβ1 subunit mutant that lacks the cytoplasmic domain can interact with Itg α subunits to form unproductive complexes that can not further transduce signals[57]. In order to generate a version of the Itgβ1 coding sequence lacking the

cytoplasmic domain, I inserted a stop codon at the position 2082bp. Then I amplified the region of interest by PCR and inserted the amplified fragment using NEBuilder HiFi DNA Assembly Cloning Kit system (New England BioLabs) into the pNeuroD-IRES-GFP construct which was previously linearized at the EcoRV site. Integrin signalling is necessary for progenitor processes such as progenitors attachment, proliferation and maintenance[69]. Thus, I chose to express ItgB1DN under the NeuroD promoter in order to restrict ItgB1DN expression to postmitotic cells and prevent disruption of progenitor function.

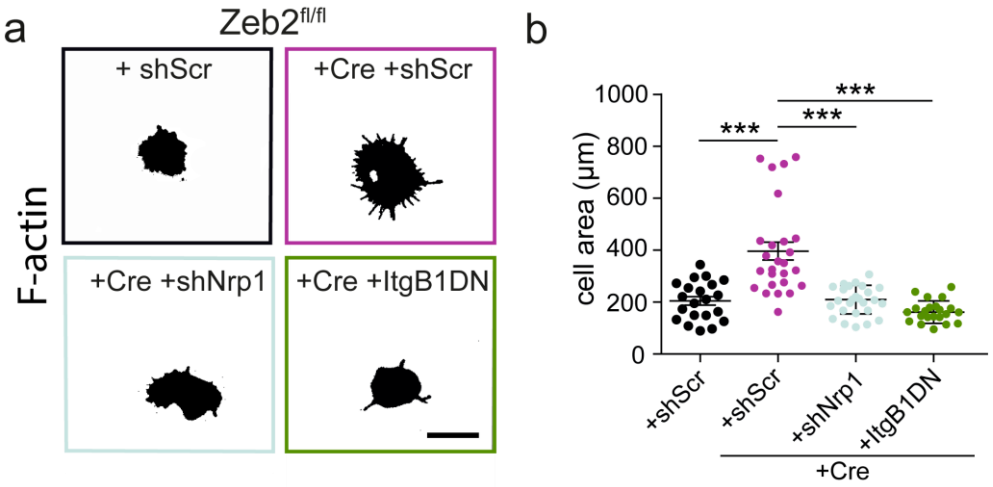

Fig. 19. Zeb2 suppresses neuronal adhesion to the extracellular matrix through Nrp1 and Itgβ1. a. Representative images of primary cortical neurons in single cell suspensions from E15.5 littermate *Zeb2*$^{fl/fl}$ embryos were nucleofected with either shScr, shNrp1 or a dominant-negative mutant of integrin β1 (Itgβ1DN) expressing construct in the presence or absence of Cre expressing construct. Neurons were plated and allowed to build up the expression for 2 days. Then neurons were detached from coated plates in the absence of proteases and allowed to adhere to laminin and poly-L-lysin coated surfaces for 2 hours, fixed, stained with phalloidin stain (marks F-actin) and imaged. Scale bar = 15µm. **b.** Quantification of lamellipodial spreading. N = 21 *Zeb2*$^{fl/fl}$ + shScr, 26 *Zeb2*$^{fl/fl}$ + Cre + shScr, 26 *Zeb2*$^{fl/fl}$ + Cre + shNrp1, 22 *Zeb2*$^{fl/fl}$ + Cre + Itgβ1DN. One-way ANOVA (Kruskal-Wallis test) with Dunn´s multiple comparison test. *** $p < 0.001$; ** $0.001 < p < 0.01$; * $0.01 < p < 0.05$. Results on the graph are represented as averages ± SD. Adapted from Epifanova et al[52].

At first, I tested whether knockdown of Nrp1 or dominant-negative Itgβ1 (Itgβ1DN) can reduce the enhanced adhesion to the extracellular matrix of Zeb2-deficient neurons. For that, I either downregulated Nrp1 or overexpressed Itgβ1DN in Zeb2-deficient neurons. I dissociated E15.5 *Zeb2*$^{fl/fl}$ cortices in the absence of proteases, nucleofected cells with either shScr, shNrp1 or Itgβ1DN expression constructs in the presence and absence of Cre expression construct and cultured neurons during 2 days to build up the expression of nucleofected constructs. After 2 days of incubation, I collected and dissociated neurons again in the absence of proteases and this single cell suspension was used in a cell-to-extracellular matrix adhesion assay as described earlier (Fig. 12). Wildtype control neurons tended to extend smaller lamellipodia than Zeb2-deficient neurons (Fig. 12 c-d). Zeb2-deficient neurons with downregulation of Nrp1 or overexpression of Itgβ1DN showed relatively normal cell body area when compared to control *Zeb2*$^{fl/fl}$ +shScr condition (Fig. 19 a-b; 205 ± 74.5µm *Zeb2*$^{fl/fl}$ +shScr, 396 ± 175µm *Zeb2*$^{fl/fl}$ + Cre +shScr, 209 ± 55 *Zeb2*$^{fl/fl}$ + Cre +shNrp1 and 162 ± 43.2 *Zeb2*$^{fl/fl}$ + Cre +Itgβ1DN; p-value *Zeb2*$^{fl/fl}$ + Cre +shScr versus *Zeb2*$^{fl/fl}$ + Cre + shNrp1 *** <0.001; p-value *Zeb2*$^{fl/fl}$ + Cre +shScr versus *Zeb2*$^{fl/fl}$ + Cre + Itgβ1DN *** <0.001).

This data showed that Nrp1 and Itgβ1 act downstream of Zeb2 and regulate the adhesion of neurons to the extracellular matrix. This is the first time that the Nrp1 has been shown to have an adhesive function in neurons.

3.1.11. Itgb1 acts downstream of Nrp1 regulating neocortical radial migration

To test whether Itgβ1 can regulate radial migration I performed several *IUE*s. At first, I *in utero* electroporated either Neurod-IRES-GFP or NeuroD-Itgβ1DN-IRES-GFP into wild type embryos at E14.5 and analysed the tissue upon completion of radial migration at E18.5. In both the wildtype control condition and the postmitotic overexpression of Itgβ1, most of the neurons migrated to the top of the CP (bin 1). It appears that postmitotic blockage of Integrin signalling does not affect radial migration (Fig. 20 a-b; p-value WT versus WT + Itgβ1DN >0.05).

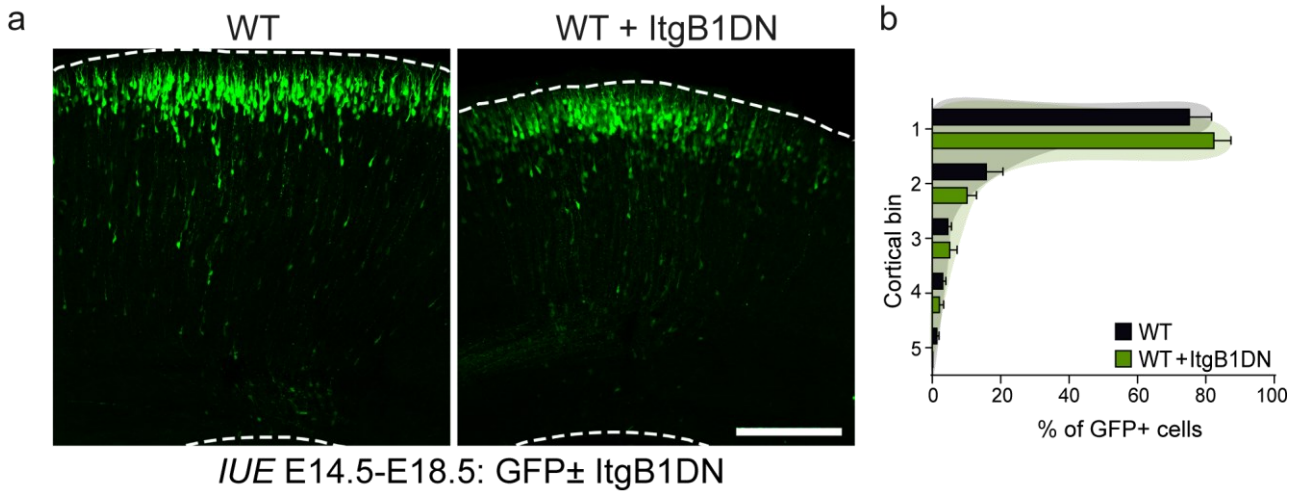

Fig. 20. Postmitotic inhibition of Integrin signalling does not alter the laminar distribution of neurons in wild type animals. a. Representative images of *in utero* electroporated at E14.5 wild type embryos with either construct with IRES driven GFP expression or the construct expressing of dominant-negative Integrin beta 1 under the Neurod1 promoter (Itgβ1DN) and IRES driven GFP expression. Animals were analysed at E18.5. Scale bar = 100μm. **b.** Quantification of the laminar distribution of GFP+ neurons *in vivo.* N = 7 control WT and 7 WT + Itgβ1DN animals. Two-way ANOVA with Bonferroni post-hoc test. *** $p < 0.001$; ** $0.001 < p < 0.01$; * $0.01 < p < 0.05$. Results on the graph are represented as averages ± SD. Adapted from Epifanova et al[52].

I then asked whether downregulation of Integrin signalling could improve the defective radial migration of Zeb2-deficient neurons. To test this, I *in utero* electroporated *Zeb2*$^{fl/fl}$ and *Zeb2*$^{fl/fl}$ *Nex*^{Cre} E14.5 embryos with either Neurod-IRES-GFP or NeuroD-Itgβ1DN-IRES-GFP constructs and analysed electroporated animals at E18.5. The laminar distribution analysis showed improved laminar positions of *in utero* electroporated Zeb2-deficient neurons in comparison to the Zeb2-deficient condition (Fig. 21 a-b, *Zeb2*$^{fl/fl}$ versus *Zeb2*$^{fl/fl}$ *Nex*^{Cre} + Itgβ1DN bins 1-5 respectively: 83.5 ± 8.595 versus 54.8 ± 11.89, p-value *** <0.001; 9.759 ± 5.543 versus 23.41 ± 5.494, p-value *** <0.001; 2.781 ± 2.057 versus 12.62 ± 4.596, p-value ** <0.01; 2.785 ± 2.710 versus 5.921 ± 3.173, p-value >0.05; 1.178 ± 1.990 versus 3.258 ± 2.187, p-value >0.05 and *Zeb2*$^{fl/fl}$ *Nex*^{Cre} versus *Zeb2*$^{fl/fl}$ *Nex*^{Cre} + Itgβ1DN bins 1-5 respectively: 30.2 ± 5.836 versus 54.8 ± 11.89, p-value *** <0.001; 23.36 ± 4.908 versus 23.41 ± 5.494, p-value >0.05; 16.56 ± 5.371 versus 12.62 ±

4.596, p-value >0.05; 15.49 ± 7.547 versus 5.921 ± 3.173, p-value * <0.05; 14.39 ± 2.080 versus 3.258 ± 2.187, p-value ** <0.01).

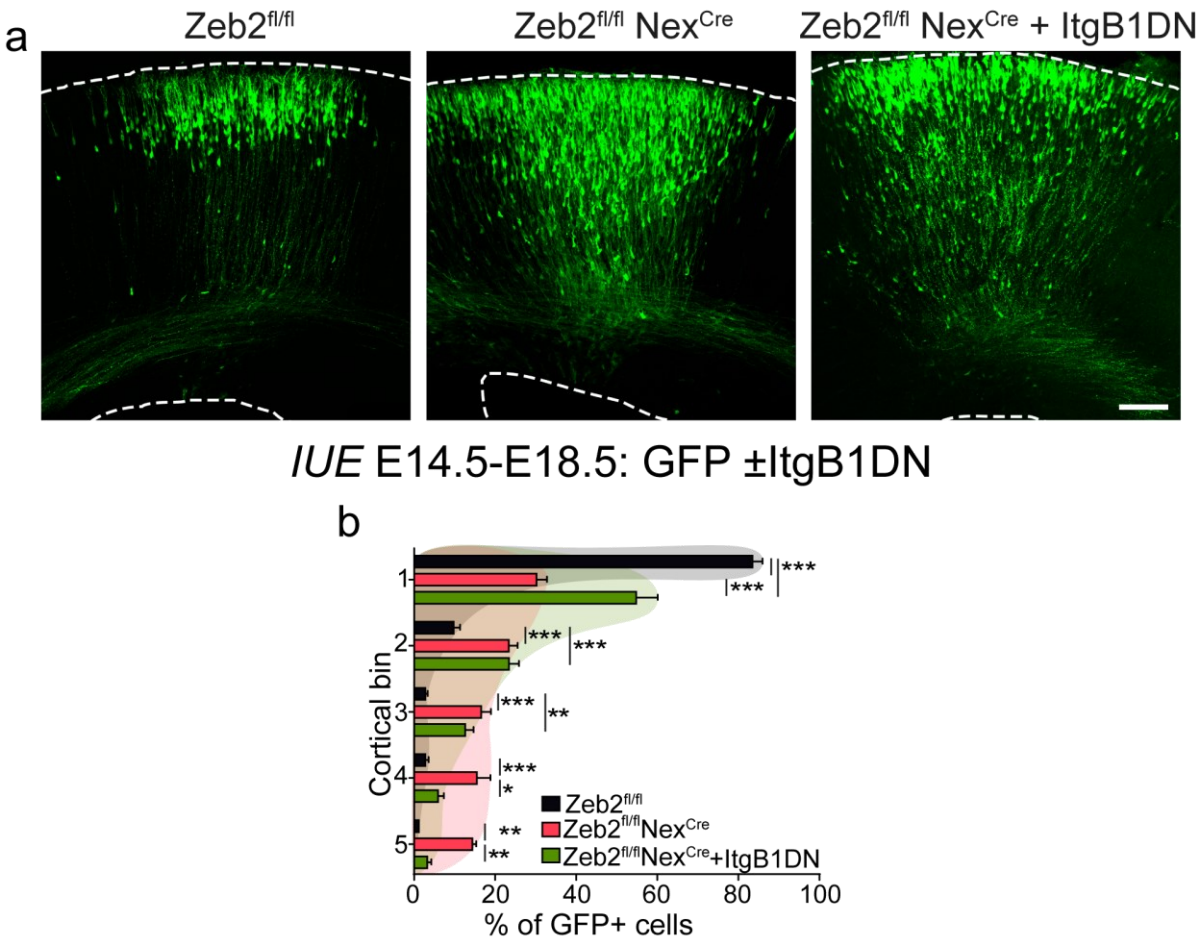

Fig. 21. Zeb2 controls neuronal radial migration through inhibition of Integrin signalling. a. Representative images of *in utero* electroporated *Zeb2*$^{fl/fl}$ and *Zeb2*$^{fl/fl}$ *Nex*^{Cre} E18.5 cortices in the presence or absence of the construct expressing of dominant-negative Integrin beta 1 under the Neurod1 promoter (Itgβ1DN) and IRES driven GFP expression. The cortical area is marked with a dotted line. Scale bar = 100μm. **b.** Quantification of the laminar position of GFP+ neurons *in vivo*. N = 12 *Zeb2*$^{fl/fl}$, 5 *Zeb2*$^{fl/fl}$ Nex^{Cre} and 5 *Zeb2*$^{fl/fl}$ *Nex*^{Cre} + Itgβ1DN animals. Two-way ANOVA with Bonferroni post-hoc test. *** $p < 0.001$; ** $0.001 < p < 0.01$; * $0.01 < p < 0.05$. Results on the graph are represented as averages ± SD. Adapted from Epifanova et al[52].

To study whether Nrp1 regulates radial migration through the Integrin pathway I conducted *IUE* of both Nrp1 and ItgB1DN expression constructs into wild type embryos at E14.5 and analysed the neurons at E18.5. Nrp1 disrupts radial migration when overexpressed in wild type neurons (Fig. 22). Neurons overexpressing Nrp1 and also ItgB1DN show only a mild defect in migration (Fig. 22 a-b; WT versus WT + Nrp1 + ItgB1DN bin 1: 75.19 ± 17.16 versus 62.78 ± 12.76, p-value * <0.05; bins 2-5 are not significantly different, p-value >0.05 and ; WT + Nrp1 versus WT + Nrp1 + ItgB1DN bin 1: 25.21 ± 13.74 versus 62.78 ± 12.76, p-value *** <0.001; bins 2-5 are not significantly different, p-value >0.05). This allows me to suggest that Nrp1 regulates the onset of the radial migration through suppression of Integrin-mediated adhesion.

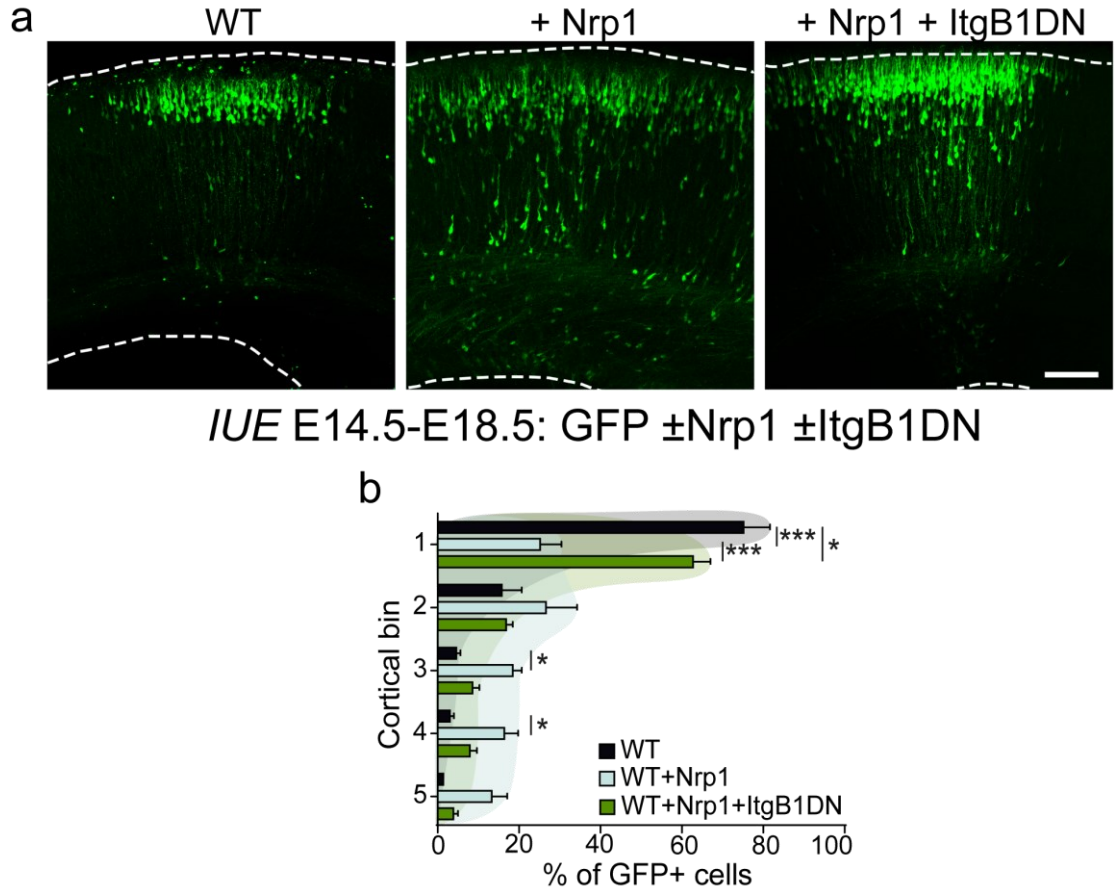

Fig. 22. Nrp1 regulates neuronal radial migration through Integrin signalling. a. Representative images of *in utero* electroporated wild type E18.5 cortices in the presence or absence of the Nrp1 expressing construct, the construct expressing of dominant-negative Integrin β1 under the Neurod1 promoter (ItgB1DN) and IRES driven GFP expression. The cortical area is marked with a dotted line. Scale bar =

100µm. **b.** Quantification of the laminar position of GFP+ neurons *in vivo*. N = 7 control WT, 7 WT + Nrp1, 9 WT + Nrp1 + Itgβ1DN animals. Two-way ANOVA with Bonferroni post-hoc test. *** $p < 0.001$; ** $0.001 < p < 0.01$; * $0.01 < p < 0.05$. Results on the graph are represented as averages ± SD. Adapted from Epifanova et al[52].

Both downregulation of Nrp1 and inhibition of Itgβ1 restored the defective laminar distribution of Zeb2-deficient neurons. I thus hypothesised that Nrp1 and Itgβ1 act within the same signalling pathway and can interact with each other directly. Nrp1 has been shown to interact with integrin subunits and form protein complexes in other cell types[65]. In order to prove a direct interaction of Nrp1 and Itgβ1 proteins in neurons, I performed PLA for endogenous Nrp1 and Itgβ1 in primary cortical neurons at DIV5 derived from E15.5 $Zeb2^{fl/fl}$ and $Zeb2^{fl/fl}$ Nex^{Cre} embryos (Fig. 23a). The PLA technique allows the detection of protein interactions with high sensitivity and specificity. Quantification of the average Nrp1+Itgβ1 PLA intensity showed that Nrp1 directly binds Itgβ1 in DIV5 cortical neurons and that this interaction is increased under loss of Zeb2 (Fig. 23b; 291082 ± 80679 $Zeb2^{fl/fl}$ versus 334587 ± 79286 $Zeb2^{fl/fl}$ Nex^{Cre}, p-value * < 0.05). Furthermore, Nrp1 and Itgβ1 form protein clusters whose presence is increased in Zeb2-deficient neurons (Fig. 23c; 0.111 ± 0.048 $Zeb2^{fl/fl}$ versus 0.203 ± 0.048 $Zeb2^{fl/fl}$ Nex^{Cre}, p-value *** <0.001). These data confirm that Nrp1 and Itgβ1 directly interact in neurons and loss of Zeb2 leads to enhanced Nrp1-Itgβ1 interaction and increased formation of Nrp1-Itgβ1 protein clusters.

Together these data demonstrate that inhibition of Integrin signalling is necessary for correct radial migration. Moreover, Zeb2 suppresses integrin-mediated adhesion of neurons to the extracellular matrix through Nrp1 and thus regulates the initiation of neuronal radial migration.

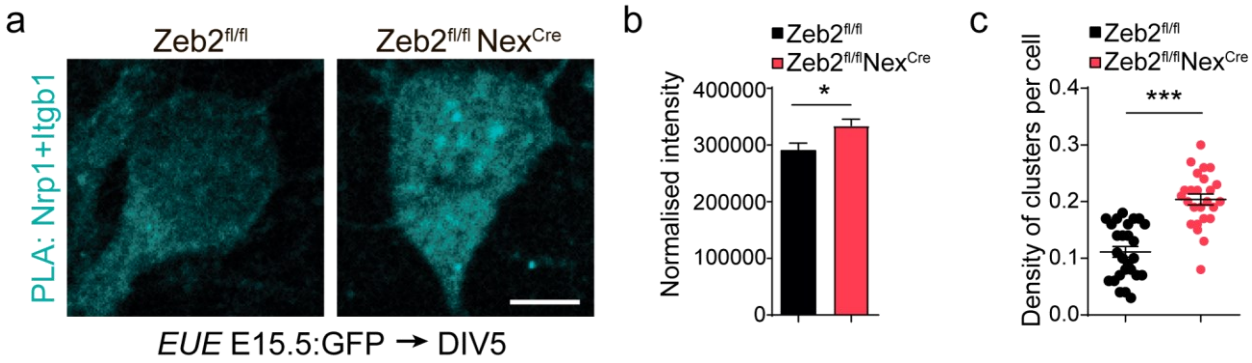

Fig. 23. Nrp1 and Itgβ1 interaction is increased in Zeb2-deficient neurons. a. Representative images of *Zeb2*$^{fl/fl}$ and *Zeb2*$^{fl/fl}$ *Nex*^{Cre} neurons that were *in utero* electroporated at E15.5 with GFP expressing construct. Proximity ligation assay (PLA) for Nrp1 and Itgβ1 was performed at DIV5 and then analysed. Scale bar = 5μm. **b.** Quantification of the average Nrp1+Itgβ1 PLA intensity per cell. N = 44 *Zeb2*$^{fl/fl}$ and 53 *Zeb2*$^{fl/fl}$ *Nex*^{Cre} cells. Unpaired *t* test. **(C)** Quantification of the density of Nrp1+Itgβ1 PLA clusters per cell. N = 26 *Zeb2*$^{fl/fl}$ and 25 *Zeb2*$^{fl/fl}$ *Nex*^{Cre} cells. Unpaired *t* test. *** $p < 0.001$; ** $0.001 < p < 0.01$; * $0.01 < p < 0.05$. Results on the graph are represented as averages ± SD. Adapted from Epifanova et al[52].

Chapter 2. Apical dendrite orientation

3.2.1. Zeb2 controls postnatally the orientation of apical dendrites

I then asked whether delayed radial migration could affect the structure of the neocortex postnatally. For that, I analysed *Zeb2*$^{fl/fl}$ and *Zeb2*$^{fl/fl}$ *Nex*^{Cre} brains stained with Golgi-Cox method at postnatal day 23 (P23). The Golgi-Cox staining was performed by others in the group. The fourth week of mouse development can be considered as the time point of neuronal maturity[70]. I studied specifically the somatosensory cortex of these brains and analysed the phenotype of upper layers and deeper layers separately. I found notable disorganization and neuronal misorientation in the outer regions of the cortex and relatively normal organisation of neurons in the deeper regions of the cortex. Generally, neurons orient their apical dendrites perpendicular to the meninges surface and parallel to each other. To obtain a measure of this disorganization, I measured the orientation of the apical dendrite of the outer and the deeper layer neurons (called UL and DL on the graph) with respect to the meningeal surface. Interestingly, neurons in the outer layer showed apical dendrite misorientation while neurons in the deeper area of cortex showed no difference in the apical dendrite orientation (Fig. 24 a-b; for UL 4.254 ± 5.310 *Zeb2*$^{fl/fl}$ versus 37. but 96 ± 40.54 *Zeb2*$^{fl/fl}$ *Nex*^{Cre}; p-value *** <0.001; for DL 6.494 ± 18.69 *Zeb2*$^{fl/fl}$ versus 4.598 ± 3.319 *Zeb2*$^{fl/fl}$ *Nex*^{Cre}; p-value >0.05).

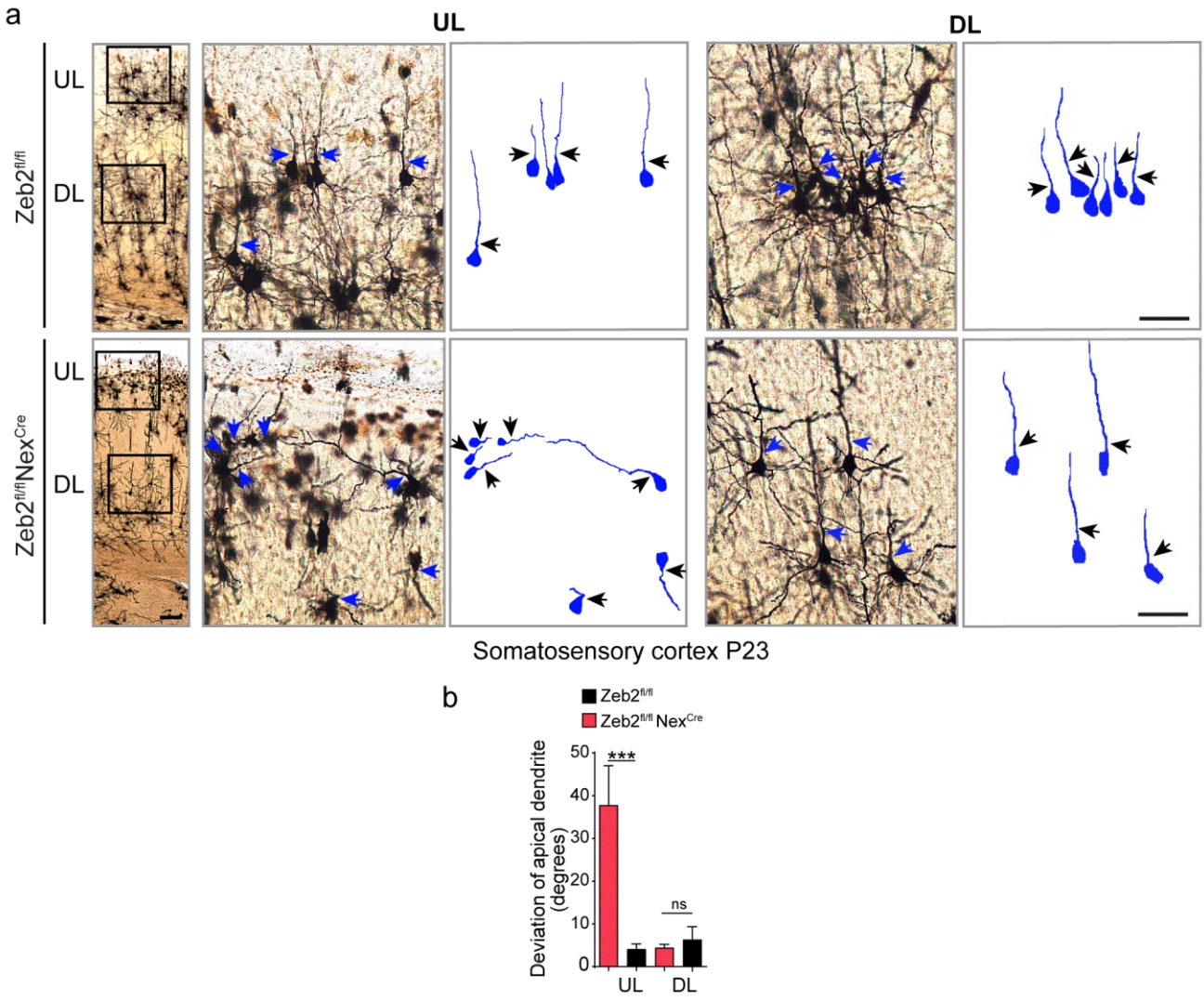

Fig. 24. Zeb2 regulates neuronal orientation of UL neurons but not DL neurons. a. Representative images of *Zeb2*$^{fl/fl}$ and *Zeb2*$^{fl/fl}$ *Nex*^{Cre} Golgi-Cox stained P23 somatosensory cortices. Boxes mark the zoomed UL and DL areas, arrows mark selected UL and DL neurons. Tracings of the soma and apical dendrite of indicated neurons are shown in blue. Scale bar of the overview pictures = 100µm. Scale bar of the zoomed areas = 50µm. **b.** Quantification of the apical dendrite deviation for UL and DL neurons. N = 23 UL and 43 DL *Zeb2*$^{fl/fl}$; 20 UL and 27 DL *Zeb2*$^{fl/fl}$ *Nex*^{Cre} cells. One-way ANOVA (Kruskal-Wallis test) with Dunn´s multiple comparison test. *** $p < 0.001$; ** $0.001 < p < 0.01$; * $0.01 < p < 0.05$. Results on the graph are represented as averages ± SD. Adapted from Epifanova et al[52].

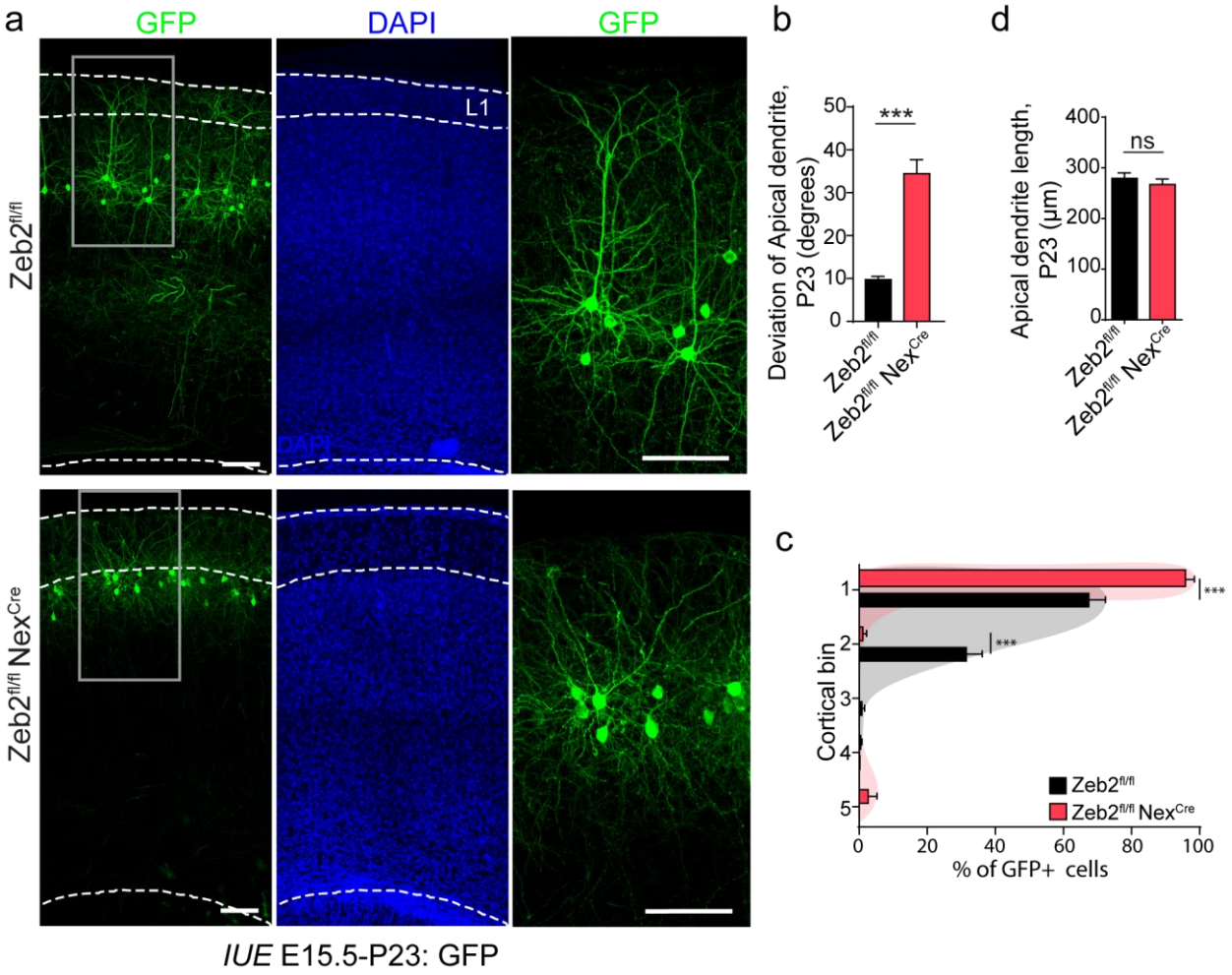

Fig. 25. Loss of Zeb2 leads to overmigration of UL neurons at P23. **a.** Representative images of *Zeb2*$^{fl/fl}$ and *Zeb2*$^{fl/fl}$ *Nex*^{Cre} *in utero* electroporated with GFP expressing construct at E15.5 somatosensory cortices analysed at P23 and stained with DAPI (nuclear marker) and anti-GFP antibody. The cortical area and layer 1 are marked with a dotted line. Boxes mark the zoomed UL areas. Scale bar of the overview pictures = 100µm. Scale bar of the zoomed areas = 50µm. **b.** Quantification of the apical dendrite deviation at P23. N = 65 *Zeb2*$^{fl/fl}$ and 65 *Zeb2*$^{fl/fl}$ *Nex*^{Cre} neurons. Mann-Whitney test. **c.** Quantification of the laminar position of GFP+ neurons *in vivo*. N = 3 brains per condition. Two-way ANOVA with Bonferroni post-hoc test. **d.** Quantification of the apical dendrite length at P23. N = 65 cells, 3 brains per condition. Welch's *t* test. *** $p < 0.001$; ** $0.001 < p < 0.01$; * $0.01 < p < 0.05$. Results on the graph are represented as averages ± SD. Adapted from Epifanova et al[52].

Next, I asked when neuronal misorientation of Zeb2-deficient neurons starts. I performed several *IUE* of E15.5 *Zeb2*$^{fl/fl}$ and *Zeb2*$^{fl/fl}$ *Nex*^{Cre} embryos and analysed them at different developmental timepoints: E18.5, P2, P7 and P23. Wild type control neurons and their apical dendrites were oriented normally (perpendicular) to the meningeal surface at all analysed time points. Zeb2-deficient neurons showed relatively normal orientation of the apical dendrite at E18.5 (Fig. 26 a-c; 2.209 ± 3.888 degrees *Zeb2*$^{fl/fl}$ versus 2.622 ± 3.189 degrees *Zeb2*$^{fl/fl}$ *Nex*^{Cre}; p-value >0.05). However, already at P2, I observed that some apical dendrites were tilted with respect to the meningeal surface (2.683 ± 2.801 degrees *Zeb2*$^{fl/fl}$ versus 22.423 ± 39.207 degrees *Zeb2*$^{fl/fl}$ *Nex*^{Cre}; p-value *** <0.001). The observed phenotype was present from P2 onward (6.572 ± 6.936 degrees *Zeb2*$^{fl/fl}$ versus 35.218 ± 33.944 degrees *Zeb2*$^{fl/fl}$ *Nex*^{Cre} at P7; p-value *** <0.001 and 9.737 ± 5.863 degrees *Zeb2*$^{fl/fl}$ versus 34.43 ± 26.41 degrees *Zeb2*$^{fl/fl}$ *Nex*^{Cre} at P23; p-value *** <0.001). Interestingly, the average angle deviation of Zeb2-deficient neurons at P2 was smaller than at P7 or P23. This angle deviation might be increasing with time due to ongoing brain growth and an increase in brain mass. Thus, misorientation of the apical dendrites of Zeb2-deficient neurons happens only after migration is complete.

Altogether, these data demonstrated that the postnatal development of Zeb2-deficient neurons was also affected. Since the apical dendrites of Zeb2-deficient neurons were specified correctly this is likely related to the defective establishment of the apical dendrite orientation with respect to the meningeal surface and did not connect to the delayed radial migration phenotype.

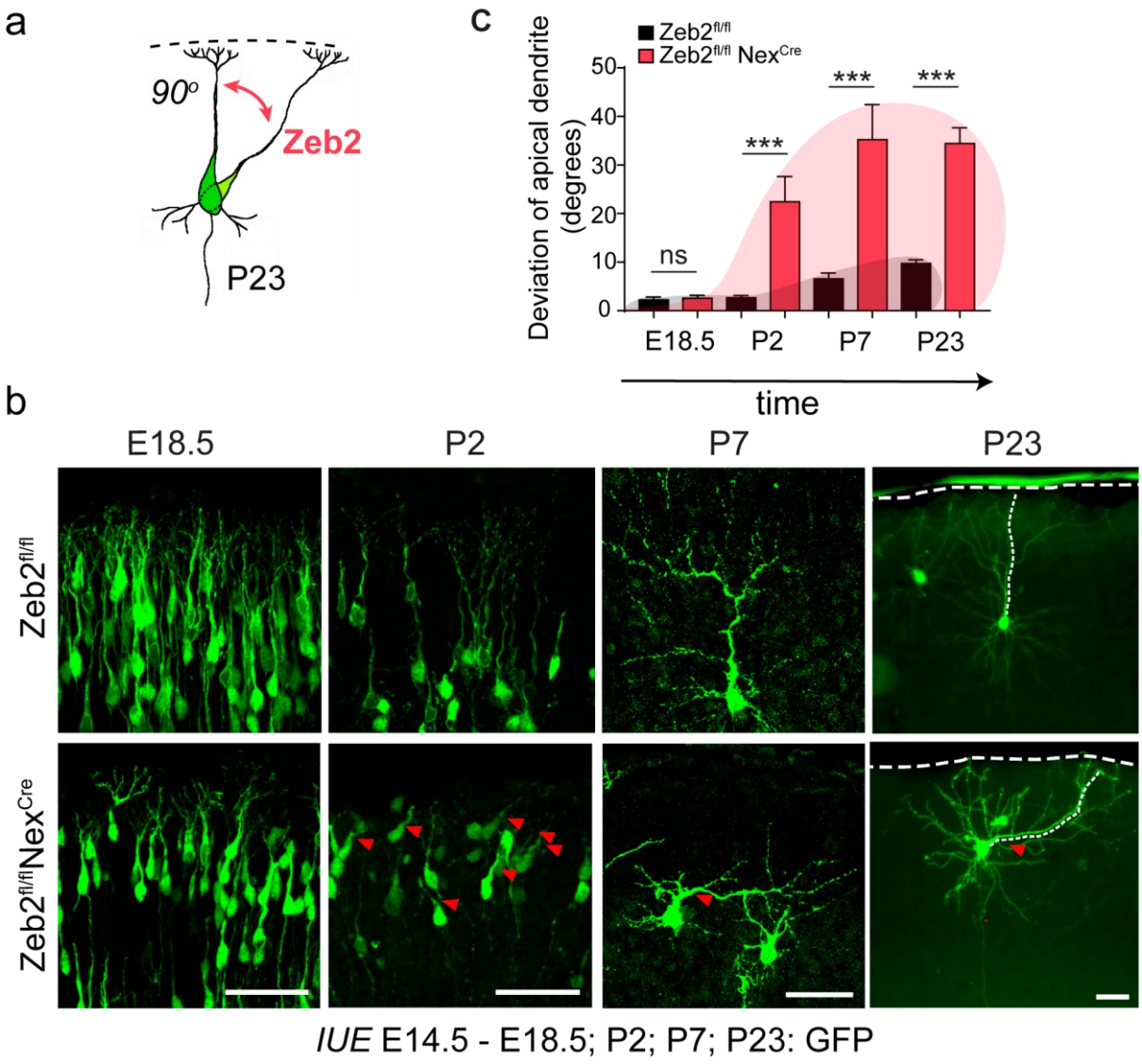

Fig. 26. Zeb2 regulates orientation of apical dendrite starting from P2 and onwards. a. Zeb2 regulates the orientation of apical dendrite**s. b.** Representative images of *Zeb2*$^{fl/fl}$ and *Zeb2*$^{fl/fl}$ *Nex*^{Cre} neurons at different developmental time points (E18.5, P2, P7, P23) *in vivo*. *Zeb2*$^{fl/fl}$ and *Zeb2*$^{fl/fl}$ *Nex*^{Cre} animals were *in utero* electroporated at E14.5 with GFP expressing construct. Red arrows indicate abnormally oriented neurons. Scale bar = 50μm. **c.** Quantification of the apical dendrite deviation at different developmental time points (E18.5, P2, P7, P23). N = 40, 36, 33, 65 *Zeb2*$^{fl/fl}$ and 33, 56, 22, 65 *Zeb2*$^{fl/fl}$ *Nex*^{Cre} neurons at E18.5, P2, P7, P23 respectively. Mann-Whitney test. *** $p < 0.001$; ** $0.001 < p < 0.01$; * $0.01 < p < 0.05$. Results on the graph are represented as averages ± SD. Adapted from Epifanova et al[52].

3.2.2. Nrp1 does not rescue apical dendrite angle deviation

I then asked whether the misorientation of the apical dendrite was related to Nrp1 signalling since Nrp1 is crucial for the onset of radial migration. To assess this, I *in utero* electroporated E15.5 *Zeb2*$^{fl/fl}$ embryos with either the control shRNA, shScr, or shNrp1 with the presence or absence of a Cre expression construct. The animals were analysed at P23 and stained with anti-GFP antibody.

Apical dendrites of wild type control neurons were oriented normally (perpendicular) to the meningeal surface while the apical dendrites of Zeb2-deficient neurons were tilted with respect to the meningeal surface. Therefore, downregulation of Nrp1 does not rescue the misorientation of the apical dendrite of Zeb2-deficient neurons (Fig. 27 a-b; 3.040 ± 4.349 degrees *Zeb2*$^{fl/fl}$ +shScr, 15.17 ± 15.10 degrees *Zeb2*$^{fl/fl}$ + Cre + shScr and 13.15 ± 16.35 degrees *Zeb2*$^{fl/fl}$ + Cre + shNrp1; p-value *Zeb2*$^{fl/fl}$ +shScr versus *Zeb2*$^{fl/fl}$ + Cre + shScr *** <0.001; *Zeb2*$^{fl/fl}$ + Cre + shScr versus *Zeb2*$^{fl/fl}$ + Cre + shNrp1 >0.05; *Zeb2*$^{fl/fl}$ +shScr versus *Zeb2*$^{fl/fl}$ + Cre + shNrp1 *** <0.001).

Moreover, I assessed whether overexpression of Nrp1 can alter the orientation of the apical dendrites. I overexpressed Npr1 (pCAG-Nrp1-IRES-GFP) by *IUE* of wild type animals at E15.5 and analysed the brains of these animals at P23. Apical dendrites of both wild type control neurons and neurons with overexpression of Nrp1 were oriented normally (perpendicular) to the meningeal surface. Thus, Nrp1 overexpression does not affect the apical dendrite (Fig. 28 a-b; 4.01 ± 4.67 degrees of WT versus 5.61 ± 6.15 degrees of WT +Nrp1; p-value >0.05).

Together, these data showed that Nrp1 does not regulate the postnatal orientation of apical dendrites.

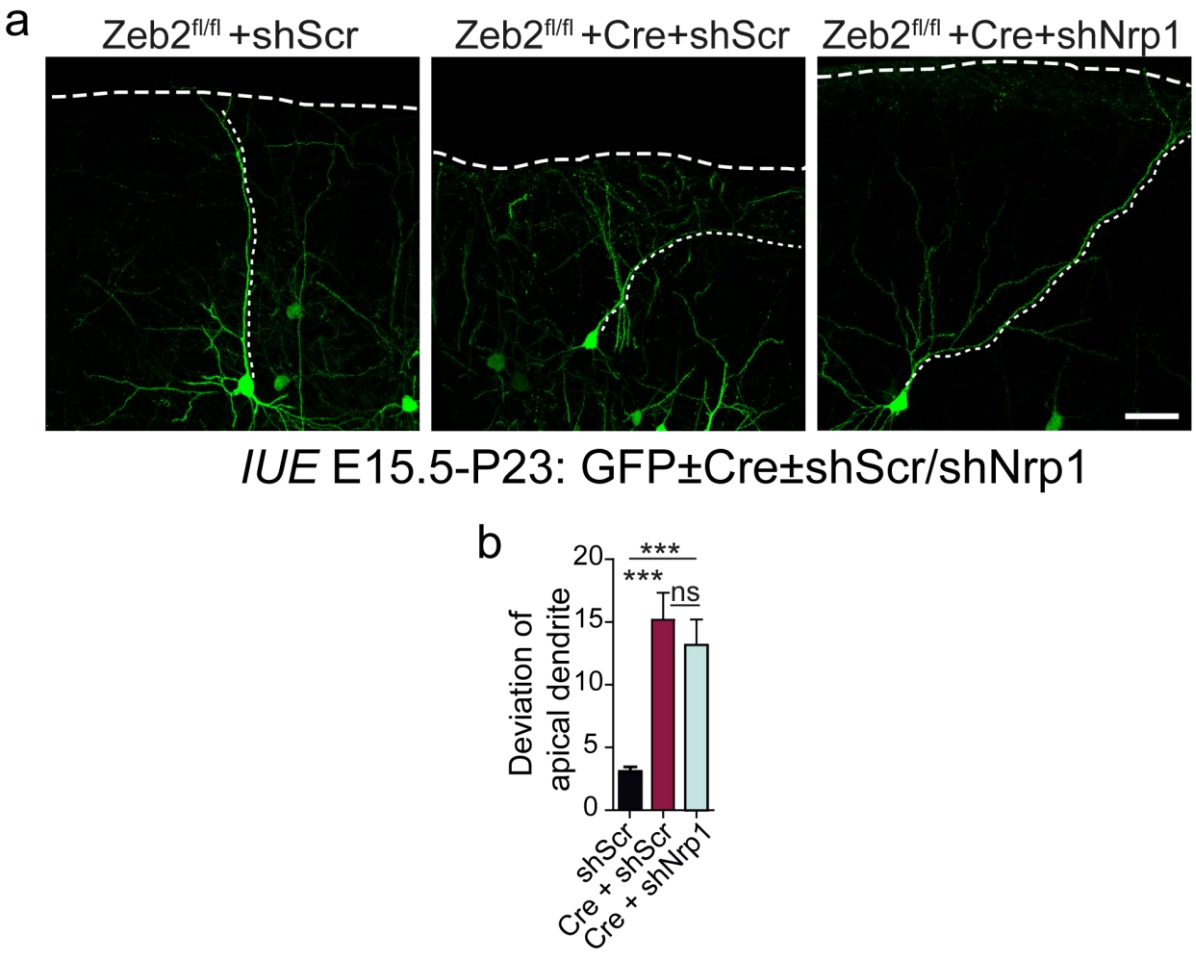

Fig. 27. Nrp1 regulates radial migration but not the orientation of the apical dendrite. a. Representative images of *in utero* electroporated *Zeb2*$^{fl/fl}$ neurons at E15.5 with GFP expressing construct, either shScr or shNrp1 in the presence or absence of Cre expressing construct and analysed at P23. The meningeal surface and apical dendrites are marked with a dotted line. Scale bar = 50µm. **b.** Quantification of apical dendrite deviation. N = 143 cells and 5 animals of *Zeb2*$^{fl/fl}$ + shScr, 49 cells and 6 animals of *Zeb2*$^{fl/fl}$ + Cre + shScr, 64 cells and 7 animals of *Zeb2*$^{fl/fl}$ + Cre + shNrp1 neurons. One-way ANOVA (Kruskal-Wallis) with Dunn´s multiple comparison test. *** $p < 0.001$; ** $0.001 < p < 0.01$; * $0.01 < p < 0.05$. Results on the graph are represented as averages ± SD. Adapted from Epifanova et al[52].

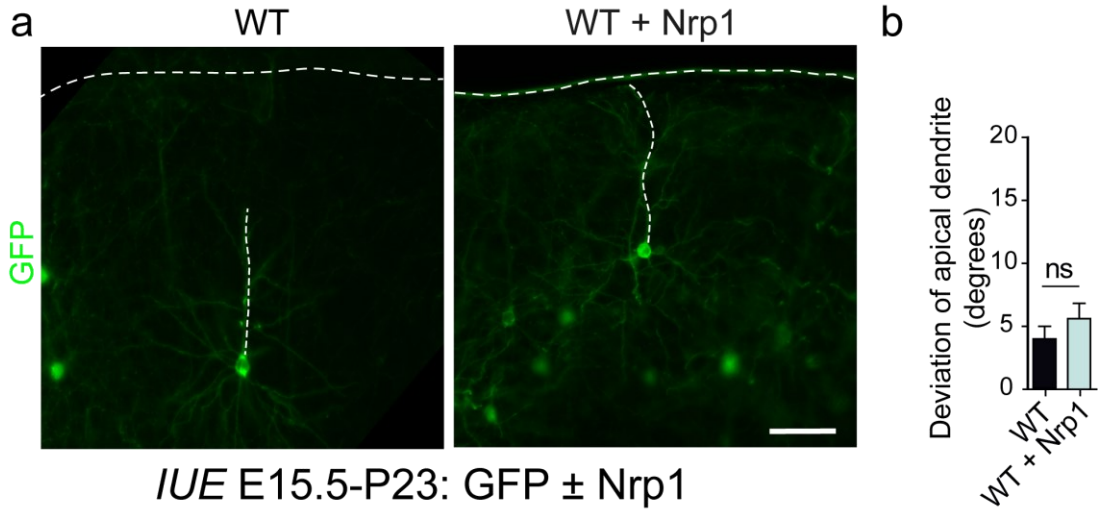

Fig. 28. Nrp1 does not control the apical dendrite orientation. a. Representative images of *in utero* electroporated wild type neurons at E15.5 with either Nrp1-IRES-GFP or IRES-GFP and analysed at P23. The meningeal surface and apical dendrites are marked with a dotted line. Scale bar = 100µm. **b.** Quantification of apical dendrite deviation. N = 22 cells and 3 animals of WT and 25 cells 3 animals of WT + Nrp1 neurons. Mann-Whitney test. *** $p < 0.001$; ** $0.001 < p < 0.01$; * $0.01 < p < 0.05$. Results on the graph are represented as averages ± SD. Adapted from Epifanova et al[52].

3.2.3. Apical dendrite misorientation of Zeb2-deficient neurons can be restored by Cdh6 downregulation

Since Nrp1 is not involved in the regulation of the apical dendrite orientation I asked whether another potential target of Zeb2 – Cdh6 – can participate in the establishment of this phenotype. At first, I assessed Cdh6 protein expression in both wildtype control and Zeb2-deficient cortices. I *in utero* electroporated E14.5 $Zeb2^{fl/fl}$ and $Zeb2^{fl/fl}$ Nex^{Cre} embryos with GFP expression construct, stained for endogenous Cdh6 using an anti-Cdh6 antibody and for GFP using an anti-GFP antibody. I analysed the embryos prenatally at E18.5 and postnatally at P2. In every analysed cortex I picked one region of interest (ROI) with the same area within MZ/Layer1 (marked as (a) on the graph) and one equal area within the outer part of the cortex (marked as (b) on the graph). I then measured the fluorescent intensity of every chosen ROI using ImageJ software and divided the intensity of the MZ- Layer1 ROI (a) by the intensity of ROI in the outer part of the cortex (b). Cdh6 protein was

significantly increased upon loss of Zeb2 both at E18.5 and P2 (Fig. 29 a, c). Then I looked at Cdh6 expression in wild type brains. In case of wild type control, at both stages, Cdh6 showed stronger signal in Layer1 area and weaker signal at the border of the marginal zone and cortical area. This pattern of Cdh6 expression coincides with the different location of shafts and tufts of apical dendrites. Dendritic shafts were located in the area with the lower Cdh6 expression, here marked as (b). The apical dendrite tufts, in turn, were located in the area with the higher Cdh6 expression, here marked as (a). In contrary to the control condition, Cdh6 expression was drastically increased in both shaft and tuft areas upon loss of Zeb2 (Fig. 29 a-d; E18.5: 1.585 ± 0.065 *Zeb2*$^{fl/fl}$ versus 1.259 ± 0.079 *Zeb2*$^{fl/fl}$ *Nex*^{Cre}; p-value ** <0.01; P2: 1.584 ± 0.118 *Zeb2*$^{fl/fl}$ versus 1.173 ± 0.115 *Zeb2*$^{fl/fl}$ *Nex*^{Cre}; p-value ** <0.01). In comparison to wild type, upon loss of Zeb2, Cdh6 protein was distributed differently in neocortex.

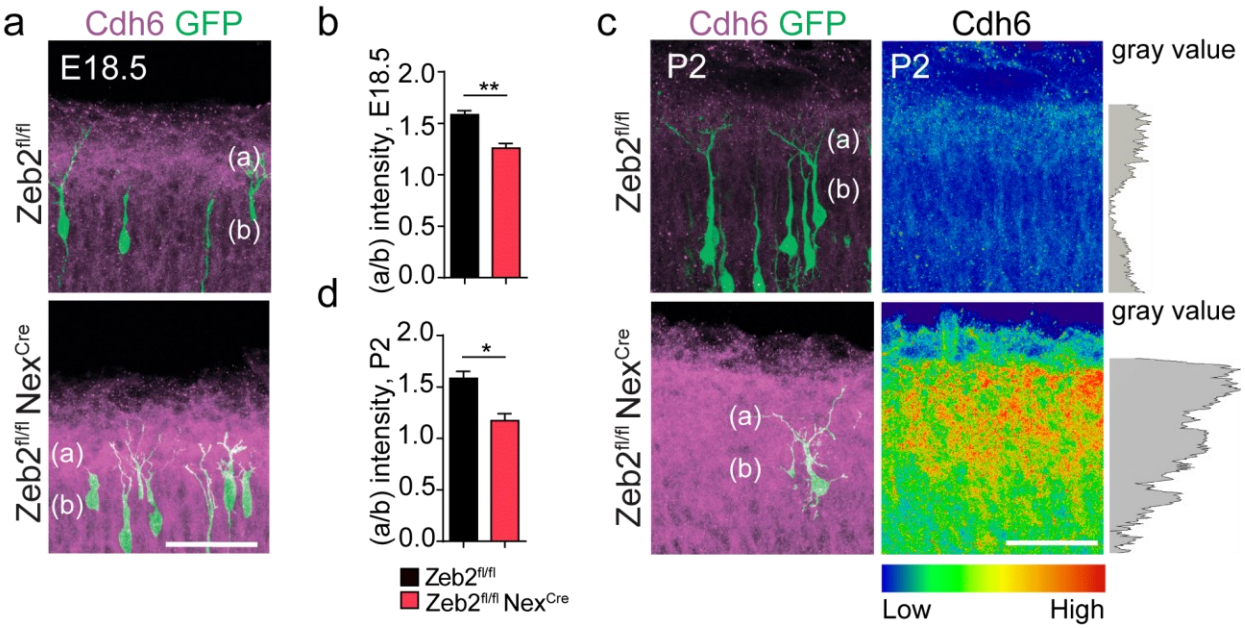

Fig. 29. Upregulation and mislocalisation of Cdh6 under loss of Zeb2. a. Representative images of *in utero* electroporated *Zeb2*$^{fl/fl}$ and *Zeb2*$^{fl/fl}$ *Nex*^{Cre} neurons at E14.5 with GFP expressing construct and analysed at prenatal stage (E18.5). Brain sections were stained with anti-GFP (in green) and anti-Cdh6 (in magenta) antibodies. Layer 1 and CP are marked with (a) and (b) respectively. Scale bar = 50µm. **b.** Quantification of Cdh6 intensity counted as the ratio of Cdh6 expression intensity in Layer 1 (a) versus the cortical area (b) at E18.5. N = 3 brains per condition. Unpaired *t* test. **c.** Representative images of *in utero* electroporated *Zeb2*$^{fl/fl}$ and *Zeb2*$^{fl/fl}$ *Nex*^{Cre} neurons at E14.5 with GFP

expressing construct and analysed at the postnatal stage (P2). Brain sections were stained with anti-GFP (in green) and anti-Cdh6 antibodies (in magenta). The heatmap and the grey plot of the Cdh6 intensity are presented on the graph. Scale bar = 50µm. **d.** Quantification of Cdh6 intensity counted as the ratio of Cdh6 expression intensity in Layer 1 versus the cortical area at P2. N = 3 brains per condition. Unpaired *t* test. *** $p < 0.001$; ** $0.001 < p < 0.01$; * $0.01 < p < 0.05$. Results on the graph are represented as averages ± SD. Adapted from Epifanova et al[52].

Prior to the experiment, I cloned Cdh6 into a pCAG-IRES-GFP construct (see section “Materials and Methods”). I then validated the shRNA against Cdh6 using *IUE* of E15.5 wild type animals and then analysed it at P23. I either electroporated only control shRNA (shScr) or shCdh6 together with Cdh6 overexpression construct. Both shScr and shCdh6 did not influence orientation of apical dendrites and shCdh6 offset the possible effect from Cdh6 overexpression (Fig. 30 a-b; 4.81 ± 4.16 WT + shScr versus 8.59 ± 12.2 WT + Cdh6 + shCdh6; p-value >0.05).

I then analysed whether Cdh6 can rescue misorientation of the apical dendrites of Zeb2-deficient neurons. I generated a mosaic Zeb2-deficient mutant by *IUE* of Cre expression construct in $Zeb2^{fl/fl}$ embryos. I downregulated Cdh6 expression using an shRNA against Cdh6. This shRNA or a control shRNA (shScr) was *IUE* into E15.5 $Zeb2^{fl/fl}$ embryos with either shScr or shCdh6 in the presence or absence of a Cre expression construct. The apical dendrites of wild type control neurons were oriented normally (perpendicular) to the meningeal surface. Surprisingly, downregulation of Cdh6 restored the abnormal apical dendrite orientation of Zeb2-deficient neurons (Fig. 31 a-c; 3.040 ± 4.349 $Zeb2^{fl/fl}$ + shScr; 44.68 ± 27.72 $Zeb2^{fl/fl}$ + Cre + shScr and 13.09 ± 12.47 $Zeb2^{fl/fl}$ + Cre + shCdh6; p-value $Zeb2^{fl/fl}$ + shScr versus $Zeb2^{fl/fl}$ + Cre + shCdh6 *** <0.001; $Zeb2^{fl/fl}$ + shScr vs $Zeb2^{fl/fl}$ + Cre + shScr *** <0.001; $Zeb2^{fl/fl}$ + Cre + shScr vs $Zeb2^{fl/fl}$ + Cre + shCdh6 *** <0.001).

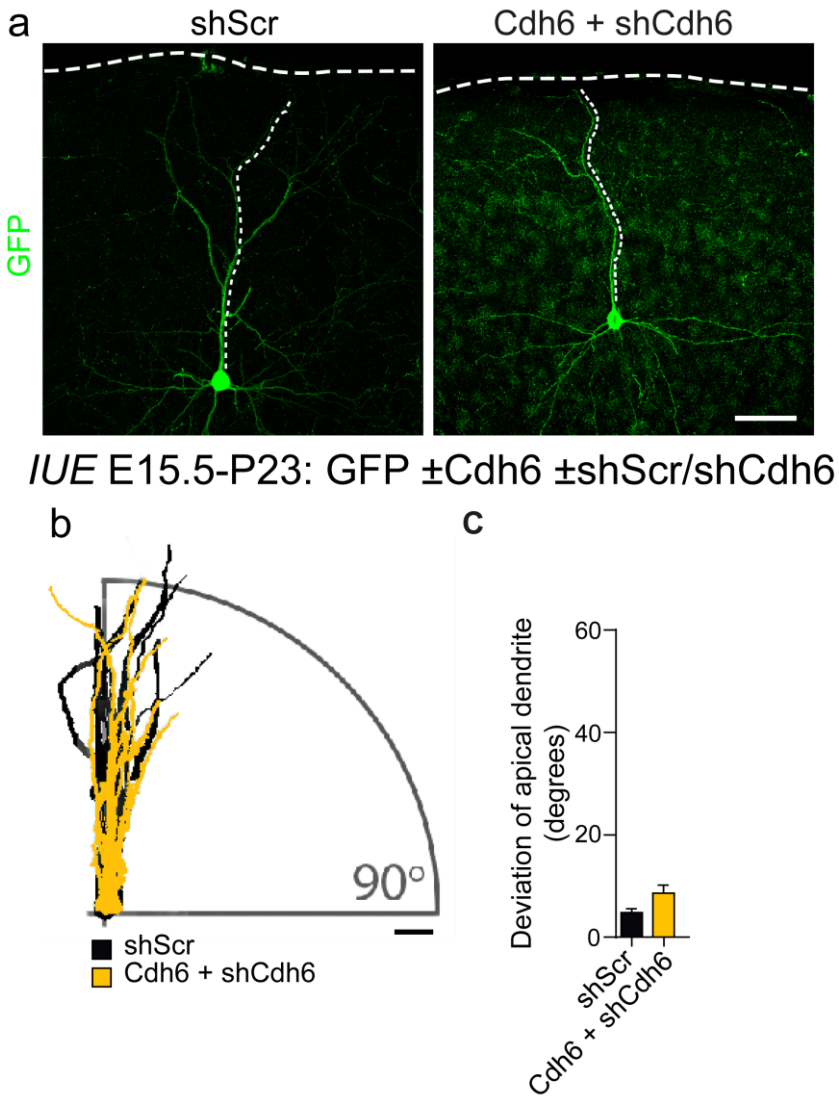

Fig. 30. Validation of the shRNA against Cdh6. a. Representative images of *in utero* electroporated wild type neurons at E15.5 with GFP expressing construct and either shScr or shCdh6 in the presence and absence of Chd6 overexpression construct, brains were analysed at P23. The meningeal surface and apical dendrites are marked with a dotted line. Scale bar = 50μm. **b.** Apical dendrite tracings showing their orientation to the meninges. Scale bar = 50μm. **c.** Quantification of apical dendrite deviation *in vivo*. N = 31 WT + shScr and 58 Cdh6 + shCdh6 cells, 3 brains per condition. One-way ANOVA with Dunn´s multiple comparison test. *** $p < 0.001$; ** $0.001 < p < 0.01$; * $0.01 < p < 0.05$. Results on the graph are represented as averages ± SD. Adapted from Epifanova et al[52].

I then asked whether Cdh6 downregulation could rescue the abnormal dendritic phenotype of the Zeb2 conditional cortical mouse mutant (*Zeb2*$^{fl/fl}$ *Nex*^{Cre}). I downregulated Cdh6 in the neocortex of *Zeb2*$^{fl/fl}$ *Nex*^{Cre} embryos by *IUE* of E15.5 embryos with shCdh6 and GFP expression construct. The wild type control condition was generated using *IUE* of E15.5 *Zeb2*$^{fl/fl}$ embryos with shScr and GFP expression constructs. Apical dendrites of wild type control neurons were oriented normally (perpendicular) to the meningeal surface. Interestingly, Cdh6 downregulation in *Zeb2*$^{fl/fl}$ *Nex*^{Cre} drastically enhanced the angle deviation of the apical dendrites (Fig. 32 a-b; 9.737 ± 5.863 *Zeb2*$^{fl/fl}$ + shScr, 34.43 ± 26.41 *Zeb2*$^{fl/fl}$ *Nex*^{Cre} + shScr and 80.11 ± 48.57 *Zeb2*$^{fl/fl}$ *Nex*^{Cre} + shCdh6; p-value *Zeb2*$^{fl/fl}$ + shScr versus *Zeb2*$^{fl/fl}$ *Nex*^{Cre} + shScr *** <0.001; *Zeb2*$^{fl/fl}$ + shScr versus *Zeb2*$^{fl/fl}$ *Nex*^{Cre} + sh Cdh6 *** <0.001; *Zeb2*$^{fl/fl}$ *Nex*^{Cre} + shScr versus *Zeb2*$^{fl/fl}$ *Nex*^{Cre} + sh Cdh6 *** <0.001).

To test whether Cdh6, like Nrp1, influences radial migration I *in utero* electroporated Cdh6 and GFP expression constructs (pCAG-Cdh6-IRES-GFP and pCAG-IRES-GFP) into E14.5 wild type embryos. The tissue was analysed 4 days later at E18.5. In both wildtype control and Cdh6 overexpression condition, most of the neurons migrated to the top of the CP (bin 1). Cdh6 did not show any influence on radial migration (Fig. 33 a-b; p-value WT versus WT + Cdh6 >0.05).

These data showed the importance of Cdh6 protein levels in the regulation of the apical dendrite orientation.

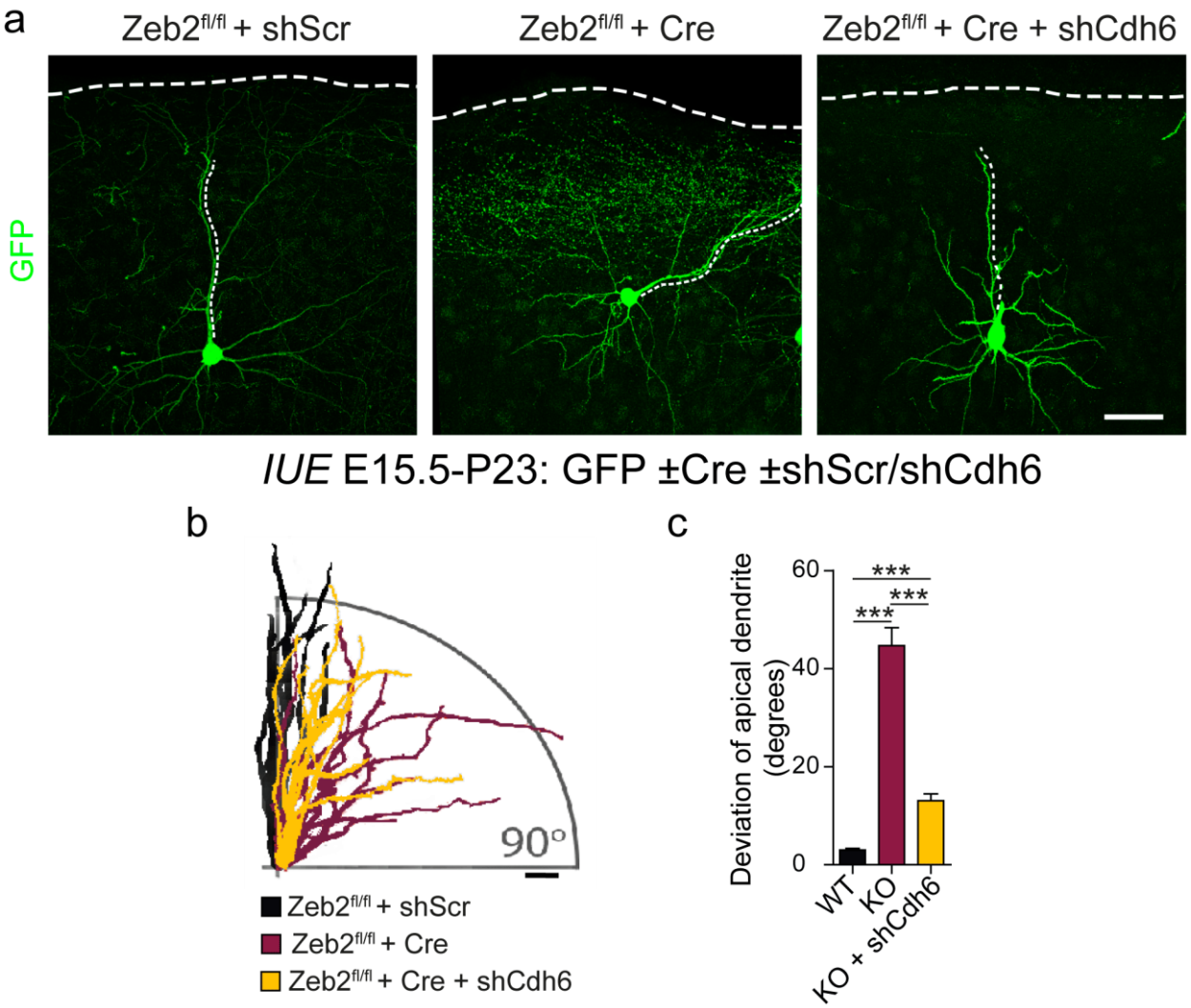

Fig. 31. Cdh6 regulates apical dendrite orientation downstream of Zeb2. a. Representative images of *in utero* electroporated *Zeb2*$^{fl/fl}$ neurons at E15.5 with GFP expressing construct, either shScr or shCdh6 in the presence or absence of Cre expressing construct and analysed at P23. The meningeal surface and apical dendrites are marked with a dotted line. Scale bar = 50μm. **b.** Apical dendrite tracings showing their orientation to the meninges. Scale bar = 50μm. **c.** Quantification of apical dendrite deviation. N = 143 cells, 7 animals of *Zeb2*$^{fl/fl}$ + shScr, 57 cells, 5 animals of *Zeb2*$^{fl/fl}$ + Cre, 85 cells, 4 animals of *Zeb2*$^{fl/fl}$ + Cre + shCdh6 cells. One-way ANOVA (Kruskal-Wallis test) with Dunn´s multiple comparison test. *** $p < 0.001$; ** $0.001 < p < 0.01$; * $0.01 < p < 0.05$. Results on the graph are represented as averages ± SD. Adapted from Epifanova et al[52].

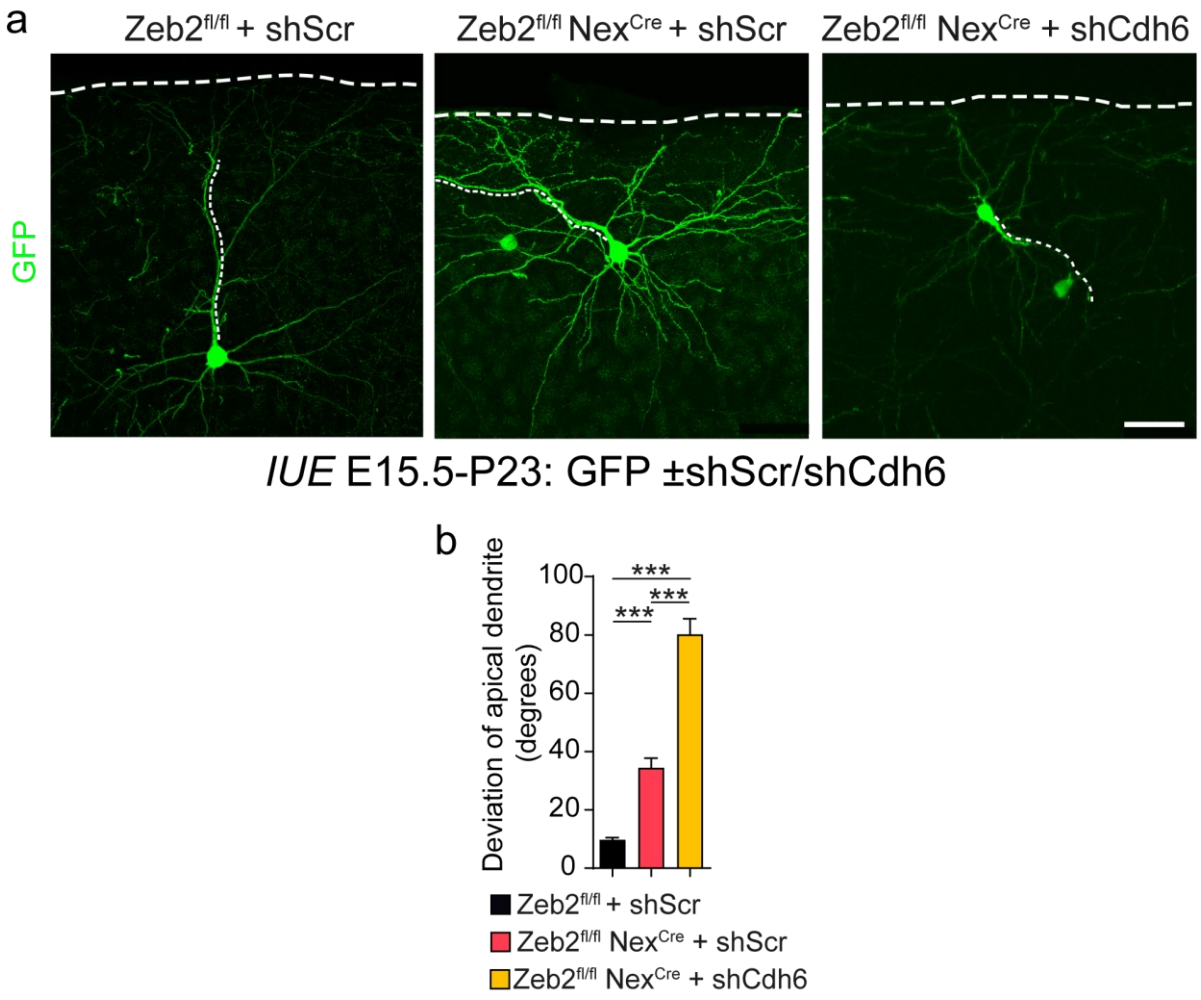

Fig. 32. A tight balance of Cdh6 is crucial for the correct apical dendrite orientation. a. Representative images of *in utero* electroporated *Zeb2*$^{fl/fl}$ and *Zeb2*$^{fl/fl}$ *Nex*^{Cre} neurons at E15.5 with GFP expressing construct and either shScr or shCdh6 and analysed at P23. The meningeal surface and apical dendrites are marked with a dotted line. Scale bar = 50μm. **b.** Quantification of apical dendrite deviation. N = 65cells, 5 animals of *Zeb2*$^{fl/fl}$ + shScr, 65 cells, 5 animals of *Zeb2*$^{fl/fl}$ *Nex*^{Cre} + shScr, 79 cells, 5 animals of *Zeb2*$^{fl/fl}$ *Nex*^{Cre} + shCdh6 cells. One-way ANOVA (Kruskal-Wallis test) with Dunn´s multiple comparison test. *** $p < 0.001$; ** $0.001 < p < 0.01$; * $0.01 < p < 0.05$. Results on the graph are represented as averages ± SD. Adapted from Epifanova et al[52].

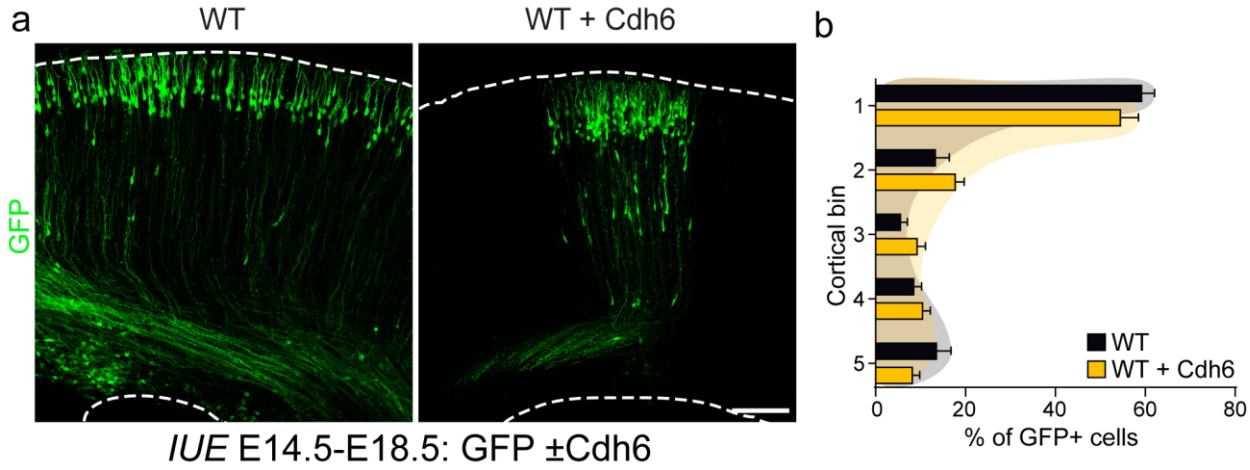

Fig. 33. Cdh6 does not regulate neuronal radial migration. a. Representative images of *in utero* electroporated wild type neurons at E14.5 with GFP expressing construct at the presence or absence of Cdh6 overexpression construct and analysed at E18.5. Cortical area is marked with a dotted line. Scale bar = 100μm. **b.** Quantification of the laminar position of GFP+ neurons *in vivo*. N = 6 WT animals and 10 WT + Cdh6 animals. Two-way ANOVA with Bonferroni post-test. *** $p < 0.001$; ** $0.001 < p < 0.01$; * $0.01 < p < 0.05$. Results on the graph are represented as averages ± SD. Adapted from Epifanova et al[52].

3.2.4. Cdh6 downregulation restores the defective adhesion of Zeb2-deficient neurons

To evaluate the role of Cdh6 in another aspect of Zeb2-deficient phenotype – enhanced cell and matrix adhesion – I analysed the influence of Cdh6 downregulation on cellular adhesion. I dissociated E15.5 *Zeb2*$^{fl/fl}$ cortices in the absence of proteases, nucleofected cells with either shScr or shCdh6 in the presence and absence of Cre expression construct and cultured neurons during 2 days to build up the expression of nucleofected constructs. After 2 days of incubation, I collected and dissociated neurons again in the absence of proteases and this single cell suspension was used primarily for the cell adhesion and cell aggregation assays as described earlier.

Firstly, I analysed the average maximal diameter of cell aggregates in cell adhesion assay. Downregulation of Cdh6 restored the cell-to-cell adhesion of the Zeb2-deficient neurons to normal levels comparable to the wild type control cells (Fig. 34 a-b; 414.780 ± 41µm *Zeb2*$^{fl/fl}$ + shScr, 1342.184 ± 143µm *Zeb2*$^{fl/fl}$ + Cre + shScr and 405.143 ± 103µm *Zeb2*$^{fl/fl}$ + Cre + shCdh6; p-value *Zeb2*$^{fl/fl}$ + shScr versus *Zeb2*$^{fl/fl}$ + Cre + shScr ** <0.01; *Zeb2*$^{fl/fl}$ + Cre + shScr versus *Zeb2*$^{fl/fl}$ + Cre + shCdh6 ** <0.01; *Zeb2*$^{fl/fl}$ + shScr versus *Zeb2*$^{fl/fl}$ + Cre + shCdh6 >0.05).

Next, I tested whether Cdh6 influenced adhesion to the extracellular matrix of Zeb2-deficient neurons. For that, I downregulated Cdh6 Zeb2-deficient neurons. I dissociated E15.5 *Zeb2*$^{fl/fl}$ cortices in the absence of proteases, nucleofected cells with either shScr or shCdh6 and prepared it in the same way as described in the previous paragraph. I then evaluated the lamellipodial spreading of these neurons. Wildtype control neurons tended to extend lamellipodia less than the Zeb2-deficient neurons (Fig. 12 c-d). I unexpectedly found out that Cdh6 also decreases the adhesion of Zeb2-deficient neurons to the extracellular matrix (Fig. 34 c-d; 205 ± 74.5µm *Zeb2*$^{fl/fl}$ + shScr, 396 ± 175µm *Zeb2*$^{fl/fl}$ + Cre + shScr and 264 ± 102.8µm *Zeb2*$^{fl/fl}$ + Cre + shCdh6; p-value *Zeb2*$^{fl/fl}$ + shScr versus *Zeb2*$^{fl/fl}$ + Cre + shScr *** <0.001; *Zeb2*$^{fl/fl}$ + Cre + shScr versus *Zeb2*$^{fl/fl}$ + Cre + shCdh6 >0.05; *Zeb2*$^{fl/fl}$ + shScr versus *Zeb2*$^{fl/fl}$ + Cre + shCdh6 ** <0.01).

Thus, Cdh6 regulates both cell-to-cell and cell-to-extracellular matrix adhesion downstream of Zeb2.

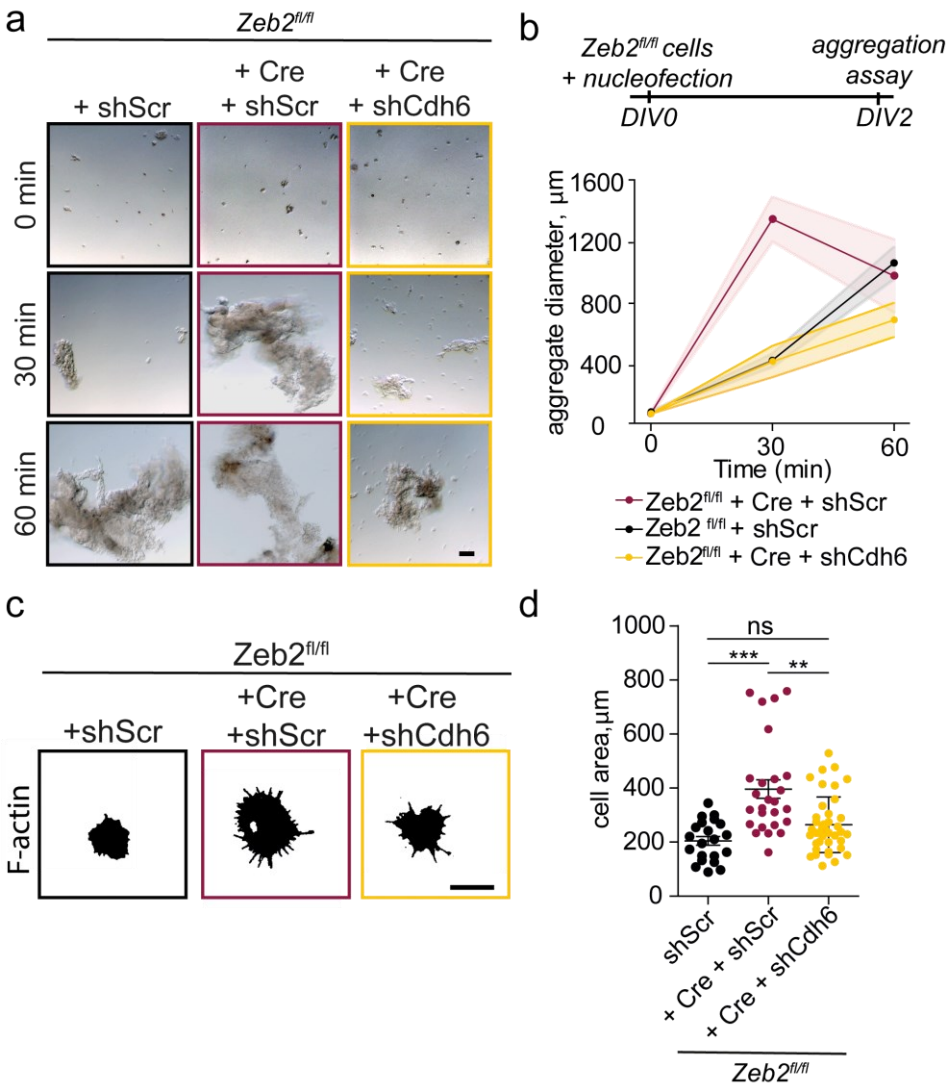

Fig. 34. Cdh6 regulates cell adhesion and adhesion to the extracellular matrix downstream of Zeb2. a-b. Abnormal cell-to-cell adhesion of Zeb2-deficient neurons rescued by Cdh6 downregulation. Aggregation assay. **a.** Representative images of primary cortical neurons in single cell suspensions from E15.5 littermate *Zeb2*$^{fl/fl}$ embryos were nucleofected with either shScr or shCdh6 in the presence or absence of Cre expressing construct. Neurons were plated and allowed to build up the expression for 2 days. Then neurons were detached from coated plates in the absence of proteases and allowed to aggregate under gentle shaking and imaged at 0, 30 and 60 minutes. Scale bar = 100µm. **b.** Quantification of cell aggregate size in cell aggregation assay. Average maximal diameter of cell aggregates was normalised to the average size of control aggregates at the 0 minutes timepoint. N = 15, 10 and 7 aggregates of *Zeb2*$^{fl/fl}$ + shScr; 12, 12, 15 aggregates of *Zeb2*$^{fl/fl}$ + Cre + shScr; 9, 7, 4 aggregates of *Zeb2*$^{fl/fl}$ +Cre + shCdh6. One-way

ANOVA (Kruskal-Wallis) with Dunn´s multiple comparison test. **c-d.** Abnormal adhesion to the extracellular matrix of Zeb2-deficient neurons rescued by Cdh6 downregulation. Adhesion assay. **c.** Representative images of primary cortical neurons in single cell suspensions from E15.5 littermate *Zeb2*$^{fl/fl}$ embryos were nucleofected with either shScr or shCdh6 in the presence or absence of Cre expressing construct. Neurons were plated and allowed to build up the expression for 2 days. Then neurons were detached from coated plates in the absence of proteases and allowed to adhere to laminin and poly-L-lysin coated surfaces for 2 hours, fixed, stained with phalloidin stain (marks F-actin) and imaged. Scale bar = 15µm. **d.** Quantification of lamellipodial spreading. N = 21 *Zeb2*$^{fl/fl}$ + shScr; 36 *Zeb2*$^{fl/fl}$ + Cre + shScr; 41 *Zeb2*$^{fl/fl}$ + Cre + shCdh6 cells. One-way ANOVA (Kruskal-Wallis test) with Dunn´s multiple comparison test. *** $p < 0.001$; ** $0.001 < p < 0.01$; * $0.01 < p < 0.05$. Results on the graph are represented as averages ± SD. Adapted from Epifanova et al[52].

3.2.5. Zeb2 directly binds the Cdh6 promoter region

I asked then whether Cdh6 is a direct downstream target of Zeb2.

Prior to the experiment using UCSC genome browser, FANTOM5 database (https://fantom.gsc.riken.jp/5/) I analysed the Cdh6 gene locus as it was described earlier (see section “Zeb2 directly binds the Nrp1 promoter region”) in order to find a potential promoter region of the Cdh6 gene. Thus, I identified two different regions (TSS1-3) in the region 4Kb upstream and one intron (Intron 2) in the region 2Kb downstream from the Cdh6 transcription start site. Given that Zeb2 is a zinc finger DNA-binding protein it is known that it recognizes one of the known E-box sequences 5’-CACCT(G)-‘3[36]. Within this 6Kb region, I identified 6 CACCTG binding sites. To each of these sites, I created a pair of qPCR primers for the following qPCR analysis (Fig. 35 a-b).

Thus, I performed chromatin immunoprecipitation (ChIP) of E15.5 *Zeb2*$^{fl/fl}$ cortices with the following qPCR analysis. I immunoprecipitated Zeb2-bound chromatin using anti-Zeb2 antibodies, then the isolated chromatin was sonicated into around 200bp pieces, cleared and used for qPCR analysis as a template. qPCR analysis of the chromatin pieces bound by Zeb2 protein showed strong enrichment in all 6 binding sites (3 experimental replicates, Fig. 35c). The previously identified Zeb2 target Ntf3[54] was used as a positive control in qPCR analysis. Enrichment was

compared to the input DNA. All 6 identified binding sites showed strong enrichment in qPCR analysis.

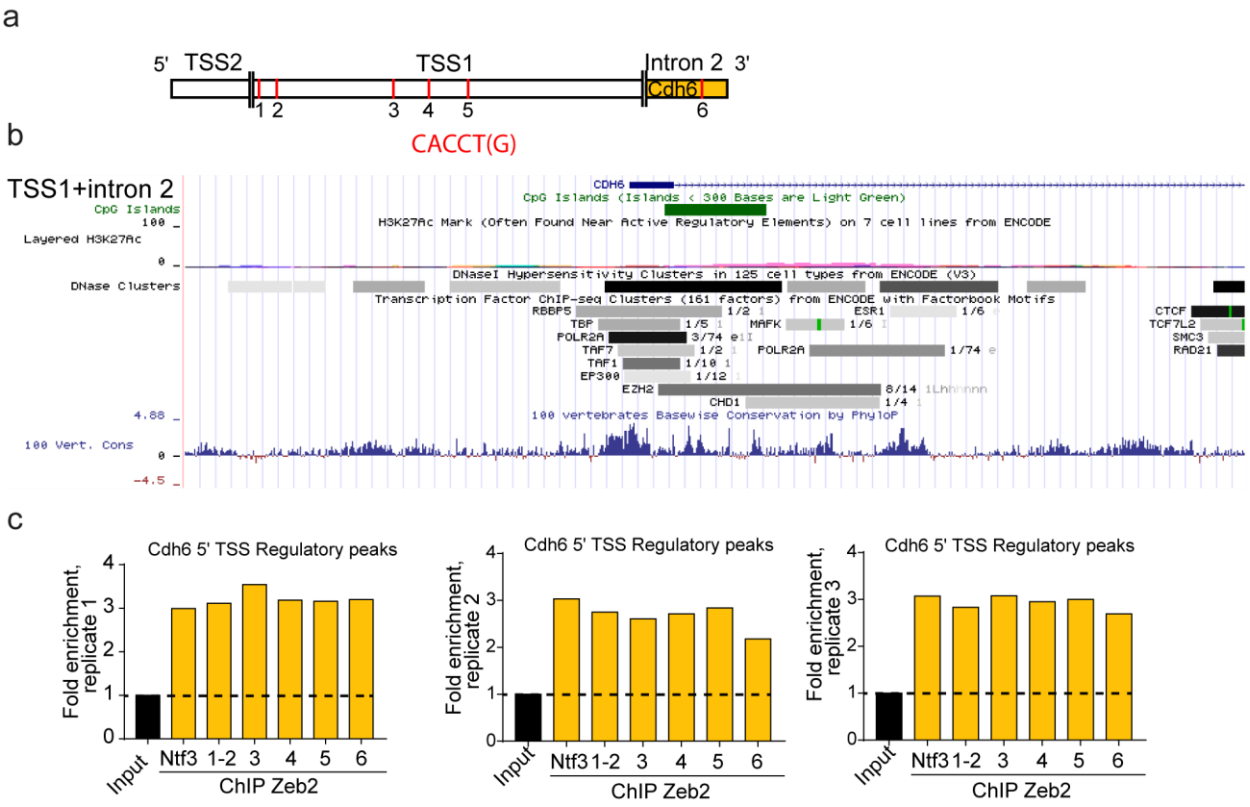

Fig. 35. Cdh6 is a novel downstream target of Zeb2. a. Schematic diagram of the genomic region enclosing 4Kb upstream and 2Kb downstream of the Cdh6 transcriptional start site. **b.** Two different potential transcription start sites (TSS1-2) and one intron region (Intron 2) were identified according to increased CpG islands, H3K27ac modification marks and DNase hypersensitivity clusters (UCSC genome browser, FANTOM5). TSS1 and Intron 2 related human genomic regions are shown. TSS1-2 and Intron 2 regions were analysed for the presence of CACCT(G) sequences which are recognised by zinc finger domains of Zeb2 (numbered 1-6). **c.** Three independent replicates of the ChIP-qPCR from E15.5 are shown. Ntf3 was used as a positive control due to its previous identification as a Zeb2-binding site upstream. Enrichment was compared to the input DNA.

Altogether these data suggested that Zeb2 directly binds the Cdh6 promoter to regulate its expression and Cdh6 is a direct downstream signalling target of Zeb2. Adapted from Epifanova et al[52].

3.2.6. Cdh6 is required for the establishment of apical dendrite orientation

Finally, I assessed the role of Cdh6 in the establishment of the apical dendrite orientation in wild type. At first, I *in utero* electroporated E15.5 wild type embryos with GFP expression construct, shScr and with or without Cdh6 overexpression construct and analysed it prenatally at E18.5 and postnatally at P7 and P23. Apical dendrites of wild type control neurons were oriented normally (perpendicular) to the meningeal surface at all analysed time points. Neurons with overexpression of Cdh6 at E18.5 also had normally oriented apical dendrites (Fig. 36 a-b; 2.801 ± 3.765 degrees WT + shScr versus 3.012 ± 2.815 degrees WT + Cdh6 +shScr; p-value >0.05). However, apical dendrite orientation was significantly affected by Cdh6 overexpression at P7 and P23 (Fig. 36 a-b; at P7: 6.572 ± 6.936 degrees WT + shScr versus 35.56 ± 37.37 degrees WT + Cdh6 + shScr; p-value *** <0.001; at P23: 4.81 ± 4.16 degrees WT + shScr versus 48.7 ± 31.8 degrees WT + Cdh6 + shScr; p-value *** <0.001). These data show that enhanced Cdh6 signalling can disrupt the correct establishment of the apical dendrite orientation with time. Cdh6 overexpression mimics the Zeb2-deficient phenotype and the temporal onset of the apical dendrite deviation happens postnatally in both cases.

Taking into account the effect of downregulation of Cdh6 in *Zeb2*$^{fl/fl}$ *Nex*^{Cre} mutant (Fig. 32) I hypothesised that the Cdh6 balance could be crucial for the correct orientation of apical dendrites also in wild type brains. Thus, I *in utero* electroporated E15.5 wild type embryos with GFP expression construct and either shScr or shCdh6 and analysed animals postnatally at P23. Apical dendrites of wild type control neurons were oriented normally to the meningeal surface. Cdh6 downregulation in wild type brains, however, altered the orientation of the apical dendrite (Fig. 37 a-b; 4.81 ± 4.16 degrees WT + shScr versus 28.1 ± 30.2 degrees WT + shCdh6; p-value *** <0.001). These data suggest that the Cdh6 balance is important for the correct orientation of the apical dendrites.

Cadherins are known to mainly regulate cell-to-cell adhesion through homophilic interactions with cadherins. It has been shown before that Cdh6 is a special cadherin among other cadherins because it contains a special RGD motif in the extracellular compartment which is known to interact with integrins. Integrins, in turn, are known to regulate cell-to-extracellular matrix adhesion. It has been shown that in some nonneuronal cell types Cdh6 with its RGD motif may participate in the signalling which regulates the adhesion of cells to the extracellular matrix[71,72].

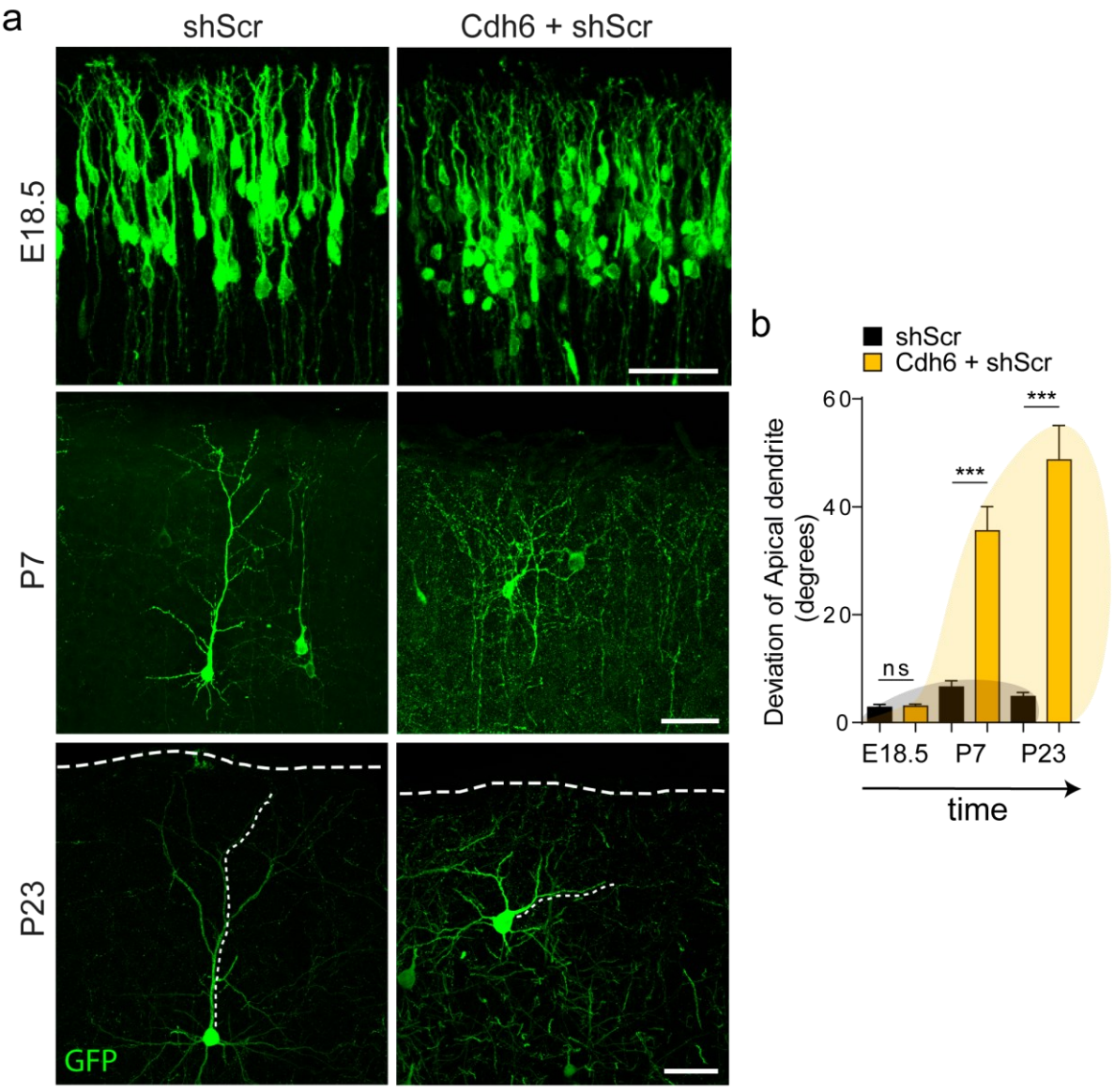

IUE E15.5-E18,5, P7, P23: GFP ±Cdh6 ±shScr

Fig. 36. Cdh6 regulates orientation of apical dendrite postnatally. a. Representative images of *in utero* electroporated at E15.5 wild type neurons with GFP expressing construct and either shScr or Cdh6 overexpression construct and analysed at different developmental time points (E18.5, P7, P23) *in vivo*. Scale bar = 50μm. **b.** Quantification of the apical dendrite deviation at different developmental time points (E18.5, P7, P23). N = 45 cells of WT E18.5 + 47 cells of of Cdh6 E18.5 + 33 cells of WT P7 + 70 cells of Cdh6 P7 + 31 cells of WT P23 + 25 cells of Cdh6 P23, 5 brains per condition. Mann-Whitney test. *** $p < 0.001$; ** $0.001 < p < 0.01$; * $0.01 < p < 0.05$. Results on the graph are represented as averages ± SD. Adapted from Epifanova et al[52].

Since I have shown that Cdh6 regulates both cell-to-cell and cell-to-extracellular matrix adhesion downstream of Zeb2 I asked how Cdh6 can influence the adhesion to the extracellular matrix. To address whether the Cdh6 regulates the apical dendrite orientation through interaction with integrins I, firstly, cloned a Cdh6 expression construct with a mutated RGD motif – Cdh6-RGDmut-IRES-GFP. In order to create a mutation, I changed the sequence for residues p.84G>A and p.85D>E of Cdh6. Similar mutations in other cadherins contained the RGD motif (Cdh5, Cdh17, Cdh16, Cdh20) have been shown to interfere with Cadherins interaction with integrins and thus adhesion to the extracellular matrix but not with interactions with other cadherins and cell-to-cell adhesion [72]. Thus, I *in utero* electroporated E15.5 wild type embryos with GFP and Cdh6-RGDmut expression constructs and compared it to the wild type control and Cdh6 overexpression conditions. Apical dendrites of wild type control neurons were oriented normally to the meningeal surface. Surprisingly, the overexpression of Cdh6-RGDmut in wild type neurons did not affect the apical dendrite orientation (Fig. 37 b-c; 4.81 ± 4.16 degrees WT + shScr, 48.7 ± 31.8 degrees WT + Cdh6 + shScr, 28.1 ± 30.2 degrees WT + shCdh6 and 8.45 ± 13.4 degrees WT + Cdh6-RGDmut + shScr; p-value WT + shScr versus WT + Cdh6-RGDmut + shScr >0.05; WT + Cdh6 +shScr versus WT + Cdh6-RGDmut + shScr *** <0.001 and WT + shCdh6 versus WT + Cdh6-RGDmut + shScr *** <0.001). These data demonstrate that Cdh6 regulates the orientation of the apical dendrite through its RGD motif.

Altogether, Cdh6 regulates cell-to-cell and cell-to-extracellular matrix adhesion *in vivo* both in wild type and Zeb2-deficient neurons. Cdh6 likely acts through downstream interaction with Integrins and it is important for the correct orientation of the apical dendrites *in vivo*.

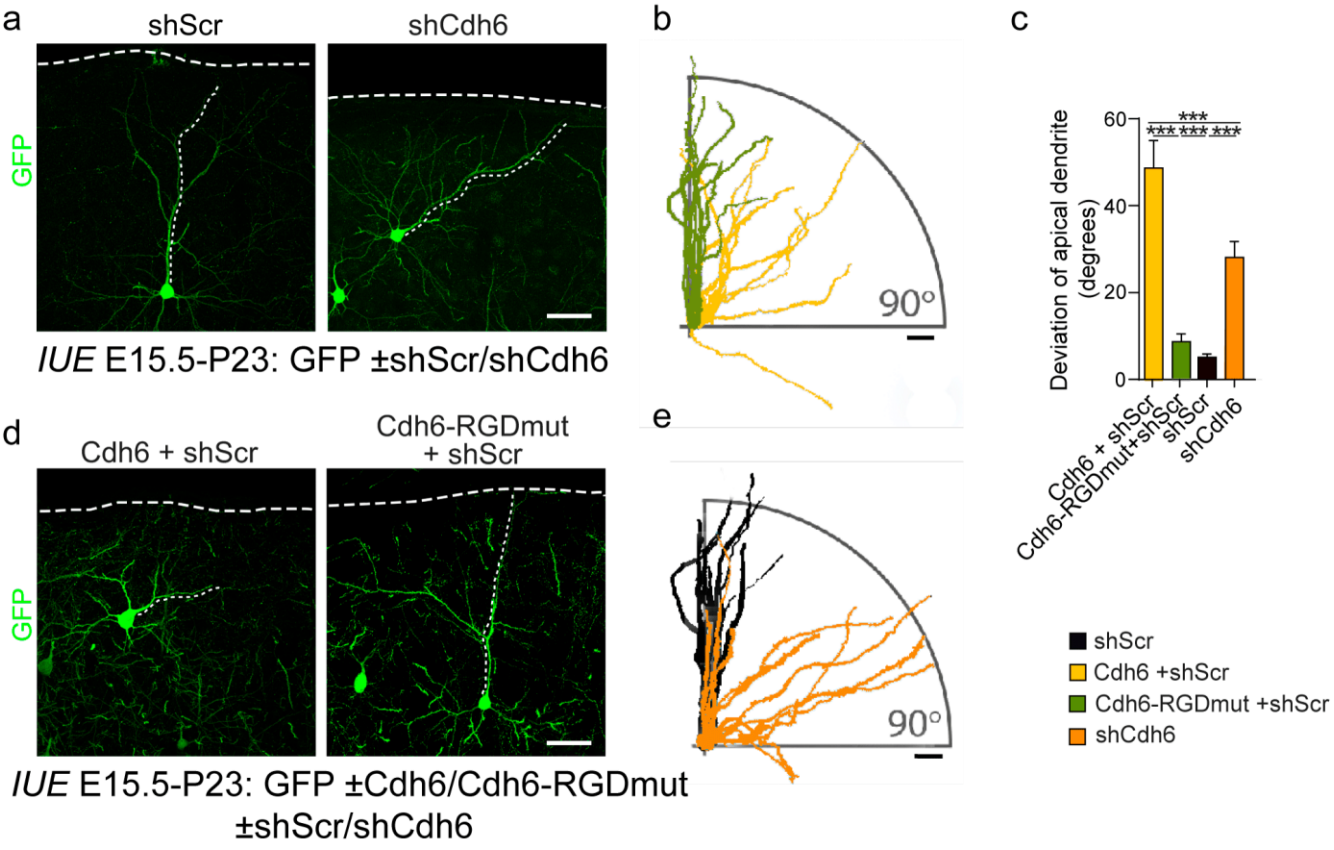

Fig. 37. Cdh6 is essential for the correct establishment of apical dendrite orientation and it regulates apical dendrite orientation through its RGD motif and Integrin signalling. a. Representative images of *in utero* electroporated *Zeb2*$^{fl/fl}$ neurons at E15.5 with GFP expressing construct and either shScr or shCdh6 at P23. The meningeal surface and apical dendrites are marked with a dotted line. Scale bar = 50μm. **b.** Apical dendrite tracings showing their orientation to the meninges. Scale bar = 50μm. **c.** Quantification of apical dendrite deviation. N = 25 cells, 3 animals of Cdh6 + shScr; 53 cells, 4 animals of Cdh6-RGDmut + shScr; 31 cells, 7 animals of shScr cells; 66 cells, 5 animals shCdh6 cells. One-way ANOVA (Kruskal-Wallis test) with Dunn´s multiple comparison test. Results on the graph are represented as averages ± SD. **d.** Representative images of *in utero* electroporated *Zeb2*$^{fl/fl}$ neurons at E15.5 with GFP expressing construct and either Cdh6

or Cdh6 with modified RGD motif (Cdh6-RGDmut) expressing constructs at P23. The meningeal surface and apical dendrites are marked with a dotted line. Scale bar = 50μm. **e.** Apical dendrite tracings showing their orientation to the meninges. Scale bar = 50μm. *** $p < 0.001$; ** $0.001 < p < 0.01$; * $0.01 < p < 0.05$. Results on the graph are represented as averages ± SD. Adapted from Epifanova et al[52].

4. Discussion

The formation of correct neocortical cytoarchitecture defines proper connectivity and functioning of the brain[3]. The data presented here have shown that transcriptional factor Zeb2 is a key regulator of neuronal adhesion in the developing cortex. Dynamic changes of neuronal adhesion define the onset of radial migration and postmigratory orientation of neurons via two independent molecular pathways: Zeb2/Nrp1/Integrin and Zeb2/Cdh6/Integrin respectively. This is the first time that these pathways have been revealed in neurons (Fig. 38).

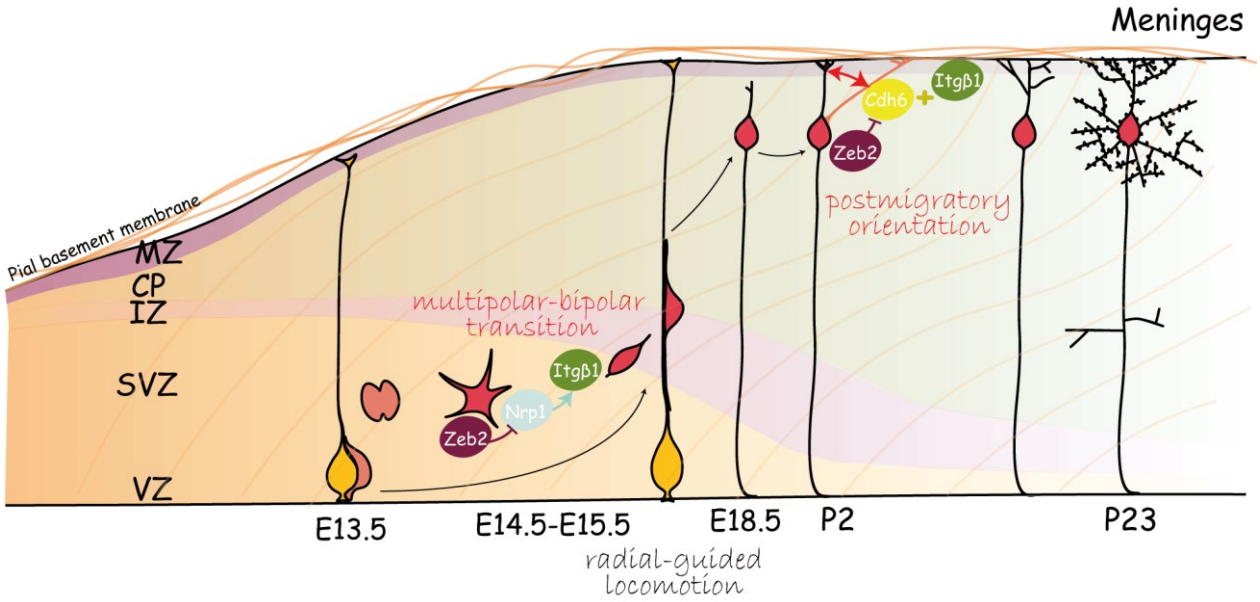

Fig. 38. Regulation of initiation of radial migration and postmigratory orientation during neocortical development. During mouse corticogenesis, new born upper layer cortical neurons (pink) arise from intermediate progenitors (orange) which in turn arise from radial glia cells (yellow). Adhesion prior to radial locomotion is tightly regulated via Zeb2- Neuropilin1- Integrinβ1 molecular pathway. Postmigratory neuronal adhesion and orientation are regulated through Zeb2- Cadherin6- Integrinβ1 molecular pathway.

4.1. Zeb2/Nrp1/Integrin pathway determines the initiation of radial migration through regulation of adhesion to the extracellular matrix

Radial migration is a key process in the development of cortical neurons. New born cortical neurons undergo several states of neuronal differentiation. Soon after birth, UL neurons acquire a multipolar shape with dynamically extended and retracted neurites in the SVZ of the developing cortex. Before the initiation of migration, neurons typically adopt a bipolar morphology, attach to the radial glia fibers and then move radially along the radial glia fibers from the SVZ through the IZ and finally reach the CP. Once neurons have reached the final position they detach from the radial glia fibers and move up towards pia via somal translocation, make contact with the MZ, orient themselves perpendicular to the meningeal surface and finally initiate the dendritic arbor maturation[7].

Multipolar stage of neuronal development is a crucial step of neuronal migration and disruption of this step has been implicated in a variety of neurodevelopmental defects[73-75]. The multipolar stage represents the transient stage between radial progenitors and polarised migrating cortical neurons[7]. It is mostly characterised by random motions as opposed to directed radial migration during the bipolar stage of neuronal development[10,76]. In this study, I have shown that the transcriptional factor Zeb2 controls the multipolar stage of cortical neurons development by restricting the adhesion of new born neurons to the extracellular matrix through suppression of neurites generation and stimulation of tangential motility of neurons in the multipolar stage (Fig. 9-12). Zeb2 inhibits the neuronal adhesion to the extracellular matrix through suppression of Nrp1/Integrin signalling (Fig. 14-23).

I have shown that Zeb2-deficient cells remain longer in the multipolar stage before the initiation of radial locomotion (Fig. 9). It has been reported before that new born neurons can remain in the multipolar stage in SVZ up to 24 hours[7]. The delay of initiation of the radial locomotion of wild type control neurons in my experiment lies relatively within the normal timing range. In case of Zeb2-deficient neurons, the pause before initiation of migration was longer than 24 hours and the proportion of cells with such a long pause was increased drastically. After all, most of the delayed Zeb2-deficient neurons managed to initiate radial locomotion (Fig. 9). This points out that the delay of radial

migration of Zeb2-deficient neurons happens due to the elongated multipolar phase of neuronal development but not as a result of the disruption of the regular neuronal movement mechanics.

The biological significance of the multipolar stage has not been described fully but there are several potential explanations. Firstly, the multipolar stage can be used for the adjustment of gene and protein expression necessary for the radial migration from the progenitor state to the state of the postmitotic neuron[52]. Secondly, neurons can exploit the multipolar stage for microenvironment exploration in order to find molecular cues for the directed migration[77]. Thirdly, the time in which neurons remain in the multipolar stage may be necessary for the tunning of timing for entering the CP[78]. My data indicate that the multipolar stage may be important for the adjustment of the cell-to-cell and cell-to-extracellular matrix interactions.

Several molecules such as Filamin A (Flna), platelet-activating factor acetylhydrolase 1b (Pafah1b1), Doublecortin (Dcx) and connexin 43 (Cx43) are known to regulate the multipolar stage. Flna, Pafah1b1, Dcx and Cx43 are necessary for neuronal exit from the multipolar stage and mainly control cytoskeleton organisation or production of cytoskeleton components[73,74,79,80]. Closer inspection of the multipolar stage of radial migration of Zeb2-deficient neurons *in vivo* also confirmed the hypothesis of disturbance of the multipolar stage of migration upon loss of Zeb2. Multipolar Zeb2-deficient neurons located in SVZ produce more neurites *in vivo* (Fig. 10). Zeb2-deficient cells may remain longer in the multipolar stage due to increased neuronal adhesion to the extracellular matrix. Moreover, the tangential motility of Zeb2-deficient neurons was significantly decreased which also correlates with the concept of increased neuronal adhesion to the extracellular matrix (Fig 7, 10). My data suggest that Zeb2-deficient neurons, via enhanced Nrp1/Integrin signalling, acquire higher adhesion to the extracellular matrix which alters the multipolar stage of radial migration and does not allow neurons to initiate the transition from the multipolar stage to the bipolar stage of migration on time.

Of note, it has been reported recently that in the non-human primate cortex, only a small fraction of early postmitotic neurons undergoes the multipolar stage while the majority of early neurons exhibit bipolar morphology. On the contrary in the rodent cortex, the majority of new born neurons undergo multipolar stage[81,82]. In primates, early born neurons skip the multipolar stage of migration and arise from polarised apical progenitors. While late born neurons exhibit multipolar stage and arise from non-polar basal progenitors. In this study, I examined

specifically late born neurons which remained longer in the multipolar stage of migration in case of loss of Zeb2. Together, this may suggest, that the multipolar stage of neuronal development seems to be especially important for UL neurons migration.

Besides the multipolar stage, multipolar-to-bipolar transition also is a critical step of migration. It requires the specification of the axon, then the formation and stabilisation of the leading process and orientation of the neuron along the radial glial fibers and perpendicular to the meningeal surface. There is unclear what comes first: the initiation of the cell transition from the multipolar to the bipolar stage or the specification of axon and establishment of neuronal polarity. Likely, these processes happen simultaneously.

The acquisition of neuronal polarity is regulated by intrinsic cell polarity signalling and extracellular signals. An example of intrinsic regulation is N-cadherin (Cdh2). Cdh2 expression is important for the interaction of neurons with radial glia fibers. Reelin/Cdh2 signalling triggers the polarization of multipolar neurons but is not required for radial-guided locomotion and does not affect the multipolar phase itself[23,83]. Furthermore, another example of cell-intrinsic regulation of cell polarity is the regulation of cytoskeletal changes which are needed for acquiring correct neuronal polarity[74,84]. As an example of extracellular regulation, extracellular factors like BDNF and IGF-1 (*in vitro*) and TGF-beta (*in vitro* and *in vivo*) are known to trigger the specification of the axonal polarity[20-22]. I have shown that Zeb2 cell-intrinsically delays multipolar-to-bipolar transition by enhancing the neuronal adhesion to the extracellular matrix. Nevertheless, Zeb2-deficient neurons, after a longer multipolar stage, manage to establish the correct neuronal polarity and progress to the bipolar stage. The enhanced adhesion to the extracellular matrix of Zeb2-deficient neurons after all may be compensated by other regulation factors. The timing of cortical development is tightly regulated and all neurogenic events are expected to take place at a specified time. Thus, the inability of Zeb2-deficient neurons to initiate radial migration on time may be a reason for formation of neurodevelopmental disorder.

Early born neurons undergoing the multipolar stage of migration first specify the pioneering axon and initiate an asymmetric growth. The longest neurite then becomes axon while other neuronal processes develop into dendrites[11]. Centrosome and Golgi complex position defines the future axon and instructs cells to initiate neuronal outgrowth[23]. Typically, the establishment of the leading process is accompanied by the reorientation of the centrosome and the Golgi complex towards the forming leading process[59,85]. Axons and dendrites differ from each other

both structurally and functionally. Comparing to axons, dendrites are less homogeneous structures and the molecular control of establishment of dendritic polarity and development of apical and basolateral dendrites is thought to be more complex[25]. Moreover, dendrite specification in general and apical dendrite in particular has not been studied enough. I have shown that in case of cultured Zeb2-deficient neurons, the centrosome and Golgi complex faced most of the times the not longest neurite (Fig. 11). If I assume that the not longest neurite corresponds to dendrite, Zeb2-deficient neurons prioritised the production of the dendrite at the expense of axonal production. Since axonal and dendritic specification are tightly connected processes, the disturbance of establishment of neuronal polarity in Zeb2-deficient neurons also maybe be the reason for the defective axonal production (multiple axons in Fig. 7 e-g) and navigation[45] and the formation of an overly complex dendritic tree[52] observed previously in the absence of Zeb2.

Neuronal cell fate remains flexible up to the multipolar stage[86]. There are two contrary views in the field as to when the cell fate of new born postmitotic neurons becomes fixed. On the one hand, the cell fate had previously been considered to be fixed at the last division of the neuronal progenitor[87]. On the other hand, it has been suggested that cell fate is predetermined but not fixed at the last division of progenitor and rather remains flexible in new born neurons[86]. Curiously, around 20% of the Zeb2-deficient cells (mostly the one in the SVZ) were negative for both UL and DL markers and did not acquire a particular neuronal cell fate (Fig. 5). This finding rather suggests that the cell fate is predetermined but not fixed and can be influenced by a variety of intracellular and extracellular cues.

4.2. Nrp1 is a novel Zeb2 target

Nrp1 is mainly known as a transmembrane receptor for class 3 semaphorins (Sema3a) and vascular endothelial growth factor (VEGF)[88]. I have shown that Nrp1 is a novel direct downstream target of Zeb2. Zeb2 typically acts as a transcriptional repressor[32]. Zeb2 directly binds the Npr1 promoter and represses Nrp1 expression (Fig. 18). I have shown that Nrp1 regulates laminar distribution of neurons by controlling the initiation of the radial migration without affecting neuronal locomotion itself (Fig. 11-14). This is associated with increased adhesion of neurons to the extracellular matrix through activation of Nrp1/Integrin signalling downstream of Zeb2 (Fig. 19-22).

In the cerebral cortex, Nrp1 is mostly known to participate in Sema3a signalling as a receptor[89]. Indeed, Sema3a acts as a chemoattractive

guidance cue for new born cortical neurons and promotes radial locomotion through interaction with Nrp1[90,91]. If I had too much Sema signalling in case of Zeb2 loss I would expect to see promoted but not delayed radial migration. Since I have shown that loss of Zeb2 specifically affects initiation of radial migration but not the radial locomotion itself, it's unlikely that disturbed neuronal laminar distribution upon Nrp1 overexpression is caused by increased Sema3a signalling.

The role of Nrp1 in radial migration is controversial. Downregulation of Nrp1 at the end of neurogenesis has been shown to cause a severe impairment of radial migration[90] while I have shown that overexpression of Nrp1 impairs laminar distribution of cortical neurons (Fig. 14-15). This controversial effect on radial migration can be explained by targeting the different cortical populations during experiments (in case of downregulation of Nrp1, *IUE* was performed at E16.5, while I carried out *IUE* at E14.5). Also, the experiments were performed using different animal models (rat versus mouse).

Integrins are highly expressed in the developing cortex. Integrins are well-known cell surface receptors for the components of the extracellular matrix such as collagens, laminins and fibronectin and they are known to mediate both cell-to-cell and cell-to-extracellular matrix adhesion. Integrins transduce signal in both directions: from the cell to outside and from the extracellular environment to the cell. In order to transduce signal integrins form a heterodimer molecule consisted of one α and one β subunit. Integrins mediate matrix remodelling[92]. There are about 20 different integrin receptors that are formed using different combinations of 18 α and 8 β subunits[93]. It has been reported that Nrp1 can promote Integrin signalling in a variety of cells (such as endothelial cells, neuroepithelial cells and several types of cancer cells) but previously there no such function was reported in neurons[66,67]. I revealed for the first time that Nrp1 directly binds to Itgβ1 under normal conditions. Moreover, I also detected an enhanced interaction of Nrp1 and Itgβ1 at the protein level in Zeb2-deficient neurons (Fig. 23).

So far, Integrin signalling in neurons has been mostly associated with neuron-to-radial glia fibers adhesion, the correct establishment and outgrowth of radial glia processes and radial glia endfeet anchorage at the pial basement membrane[94]. Itgβ1, in particular, is highly expressed in radial glia cells and required for their proper development[95]. On the contrary, another subunit of a typical Integrin heterodimer - Itgα3, is mostly expressed in migrating neurons and mediates neuron-glial fibers interaction during radial migration[96]. It has been previously reported that Itgβ1 is not essential in migrating neurons for the proper radial glia

guided migration[94,95]. My data indicates that Integrin signalling is important for neuronal adhesion to the extracellular matrix and initiation of radial locomotion. Interestingly though, disturbed laminar distribution of Zeb2-deficient neurons can be restored by inhibition of Integrin signalling through either: downregulation of Nrp1 or overexpression of a dominant-negative form of Itgβ1 (Fig. 14, 21). This suggests that regulation of cortical laminar distribution by Itgβ1 occurs not due to influence of locomotion itself but the multipolar stage preceding radial locomotion through inhibition of adhesion of neurons to the extracellular matrix.

4.3. Zeb2/Cdh6/Integrin pathway controls the postmigratory orientation of neurons through regulation of both: cell-to-cell and cell-to-extracellular matrix adhesion

Correct cortical cytoarchitecture is defined by many factors. Cortical neurons are typically strictly organised into cortical layers. Moreover, neuronal cell bodies and apical dendrites within these layers are normally oriented perpendicular to the meningeal surface and parallel to each other. Despite extensive studies on neuronal development some questions related to neuronal orientation remained unanswered. Does the orientation of the leading process during radial migration define later the orientation of the apical dendrite? And what are the molecules controlling neuronal orientation? In this study, I have identified mechanisms regulating postmigratory orientation of UL neurons. I have shown that postmigratory orientation of neurons occurs independently of radial migration through the major regulation of neuronal adhesion by Zeb2-Cdh6-Integrin pathway.

It is generally believed in the field, that the leading process of most migrating neurons becomes the future apical dendrite[97,98]. That said, it has remained unclear how the leading process transforms into an apical dendrite and how, in particular, the vertical orientation of apical dendrites establishes during neuronal development. The orientation of the leading process during radial migration of neurons is likely determined by attachment to the parallel-oriented radial glial fibers. The correct orientation and growth of radial glia fibers are controlled by Reelin signalling[99]. During embryonic development, Reelin is mostly secreted by Cajal-Retzius cells[100] and specifically regulates attachment of migrating

neurons to the radial glia fibers via N-cadherin-mediated cell adhesion[83,101]. Reelin, through binding to its receptors, promotes the phosphorylation of Dab1. Dab1 acts as an adaptor protein for Reelin and transduces signal inside the cell. This leads to stabilisation of leading processes of migrating neurons during the last stage of radial migration – terminal somal translocation[102]. It has been shown that both losses of Dab1 and Reelin lead to neuronal misorientation similar to a Zeb2-deficient phenotype[103]. Upon loss of Zeb2, misorientation of apical dendrites occurs when radial migration is finished while in case of Reelin deficiency misorientation takes place during the last phase of radial migration. I have revealed that the postmigratory orientation of neurons occurs independently of radial migration and it is established postnatally around P2 (Fig. 26).

Last but not least, Sema3a is also known to regulate the orientation of the apical dendrite towards the meningeal surface. It is highly expressed on the top of the cortex below the MZ[91]. It has been shown that apical dendrite orientation is regulated by Sema3a through Nrp1[91] and Fyn-Cdk5 pathways in cultured slices[104]. Both, Reelin and Sema3a can regulate cytoskeleton organisation and therefore dendritic orientation through a common signalling pathway - Fyn-Cdk5[104]. Although it has been shown that Fyn promotes integrin-mediated adhesion in oligodendrocytes[105], it's not clear whether it does the same in neurons. Remarkably, loss of Reelin or Sema3a also disrupts radial migration[83,90], while loss of Cdh6 does not (Fig. 33). This shows that in case of Reelin and Sema3a signalling neuronal orientation is dependent on radial migration. While in case of Zeb2/Cdh6, radial migration and postmigratory orientation are two independent processes. Thus, it is likely that Zeb2-Cdh6-Integrin pathway controls the orientation of the apical dendrites independently from the molecular pathways described above.

The MZ contains Cajal-Retzius cells that strongly express Reelin. Reeler mice are characterized by the invasion of migrating neurons into MZ[83]. So Reelin likely arrests the neuronal radial migration near MZ. I observed that Zeb2 misoriented cortical neurons are located closer to the meningeal surface (Fig. 25). I have not observed neuronal invasions into the MZ upon loss of Zeb2 or Cdh6. Also, Cdh6 did not affect radial migration. Close position of Zeb2 misoriented neurons is unlikely to happen due to affected radial migration or Reelin signalling but rather connected to abnormal orientation of the apical dendrites, observed upon loss of Zeb2. Also, Zeb2-deficient neurons showed normal apical dendrite length which means that in case of Zeb2 deficiency, unlike Reelin or Sema3a, growth of apical dendrites was not affected. This

allows me to hypothesise that postmigratory orientation also influences the proximity of UL neurons to the meningeal surface and it is not dependent on radial migration.

4.4. Cdh6 is a novel Zeb2 target

Cdh6 is a novel downstream target of Zeb2 and like other members of the Cadherin family, it is known to mediate calcium-dependent cell-to-cell adhesion. The most studied members of Cadherin family are E-cadherin (Cdh1) and N-cadherin (Cdh2) which are known to regulate epithelial–mesenchymal transition[106]. Cadherins preferentially form homodimers but can also signal via heterophilic interactions with other cadherins. Each cadherin typically have a small C-terminal cytoplasmic domain, transmembrane domain and extracellular domain[71]. Cdh6, in particular, is widely expressed in the central nervous system and has been shown to regulate neural tube development[107], axon-target matching in retinal ganglion cells[108] and organisation of hippocampal and neocortical chandelier cells[109].

Cdh6 is one of the atypical cadherins that has an RGD motif in its extracellular part. There are over a hundred Cadherins but only a few have RGD motif - Cdh5, Cdh17, Cdh16 and Cdh20[72]. RGD motif consists of arginine, glycine, and aspartic acid. It has been identified in several extracellular matrix proteins such as fibronectin, laminin and vitronectin which are known Integrin ligands. RGD motif is mainly recognized by Integrins and therefore regulates the adhesion of cells to the extracellular matrix. RGD motif is present in many mammalian species[72]. Altogether, this may indicate that RGD motif is highly specialised and evolutionarily important. Cdh6 typically interacts with other cadherins expressed on cell membranes of other cells promoting cell-to-cell adhesion but also can interact through its RGD motif with integrin heterodimers activating its affinity to integrin ligands[72]. So far Integrin-mediated adhesion through interaction with RGD on Cdh6 has been shown only in non-neuronal cells such as platelets[110] and cancer cells[111].

Both overexpression and downregulation of Cdh6 lead to a severe disturbance of neuronal orientation (Fig. 36, 37). Curiously, Cdh6 protein expression is enriched in the outermost layer of the cerebral cortex – MZ (future Layer 1), where apical dendrite tufts reside, around E18.5-P2. And it is decreased just below the MZ, where apical dendrite shafts can be found (Fig. 29). This provides a gradient of Cdh6 expression which may be used by apical dendrites tips as a key to the establishment of correct postmigratory neuronal orientation. The enrichment of Cdh6

protein expression in the MZ coincides with the presence of the basement membrane in the pia, just above the MZ. Integrin ligands are highly expressed in meningeal basement membrane[112]. The basement membrane is composed of extracellular matrix components: for example, laminins, collagens, nidogen, perlecan, agrin, and fibronectin which are known to be integrin ligands. Integrins ligands are also enriched in the MZ. It has also been shown that Itgβ1 is necessary for the integrity of the basement membrane. Mutation in laminin, the major component of the basement membrane, disrupts the attachment of radial glia cells to the meningeal surface and therefore radial migration. It also affects Cajal-Retzius cells migration into the MZ[113]. Thus, both Cdh6 and Integrin ligands are highly expressed in similar cortical areas: the basement membrane and the MZ and may instruct neurons in which direction postmigratory neuronal orientation should occur. Cdh6 regulates postmigratory neuronal orientation *in vivo* through RGD-mediated integrin binding. Indeed, I have shown that in dissociated cortical neurons Cdh6 promotes not only cell-to-cell adhesion but also cell-to-extracellular matrix adhesion to a similar extent as cells with downregulated Integrin signalling (Fig. 34).

Interestingly, RGD motif is evolutionarily old. Lizards, crocodiles and birds have a mutated version of the RGD motif – KGD. The RGD motif in Cdh17 and vascular endothelial cadherin (VE-Cdh) are evolutionary recent and are present only in placental mammals with the exception of rodents, lagomorphs and carnivores[72]. Cdh6 is the only cadherin whose RGD motif is conserved in human, mouse, and almost any investigated species so far. In mouse, Cdh6 is the only RGD containing Cadherin[112]. This could indicate a crucial function of the Cdh6 RGD domain in brain development.

Not much is known about Cdh6 function in the neocortex. Cdh6 is known to regulate the morphology of the murine barrel cortex and is necessary for the establishment of correct functional areas of layer 4 neurons within the barrel cortex[114]. When overexpressed, Cdh6 disrupts area-specific cell organization in the barrel field. In the light of this, I hypothesize that Cdh6 function in the human cortex might be involved in the formation of cortical columns, which are known to act as functional units of information processing[115]. Moreover, gyrification problems (polymicrogyria and pachygyria) have been reported in some Mowat-Wilson patients[116,117]. This may be related to the misorientation of the apical dendrites upon loss of Zeb2.
It has been shown recently that modulation of the extracellular matrix adhesion can affect folding of the developing brain in humans. Addition of a mixture of hyaluronan and proteoglycan link protein 1 (HAPLN1),

lumican and collagen I to cultures of human fetal neocortex leads to local changes in tissue stiffness and induction of folding of CP. This depends on downstream regulation of ERK signalling[118]. These extracellular matrix components can be recognized by integrins. I have shown that Cdh6 regulates extracellular adhesion through integrin signalling in an RGD-dependent manner. Since gyrification does not take place in the mouse it is impossible to address it using mouse models.

All in all, this study revealed that the transcriptional factor Zeb2 independently regulates both the timely initiation of radial migration and the post-migratory orientation of neurons. This happens through suppression of neuronal adhesion via Nrp1/Integrin and Cdh6/Integrin pathways respectively.

5. Supplementary information

Table 5 (refers to Fig. 4b): Quantification of the laminar distribution of GFP+ neurons in *Zeb2$^{fl/fl}$* and *Zeb2$^{fl/fl}$ Nex^{Cre}* brains *in vivo*

Cortical bin	Zeb2fl/fl	Zeb2fl/fl NexCre	p-value
5	1.178 ± 1.990	14.39 ± 2.080	*** <0.001
4	2.785 ± 2.710	15.49 ± 7.547	*** <0.001
3	2.781 ± 2.057	16.56 ± 5.371	*** <0.001
2	9.759 ± 5.543	23.36 ± 4.908	*** <0.001
1	83.50 ± 8.595	30.20 ± 5.836	*** <0.001
N. of brains	12	5	
N. of cells counted	4029	2639	

Mean ± SD are shown. Statistics: two-way ANOVA with Bonferroni post-hoc test

Table 6 (refers to Fig. 5b): Proportion of GFP+ cells expressing Satb2 or Ctip2

	% Satb+ GFP+ cells		% Ctip2+ GFP+ cells		
	Zeb2fl/fl	Zeb2fl/fl NexCre	Zeb2fl/fl	Zeb2fl/fl NexCre	p-value
Mean ± SD	96.53 ± 1.06	76.5 ± 11.68	0% ± 0	0.09 ± 0.16	* < 0.05
Number of values	3 animals				

Statistics: Two-way ANOVA with Bonferroni post-hoc test

Table 7 (refers to Fig. 6b): Quantification of the laminar distribution of control and cre expressing *Zeb2$^{fl/fl}$* neurons in vivo

Cortical bin	Zeb2fl/fl control	Zeb2fl/fl + Cre	p-value
5	0.938 ± 2.08	17.29 ± 13.16	*** <0.001
4	3.580 ± 3.022	19.68 ± 8.442	*** <0.001
3	3.290 ± 1.874	10.52 ± 5.119	>0.05
2	9.849 ± 4.307	16.94 ± 3.748	>0.05
1	82.34 ± 7.728	35.55 ± 16.23	*** <0.001
N. of brains	11	6	
N. of cells counted	2308	1440	

Mean ± SD are shown. Statistics: two-way ANOVA with Bonferroni post-hoc test

Table 8 (refers to Fig. 7b): Quantification of the number of neurites per cell in control and cre-expressing *Zeb2*$^{fl/fl}$ neurons in SVZ at E18.5

	Zeb2fl/fl control	Zeb2fl/fl + cre	p-value
Mean ± SD	3.000 ± 1.069	5.267 ± 1.280	*** <0.001
Number of values	15	15	

Statistics: unpaired *t* test

Table 9 (refers to Fig. 7c): Quantification of the number of neurites per cell in control and cre-expressing *Zeb2*$^{fl/fl}$ neurons in IZ at E18.5

	Zeb2fl/fl control	Zeb2fl/fl + cre	p-value
Mean ± SD	2.267 ± 0.593	2.533 ± 0.639	>0.05
Number of values	15	15	

Statistics: Mann-Whitney test

Table 10 (refers to Fig. 7d): Quantification of the number of neurites per cell in control and cre-expressing *Zeb2*$^{fl/fl}$ neurons in CP at E18.5

	Zeb2fl/fl control	Zeb2fl/fl + cre	p-value
Mean ± SD	2.400 ± 0.632	3.800 ± 1.521	** <0.01
Number of values	15	15	

Statistics: Mann-Whitney test

Table 11 (refers to Fig. 7e): Quantification of the GFP+ neurons with one or multiple axons in control and *Zeb2*$^{fl/fl}$ *NeuroD1*^{Cre} brains at E18.5

	Zeb2fl/fl		Zeb2fl/fl NexCre		
	One axon	Multiple axons	One axon	Multiple axons	p-value
Mean ± SD	0.818% ± 0.024	0.181% ± 0.024	0.504% ± 0.010	0.495% ± 0.010	*** <0.001
Number of brains	3		3		
Number of cells	194		567		

Statistics: Two-way ANOVA with Bonferroni post-hoc test

Table 12 (refers to Fig. 7f): Quantification of the GFP+ neurons with one or multiple axons in IZ of control and *Zeb2$^{fl/fl}$ NeuroD1^{Cre}* brains at E18.5

	Zeb2fl/fl		Zeb2fl/fl NexCre		
	One axon	Multiple axons	One axon	Multiple axons	p-value
Mean ± SD	0.818% ± 0.024	0.181% ± 0.024	0.504% ± 0.010	0.495% ± 0.010	* < 0.05
Number of brains	3		3		
Number of cells	12		137		

Statistics: Two-way ANOVA with Bonferroni post-hoc test

Table 13 (refers to Fig. 7g): Quantification of the GFP+ neurons with one or multiple axons in *Zeb2$^{fl/fl}$ NexCre* brains in CP versus IZ at E18.5

	IZ		CP		
	One axon	Multiple axons	One axon	Multiple axons	p-value
Mean ± SD	0.5491% ± 0.1031	0.4509% ± 0.1031	0.499% ± 0.006	0.5% ± 0.006	>0.05
Number of brains	3				
Number of cells	137		215		

Statistics: Two-way ANOVA with Bonferroni post-hoc test

Table 14 (refers to Fig. 8b): Validation of the fl-mCherry-stop-fl-GFP reporter construct

Cortical bin	mCherry+ cells	GFP+ cells	p-value
5	27.24 ± 12.42	29.37 ± 10.17	>0.05
4	37.97 ± 10.62	44.35 ± 5.123	>0.05
3	21.06 ± 5.135	16.84 ± 11.00	>0.05
2	11.03 ± 7.491	6.519 ± 3.220	>0.05
1	2.710 ± 4.556	2.921 ± 4.165	>0.05
N. of brains	4		
N. of cells counted	568	558	

Mean ± SD shown. Statistics: Two-way ANOVA with Bonferroni post-hoc test

Table 15 (refers to Fig. 9d): Percentage of mCherry+ (WT) or GFP+ (KO) cells that initiated radial migration during the imaged period

Initiation of migration	mCherry+ (WT)	GFP+ (KO)
0-6 h	0.351	0.029
6-12 h	0.189	0.029
12-24 h	0.081	0.206
24-50 h	0	0.206
Do not migrate	0.378	0.529
Number of values	37	34

Table 16 (refers to Fig. 9f): The timepoints of initiation of radial migration

	mCherry+ cells	GFP+ cells	p-value
Mean ± SD	8.870 ± 5.764	25.85 ± 8.401	*** <0.0001
Number of values	46	41	

Statistics: Mann-Whitney test

Table 17 (refers to Fig. 9g): Speed of cells that started radial migration

	mCherry+ cells	GFP+ cells	p-value
Mean ± SD	11.1 ± 3.54	8.19 ± 3.02	* < 0.05
Number of values	46	41	

Statistics: unpaired *t* test

Table 18 (refers to Fig. 9h): Zeb2 regulates multipolar to bipolar transition

Time (hrs)	mCherry+ cells	GFP+ cells
1	69 .23077	74 .19
2	69 .23077	74 .19
3	69 .23077	74 .19
4	69 .23077	74 .19
5	61 .53846	74 .19
6	61 .53846	74 .19
7	61 .53846	74 .19
8	53 .84615	70 .97
9	53 .84615	70 .97
10	53 .84615	70 .97
11	53 .84615	70 .97
12	53 .84615	70 .97
13	50.0000	70 .97

14	50.00	70 .97
15	50.00	70 .97
16	46 .15385	67 .74
17	42 .30769	67 .74
18	42 .30769	70 .97
19	38 .46154	70 .97
20	34 .61538	70 .97
21	34 .61538	70 .97
22	26 .92308	70 .97
23	23 .07692	70 .97
24	23 .07692	67 .74
25	23 .07692	64 .52
26	23 .07692	64 .52
27	23 .07692	64 .52
28	23 .07692	64 .52
29	23 .07692	61 .29
30	23 .07692	61 .29
31	15 .38461	61 .29
32	15 .38461	58 .06
33	15 .38461	58 .06
34	15 .38461	58 .06
35	11 .53846	58 .06
36	7 .692307	58 .06
37	7 .692307	58 .06
38	7 .692307	58 .06
39	7 .692307	58 .06
40	7 .692307	58 .06
41	7 .692307	54 .84
42	7 .692307	54 .84
43	7 .692307	54 .84
44	3 .846154	54 .84
45	3 .846154	54 .84
46	3 .846154	54 .84
47	3 .846154	54 .84
48	3 .846154	48 .39
49	3 .846154	48 .39
50	3 .846154	48 .39
51	3 .846154	48 .39
52	3 .846154	48 .39
53	3 .846154	48 .39
54	3 .846154	48 .39
55	3 .846154	50 .00
56	3 .846154	50 .00
57	3 .846154	50 .00
58	3 .846154	50 .00
59	3 .846154	50 .00
60	3 .846154	50 .00

61	3 .846154	50 .00
62	3 .846154	50 .00
63	3 .846154	50 .00
64	3 .846154	50 .00
65	3 .846154	50 .00
66	3 .846154	50 .00
67	3 .846154	50 .00
68	3 .846154	50 .00
69	3 .846154	50 .00
70	3 .846154	50 .00
71	3 .846154	50 .00
72	3 .846154	50 .00
73	3 .846154	50 .00
74	3 .846154	50 .00
75	3 .846154	50 .00
76	0 .00	50 .00
77	0 .00	50 .00
78	0 .00	50 .00
79	0 .00	50 .00
80	0 .00	50 .00
81	0 .00	50 .00
82	0 .00	50 .00
83	0 .00	46 .67
84	0 .00	43 .33
85	0 .00	43 .33
86	0 .00	43 .33
87	0 .00	43 .33
88	0 .00	43 .33
89	0 .00	43 .33
90	0 .00	40 .00
91	0 .00	40 .00
92	0 .00	40 .00
93	0 .00	40 .00
94	0 .00	40 .00
95	0 .00	40 .00
96	0 .00	36 .67
97	0 .00	33 .33
98	0 .00	33 .33
99	0 .00	33 .33
100	0 .00	33 .33
101	0 .00	31 .03
102	0 .00	31 .03
103	0 .00	31 .03
104	0 .00	31 .03
105	0 .00	31 .03
106	0 .00	31 .03
107	0 .00	31 .03

108	0 .00	31 .03
109	0 .00	31 .03
110	0 .00	31 .03
111	0 .00	31 .03
112	0 .00	31 .03
113	0 .00	31 .03
114	0 .00	31 .03
115	0 .00	31 .03
116	0 .00	31 .03
117	0 .00	31 .03
118	0 .00	31 .03
119	0 .00	31 .03
120	0 .00	31 .03
121	0 .00	31 .03
122	0 .00	27 .59
123	0 .00	27 .59
124	0 .00	27 .59
125	0 .00	27 .59
126	0 .00	27 .59
127	0 .00	27 .59
128	0 .00	27 .59
129	0 .00	27 .59
130	0 .00	27 .59
131	0 .00	27 .59
132	0 .00	27 .59
133	0 .00	24 .14
134	0 .00	24 .14
135	0 .00	24 .14
136	0 .00	24 .14
137	0 .00	24 .14
138	0 .00	24 .14
139	0 .00	24 .14
140	0 .00	24 .14
141	0 .00	24 .14
142	0 .00	24 .14
143	0 .00	24 .14
144	0 .00	24 .14
145	0 .00	24 .14
146	0 .00	24 .14
147	0 .00	24 .14
148	0 .00	24 .14
149	0 .00	24 .14
150	0 .00	24 .14
151	0 .00	24 .14
152	0 .00	24 .14
153	0 .00	24 .14
154	0 .00	24 .14

155	0 .00	24 .14
156	0 .00	24 .14
157	0 .00	24 .14
158	0 .00	24 .14
159	0 .00	24 .14
160	0 .00	24 .14
161	0 .00	24 .14
162	0 .00	24 .14
163	0 .00	20 .69

Table 19 (refers to Fig. 9j): Zeb2 controls the tangential motility of new born neurons

	WT	KO	p-value
Mean ± SD	9.288 ± 4.707	4.333 ± 1.605	*** <0.001
Number of values	15	15	

Statistics: unpaired *t* test

Table 20 (refers to Fig. 9k): Zeb2 controls the speed of tangential motility

	WT	KO	p-value
Mean ± SD	2.051 ± 0.649	1.216 ± 0.376	*** <0.001
Number of values	15	15	

Statistics: unpaired *t* test

Table 21 (refers to Fig. 10b): Zeb2 controls neuronal multipolar stage

	Zeb2$^{fl/fl}$	*Zeb2*$^{fl/fl}$ *Nex*^{Cre}	p-value
Mean ± SD	5.35 ± 1.496	7.8 ± 1.989	*** <0.001
Number of values	20 cells	20 cells	
	3 animals	3 animals	

Statistics: unpaired *t* test

Table 22 (refers to Fig. 11b): Zeb2 regulates centrosome and Golgi complex position in young neurons

Mean ± SD	*Zeb2*$^{fl/fl}$	*Zeb2*$^{fl/fl}$ *Nex*^{Cre}	p-value
Longest neurite	62.18 ± 5.358	23.54 ± 7.097	*** <0.001
Not longest neurite	32.7 ± 5.143	64.91 ± 7.259	** <0.01
Random position	13.10 ± 12.54	14.94 ± 7.958	>0.05
Number of values	39 cells	102 cells	
	3 animals	4 animals	

Statistics: unpaired *t* test

Table 23 (refers to Fig. 12b): Zeb2 suppresses neuronal adhesion to other cells

Time (min)	*Zeb2*$^{fl/fl}$		*Zeb2*$^{fl/fl}$ *Nex*^{Cre}		p-value
	Mean ± SEM	N. of values	Mean ± SEM	N. of values	
0	1.000 ± 0.140	15	1.031 ± 0.119	12	>0.05
30	0.946 ± 0.124	10	3.709 ± 0.752	12	** <0.01
60	3.264 ± 1.097	7	4.04 ± 0.79	15	>0.05

Statistics: One-way ANOVA with Kruskal-Wallis test

Table 24 (refers to Fig. 12d): Zeb2 suppresses neuronal adhesion to the extracellular matrix

	Zeb2$^{fl/fl}$	*Zeb2*$^{fl/fl}$ *Nex*^{Cre}	p-value
Mean ± SD	319± 245	485±197	*** <0.001
Number of values	43	56	

Statistics: Mann-Whitney test

Table 25 (refers to Fig. 14b): Zeb2 controls neuronal laminar distribution through the repression of Nrp1

Cortical bin	*Zeb2*$^{fl/fl}$ + shScr	*Zeb2*$^{fl/fl}$ + Cre + shScr	*Zeb2*$^{fl/fl}$ + Cre + shNrp1	p-value
5	0.92 ± 2.18	16.08 ± 9.09	4.69 ± 3.86	*Zeb2*$^{fl/fl}$ + shScr vs *Zeb2*$^{fl/fl}$ + Cre ** <0.01 *Zeb2*$^{fl/fl}$ + Cre + shScr vs *Zeb2*$^{fl/fl}$ + Cre + shNrp1 >0.05 *Zeb2*$^{fl/fl}$ + shScr vs *Zeb2*$^{fl/fl}$ + Cre + shNrp1 >0.05
4	3.51 ± 2.81	23.51 ± 14.61	9.53 ± 5.09	*Zeb2*$^{fl/fl}$ + shScr vs *Zeb2*$^{fl/fl}$ + Cre *** <0.001 *Zeb2*$^{fl/fl}$ + Cre + shScr vs *Zeb2*$^{fl/fl}$ + Cre + shNrp1 * <0.05 *Zeb2*$^{fl/fl}$ + shScr vs *Zeb2*$^{fl/fl}$ + Cre + shNrp1 >0.05
3	3.25 ± 1.93	15.57 ± 4.39	7.35 ± 3.69	*Zeb2*$^{fl/fl}$ + shScr vs *Zeb2*$^{fl/fl}$ + Cre * <0.05 *Zeb2*$^{fl/fl}$ + Cre + shScr vs *Zeb2*$^{fl/fl}$ + Cre + shNrp1 >0.05 Zeb2fl/fl + shScr vs *Zeb2*$^{fl/fl}$ + Cre + shNrp1 >0.05
2	9.75 ± 4.53	29.21 ± 26.89	15.63 ± 8.23	Zeb2fl/fl + shScr vs *Zeb2*$^{fl/fl}$ + Cre *** <0.001

				Zeb2$^{fl/fl}$ + Cre + shScr vs *Zeb2*$^{fl/fl}$ + Cre + shNrp1 * <0.05 Zeb2fl/fl + shScr vs Zeb2fl/fl + Cre + shNrp1 >0.05
1	82.57 ± 7.76	15.64 ± 7.48	62.80 ± 14.11	*Zeb2*$^{fl/fl}$ + shScr vs *Zeb2*$^{fl/fl}$ + Cre *** <0.001 *Zeb2*$^{fl/fl}$ + Cre + shScr vs *Zeb2*$^{fl/fl}$ + Cre + shNrp1 *** <0.001 *Zeb2*$^{fl/fl}$ + shScr vs *Zeb2*$^{fl/fl}$ + Cre + shNrp1 *** <0.001
N. of brains	11	5	7	
N. of cells counted	2712	2066	1813	

Mean ± SEM are shown. Statistics: Two-way ANOVA with Bonferroni post-hoc test

Table 26 (refers to Fig. 15b): Nrp1 overexpression disturbs the laminar distribution of UL cortical neurons

Cortical bin	WT	WT+ Nrp1	p-value
5	1.388 ± 1.66	13.29 ± 10.09	WT vs. WT + Nrp1 >0.05
4	3.059 ± 2.55	16.40 ± 8.94	WT vs. WT + Nrp1 * < 0.05
3	4.567 ± 2.79	18.48 ± 5.82	WT vs. WT + Nrp1 * < 0.05
2	15.79 ± 12.99	26.61 ± 20.24	WT vs. WT + Nrp1 >0.05
1	75.19 ± 17.16	25.21 ± 13.74	WT vs. WT + Nrp1 *** <0.001
N. of brains	7	7	
N. of cells counted	1499	1188	

Mean ± SEM are shown. Statistics: Two-way ANOVA with Bonferroni post-hoc test

Table 27 (refers to Fig. 16c): Nrp1 controls the initiation of neuronal radial migration downstream of Zeb2

Time window for initiation of migration (h)	*Zeb2*$^{fl/fl}$ + shScr (WT+ shScr)	*Zeb2*$^{fl/fl}$ +*Cre* + shScr (KO + shScr)	*Zeb2*$^{fl/fl}$ +*Cre* + shNrp1 (KO + shNrp1)	p-value
0-6	74.54546 ± 13.75704	7.792206 ± 7.230861	34.49573 ± 11.12257	WT vs KO *** <0.001 KO vs KO + shNrp1 ** <0.01 WT vs KO + shNrp1 *** <0.001
6-12	9.39394 ± 9.106049	9.752991 ± 4.240621	14.47008 ± 7.675892	WT vs KO >0.05 KO vs KO + shNrp1 >0.05 WT vs KO + shNrp1 >0.05
12-24	0.000 ± 0.000	18.66565 ± 4.640804	29.68376 ± 13.29325	WT vs KO * <0.05 KO vs KO + shNrp1 >0.05 WT vs KO + shNrp1 *** <0.001
24-50	0.000 ± 0.000	22.11612 ± 4.849528	9.34188 ± 2.324205	WT vs KO ** <0.01 KO vs KO + shNrp1 >0.05 WT vs KO + shNrp1 >0.05
None	16.06061 ± 5.326787	41.67304 ± 9.763899	12.00855 ± 6.928219	WT vs KO ** <0.01 KO vs KO + shNrp1 *** <0.001 WT vs KO + shNrp1 >0.05

Number of brains	3	3	3	

Mean ± SD are shown. Statistics: Two-way ANOVA with Bonferroni post-hoc test

Table 28 (refers to Fig. 16d): Nrp1 controls multipolar to bipolar transition downstream of Zeb2

Time (hrs.)	*Zeb2*$^{fl/fl}$ + shScr (WT+ shScr)	*Zeb2*$^{fl/fl}$ +*Cre* + shScr (KO + shScr)	*Zeb2*$^{fl/fl}$ +*Cre* + shNrp1 (KO + shNrp1)
1	69 .23077	74 .19	84 .00
2	69 .23077	74 .19	84 .00
3	69 .23077	74 .19	84 .00
4	69 .23077	74 .19	84 .00
5	61 .53846	74 .19	84 .00
6	61 .53846	74 .19	84 .00
7	61 .53846	74 .19	84 .00
8	53 .84615	70 .97	84 .00
9	53 .84615	70 .97	84 .00
10	53 .84615	70 .97	84 .00
11	53 .84615	70 .97	84 .00
12	53 .84615	70 .97	84 .00
13	50.0000	70 .97	80 .00
14	50.00	70 .97	80 .00
15	50.00	70 .97	84 .00
16	46 .15385	67 .74	84 .00
17	42 .30769	67 .74	84 .00
18	42 .30769	70 .97	84 .00
19	38 .46154	70 .97	84 .00
20	34 .61538	70 .97	84 .00
21	34 .61538	70 .97	84 .00
22	26 .92308	70 .97	84 .00
23	23 .07692	70 .97	84 .00
24	23 .07692	67 .74	84 .00
25	23 .07692	64 .52	84 .00
26	23 .07692	64 .52	84 .00
27	23 .07692	64 .52	84 .00
28	23 .07692	64 .52	84 .00
29	23 .07692	61 .29	84 .00
30	23 .07692	61 .29	84 .00
31	15 .38461	61 .29	84 .00
32	15 .38461	58 .06	84 .00

33	15 .38461	58 .06	84 .00
34	15 .38461	58 .06	84 .00
35	11 .53846	58 .06	84 .00
36	7 .692307	58 .06	84 .00
37	7 .692307	58 .06	80 .00
38	7 .692307	58 .06	80 .00
39	7 .692307	58 .06	80 .00
40	7 .692307	58 .06	80 .00
41	7 .692307	54 .84	80 .00
42	7 .692307	54 .84	76 .00
43	7 .692307	54 .84	72 .00
44	3 .846154	54 .84	72 .00
45	3 .846154	54 .84	72 .00
46	3 .846154	54 .84	64 .00
47	3 .846154	54 .84	60 .00
48	3 .846154	48 .39	56 .00
49	3 .846154	48 .39	56 .00
50	3 .846154	48 .39	56 .00
51	3 .846154	48 .39	48 .00
52	3 .846154	48 .39	44 .00
53	3 .846154	48 .39	44 .00
54	3 .846154	48 .39	44 .00
55	3 .846154	50 .00	44 .00
56	3 .846154	50 .00	44 .00
57	3 .846154	50 .00	40 .00
58	3 .846154	50 .00	40 .00
59	3 .846154	50 .00	40 .00
60	3 .846154	50 .00	36 .00
61	3 .846154	50 .00	29 .17
62	3 .846154	50 .00	29 .17
63	3 .846154	50 .00	29 .17
64	3 .846154	50 .00	29 .17
65	3 .846154	50 .00	25 .00
66	3 .846154	50 .00	25 .00
67	3 .846154	50 .00	25 .00
68	3 .846154	50 .00	25 .00
69	3 .846154	50 .00	25 .00
70	3 .846154	50 .00	25 .00
71	3 .846154	50 .00	25 .00
72	3 .846154	50 .00	25 .00
73	3 .846154	50 .00	25 .00
74	3 .846154	50 .00	25 .00
75	3 .846154	50 .00	25 .00
76	0 .00	50 .00	25 .00

77	0 .00	50 .00	25 .00
78	0 .00	50 .00	20 .83
79	0 .00	50 .00	20 .83
80	0 .00	50 .00	20 .83
81	0 .00	50 .00	20 .83
82	0 .00	50 .00	20 .83
83	0 .00	46 .67	20 .83
84	0 .00	43 .33	20 .83
85	0 .00	43 .33	20 .83
86	0 .00	43 .33	20 .83
87	0 .00	43 .33	20 .83
88	0 .00	43 .33	20 .83
89	0 .00	43 .33	20 .83
90	0 .00	40 .00	20 .83
91	0 .00	40 .00	16 .67
92	0 .00	40 .00	16 .67
93	0 .00	40 .00	16 .67
94	0 .00	40 .00	12 .50
95	0 .00	40 .00	12 .50
96	0 .00	36 .67	8 .33
97	0 .00	33 .33	8 .33
98	0 .00	33 .33	8 .33
99	0 .00	33 .33	8 .33
100	0 .00	33 .33	4 .35
101	0 .00	31 .03	4 .35
102	0 .00	31 .03	4 .35
103	0 .00	31 .03	0 .00
104	0 .00	31 .03	0 .00
105	0 .00	31 .03	0 .00
106	0 .00	31 .03	0 .00
107	0 .00	31 .03	0 .00
108	0 .00	31 .03	0 .00
109	0 .00	31 .03	0 .00
110	0 .00	31 .03	0 .00
111	0 .00	31 .03	0 .00
112	0 .00	31 .03	0 .00
113	0 .00	31 .03	0 .00
114	0 .00	31 .03	0 .00
115	0 .00	31 .03	0 .00
116	0 .00	31 .03	0 .00
117	0 .00	31 .03	0 .00
118	0 .00	31 .03	0 .00
119	0 .00	31 .03	0 .00
120	0 .00	31 .03	0 .00

121	0 .00	31 .03	0 .00
122	0 .00	27 .59	0 .00
123	0 .00	27 .59	0 .00
124	0 .00	27 .59	0 .00
125	0 .00	27 .59	0 .00
126	0 .00	27 .59	0 .00
127	0 .00	27 .59	0 .00
128	0 .00	27 .59	0 .00
129	0 .00	27 .59	0 .00
130	0 .00	27 .59	0 .00
131	0 .00	27 .59	0 .00
132	0 .00	27 .59	0 .00
133	0 .00	24 .14	0 .00
134	0 .00	24 .14	0 .00
135	0 .00	24 .14	0 .00
136	0 .00	24 .14	0 .00
137	0 .00	24 .14	0 .00
138	0 .00	24 .14	0 .00
139	0 .00	24 .14	0 .00
140	0 .00	24 .14	0 .00
141	0 .00	24 .14	0 .00
142	0 .00	24 .14	0 .00
143	0 .00	24 .14	0 .00
144	0 .00	24 .14	0 .00
145	0 .00	24 .14	0 .00
146	0 .00	24 .14	0 .00
147	0 .00	24 .14	0 .00
148	0 .00	24 .14	0 .00
149	0 .00	24 .14	0 .00
150	0 .00	24 .14	0 .00
151	0 .00	24 .14	0 .00
152	0 .00	24 .14	0 .00
153	0 .00	24 .14	0 .00
154	0 .00	24 .14	0 .00
155	0 .00	24 .14	0 .00
156	0 .00	24 .14	0 .00
157	0 .00	24 .14	0 .00
158	0 .00	24 .14	0 .00
159	0 .00	24 .14	0 .00
160	0 .00	24 .14	0 .00
161	0 .00	24 .14	0 .00
162	0 .00	24 .14	0 .00
163	0 .00	20 .69	0 .00

Table 29 (refers to Fig. 16e): Nrp1 controls the speed of migration downstream of Zeb2

	Zeb2$^{fl/fl}$ + shScr (WT+ shScr)	*Zeb2*$^{fl/fl}$ +*Cre* + shScr (KO + shScr)	*Zeb2*$^{fl/fl}$ +*Cre* + shNrp1 (KO + shNrp1)	p-value
Mean ± SD	8.492 ± 4.272	4.249 ± 2.108	5.899 ± 3.662	*Zeb2*$^{fl/fl}$ + shScr vs *Zeb2*$^{fl/fl}$ *Nex*^{Cre} + shScr * <0.05 *Zeb2*$^{fl/fl}$ *Nex*^{Cre} + shScr vs *Zeb2*$^{fl/fl}$ *Nex*^{Cre} + shNrp1 >0.05 *Zeb2*$^{fl/fl}$ + shScr *Zeb2*$^{fl/fl}$ *Nex*^{Cre} + shScr shNrp1 >0.05
Number	9	9	19	

Statistics: One-way ANOVA (Kruskal-Wallis) with Dunn´s multiple comparison test

Table 30 (refers to Fig. 17b): Nrp1 does not regulate centrosome and Golgi complex position in young neurons downstream of Zeb2

Mean ± SD	*Zeb2*$^{fl/fl}$	*Zeb2*$^{fl/fl}$ *Nex*^{Cre}	*Zeb2*$^{fl/fl}$ *Nex*^{Cre} +shNrp1	p-value
Longest neurite	62.18 ± 5.358	23.54 ± 7.097	32.5 ± 6.455	*Zeb2*$^{fl/fl}$ vs *Zeb2*$^{fl/fl}$ *Nex*^{Cre} *** <0.001 *Zeb2*$^{fl/fl}$ vs *Zeb2*$^{fl/fl}$ *Nex*^{Cre} *+shNrp1*** <0.001 *Zeb2*$^{fl/fl}$ *Nex*^{Cre} vs *Zeb2*$^{fl/fl}$ *Nex*^{Cre} *+shNrp1* >0.05
Not longest neurite	32.7 ± 5.143	64.91 ± 7.259	54.06 ± 9.540	*Zeb2*$^{fl/fl}$ vs *Zeb2*$^{fl/fl}$ *Nex*^{Cre} ** <0.01 *Zeb2*$^{fl/fl}$ vs *Zeb2*$^{fl/fl}$ *Nex*^{Cre} *+shNrp1* ** <0.01 *Zeb2*$^{fl/fl}$ *Nex*^{Cre} vs *Zeb2*$^{fl/fl}$ *Nex*^{Cre} *+shNrp1* >0.05
Random position	13.10 ± 12.54	14.94 ± 7.958	20.08 ± 11.36	*Zeb2*$^{fl/fl}$ vs *Zeb2*$^{fl/fl}$ *Nex*^{Cre} >0.05 *Zeb2*$^{fl/fl}$ vs *Zeb2*$^{fl/fl}$ *Nex*^{Cre} *+shNrp1* >0.05

				Zeb2$^{fl/fl}$ *Nex*^{Cre} vs *Zeb2*$^{fl/fl}$ *Nex*^{Cre} *+shNrp1* >0.05
Number of values	39 cells	102 cells	73 cells	
	3 animals	4 animals	5 animals	

Mean ± SD shown. Statistics: Two-way ANOVA with Bonferroni post-hoc test

Table 31 (refers to Fig. 18c): Nrp1 is a novel downstream target of Zeb2. ChIP-qPCR

Fold enrichment	Replicate 1	Replicate 2	Replicate 3
Ntf3	2.991	3.070	3.031
Nrp1-1-2	3.173	3.426	3.300
Nrp1-3	2.969	3.243	3.106
Nrp1-4	3.012	2.488	2.750
Nrp1-5	3.162	3.199	3.180
Nrp1-6	2.944	3.203	3.074
Nrp1-7	2.937	3.279	3.108
Nrp1-8	3.292	3.294	3.293
Nrp1-9	2.990	2.787	2.889
Nrp1-10	1.000	2.838	3.185
Nrp1-11	3.261	3.087	3.174

Table 32 (refers to Fig. 19b): Zeb2 suppresses neuronal adhesion to the extracellular matrix through Nrp1 and ItgB1

	Zeb2$^{fl/fl}$ + shScr	*Zeb2*$^{fl/fl}$ *+Cre* + shScr	*Zeb2*$^{fl/fl}$ *+Cre* + shNrp 1	*Zeb2*$^{fl/fl}$ *+Cre* + ItgB1DN	p-value
Mean ± SD	205± 74.5	396± 175	209± 55	162± 43.2	*Zeb2*$^{fl/fl}$ + shScr vs. *Zeb2*$^{fl/fl}$ *+Cre* + shScr *** <0.001 *Zeb2*$^{fl/fl}$ + shScr vs. *Zeb2*$^{fl/fl}$ *+Cre* + shNrp1 >0.05

					Zeb2$^{fl/fl}$ + shScr vs. *Zeb2*$^{fl/fl}$ +*Cre* + ItgB1DN >0.05 *Zeb2*$^{fl/fl}$ +*Cre* + shScr vs. *Zeb2*$^{fl/fl}$ +*Cre* + shNrp1 *** <0.001 *Zeb2*$^{fl/fl}$ +*Cre* + shScr vs. *Zeb2*$^{fl/fl}$ +*Cre* + ItgB1DN *** <0.001 *Zeb2*$^{fl/fl}$ +*Cre* + shNrp1 vs. *Zeb2*$^{fl/fl}$ +*Cre* + ItgB1DN >0.05
N	21	26	26	22	

Statistics: One-way ANOVA (Kruskal-Wallis test) with Dunn´s multiple comparison test

Table 33 (refers to Fig. 20b): Postmitotic inhibition of Integrin signalling does not alter the laminar distribution of neurons in wildtype animals

Cortical bin	WT	WT + ItgB1DN	p-value
5	1.388 ± 1.663	0.220 ± 0.377	>0.05
4	3.059 ± 2.548	2.105 ± 3.332	>0.05
3	4.567 ± 2.795	5.122 ± 5.838	>0.05
2	15.79 ± 12.99	10.20 ± 7.398	>0.05
1	75.19 ± 17.16	82.36 ± 13.28	>0.05
N. of brains	7	7	
N. of cells counted	1499	992	

Mean ± SD shown. Statistics: Two-way ANOVA with Bonferroni post-hoc test

Table 34 (refers to Fig. 21b): Zeb2 controls neuronal radial migration through inhibition of Integrin signalling

Cortical bin	*Zeb2*$^{fl/fl}$	*Zeb2*$^{fl/fl}$ *Nex*^{Cre}	*Zeb2*$^{fl/fl}$ *Nex*^{Cre} + ItgBDN	p-value
5	1.178 ± 1.990	14.39 ± 2.080	3.258 ± 2.187	*Zeb2*$^{fl/fl}$ vs. *Zeb2*$^{fl/fl}$ *Nex*^{Cre} *** <0.001 *Zeb2*$^{fl/fl}$ vs. *Zeb2*$^{fl/fl}$ *Nex*^{Cre} +pNeuroD-ItgB1DN >0.05 *Zeb2*$^{fl/fl}$ *Nex*^{Cre} vs. *Zeb2*$^{fl/fl}$ *Nex*^{Cre} +pNeuroD-ItgB1DN ** <0.01
4	2.785 ± 2.710	15.49 ± 7.547	5.921 ± 3.173	*Zeb2*$^{fl/fl}$ vs. *Zeb2*$^{fl/fl}$ *Nex*^{Cre} *** <0.001 *Zeb2*$^{fl/fl}$ vs. *Zeb2*$^{fl/fl}$ *Nex*^{Cre} +pNeuroD-ItgB1DN >0.05 *Zeb2*$^{fl/fl}$ *Nex*^{Cre} vs. *Zeb2*$^{fl/fl}$ *Nex*^{Cre} +pNeuroD-ItgB1DN * <0.05
3	2.781 ± 2.057	16.56 ± 5.371	12.62 ± 4.596	*Zeb2*$^{fl/fl}$ vs. *Zeb2*$^{fl/fl}$ *Nex*^{Cre} *** <0.001 *Zeb2*$^{fl/fl}$ vs. *Zeb2*$^{fl/fl}$ *Nex*^{Cre} +pNeuroD-ItgB1DN ** <0.01 *Zeb2*$^{fl/fl}$ *Nex*^{Cre} vs. *Zeb2*$^{fl/fl}$ *Nex*^{Cre} +pNeuroD-ItgB1DN >0.05
2	9.759 ± 5.543	23.36 ± 4.908	23.41 ± 5.494	*Zeb2*$^{fl/fl}$ vs. *Zeb2*$^{fl/fl}$ *Nex*^{Cre} *** <0.001 *Zeb2*$^{fl/fl}$ vs. *Zeb2*$^{fl/fl}$ *Nex*^{Cre} +pNeuroD-ItgB1DN *** <0.001 *Zeb2*$^{fl/fl}$ *Nex*^{Cre} vs. *Zeb2*$^{fl/fl}$ *Nex*^{Cre} +pNeuroD-ItgB1DN >0.05
1	83.5 ± 8.595	30.2 ± 5.836	54.8 ± 11.89	*Zeb2*$^{fl/fl}$ vs. *Zeb2*$^{fl/fl}$ *Nex*^{Cre} *** <0.001 *Zeb2*$^{fl/fl}$ vs. *Zeb2*$^{fl/fl}$ *Nex*^{Cre} +pNeuroD-ItgB1DN *** <0.001 *Zeb2*$^{fl/fl}$ *Nex*^{Cre} vs. *Zeb2*$^{fl/fl}$ *Nex*^{Cre} +pNeuroD-ItgB1DN *** <0.001
N. of brains	12	5	5	

N. of cells counted	4029	2639	2588	

Mean ± SD are shown. Statistics: two-way ANOVA with Bonferroni post-hoc test

Table 35 (refers to Fig. 22b): Nrp1 regulates neuronal radial migration through Integrin signalling

Cortical bin	WT	WT+ Nrp1	WT + Nrp1 + ItgB1DN	p-value
5	1.388 ± 1.66	13.29 ± 10.09	3.888 ± 3.423	WT vs. WT + Nrp1 >0.05 WT vs. WT + Nrp1 + pNeuroD-ItgB1DN >0.05 WT + Nrp1 vs. WT + Nrp1 + pNeuroD-ItgB1DN >0.05
4	3.059 ± 2.55	16.40 ± 8.94	7.939 ± 5.214	WT vs. WT + Nrp1 * < 0.05 WT vs. WT + Nrp1 + pNeuroD-ItgB1DN >0.05 WT + Nrp1 vs. WT + Nrp1 + pNeuroD-ItgB1DN >0.05
3	4.567 ± 2.79	18.48 ± 5.82	8.589 ± 5.068	WT vs. WT + Nrp1 * < 0.05 WT vs. WT + Nrp1 + pNeuroD-ItgB1DN >0.05 WT + Nrp1 vs. WT + Nrp1 + pNeuroD-ItgB1DN >0.05
2	15.79 ± 12.99	26.61 ± 20.24	16.81 ± 4.958	WT vs. WT + Nrp1 >0.05 WT vs. WT + Nrp1 + pNeuroD-ItgB1DN >0.05 WT + Nrp1 vs. WT + Nrp1 + pNeuroD-ItgB1DN >0.05
1	75.19 ± 17.16	25.21 ± 13.74	62.78 ± 12.76	WT vs. WT + Nrp1 *** <0.001 WT vs. WT + Nrp1 + pNeuroD-ItgB1DN * < 0.05

				WT + Nrp1 vs. WT + Nrp1 + pNeuroD-ItgB1DN *** <0.001
N. of brains	7	7	9	
N. of cells counted	1499	1188	3249	

Mean ± SEM are shown. Statistics: Two-way ANOVA with Bonferroni post-hoc test

Table 36 (refers to Fig. 23b): Nrp1 and ItgB1 interaction is increased in Zeb2-deficient neurons. Quantification of PLA intensity

	Zeb2$^{fl/fl}$	*Zeb2*$^{fl/fl}$ *Nex*^{Cre}	p-value
Mean ± SD	291082 ± 80679	334587 ± 79286	* < 0.05
Number of values	44	53	

Statistics: unpaired *t* test

Table 37 (refers to Fig. 23c): Nrp1 and ItgB1 interaction is increased in Zeb2-deficient neurons. Quantification of PLA clusters per cell

	Zeb2$^{fl/fl}$	*Zeb2*$^{fl/fl}$ *Nex*^{Cre}	p-value
Mean ± SD	0.111 ± 0.048	0.203 ± 0.048	*** <0.001
Number of values	26	25	

Statistics: unpaired *t* test

Table 38 (refers to Fig. 24b): Zeb2 regulates the neuronal orientation of UL neurons but not DL neurons

	Zeb2$^{fl/fl}$		*Zeb2*$^{fl/fl}$ *Nex*^{Cre}		p-value
	UL	DL	UL	DL	
Mean ± SD	4.254± 5.310	6.494± 18.69	37.96± 40.54	4.598± 3.319	UL*** <0.001 DL >0.05
Number of values	23	43	20	27	

Statistics: One-way ANOVA (Kruskal-Wallis test) with Dunn´s multiple comparison test

Table 39 (refers to Fig. 25c): Loss of Zeb2 leads to overmigration of UL neurons at P23

Cortical bin	*Zeb2*$^{fl/fl}$ control	*Zeb2*$^{fl/fl}$ + Cre	p-value
5	0±0	2.63±4.56	>0.05
4	0.22±0.37	0.44±0.76	>0.05
3	0.80±1.39	0±0	>0.05
2	31.49±8.04	1.09±1.89	*** <0.001
1	67.49±8.43	95.84±4.67	*** <0.001
N. of brains	3	3	
N. of cells counted	254	183	

Mean ± SD shown. Statistics: Two-way ANOVA with Bonferroni post-hoc test

Table 40 (refers to Fig. 25d): Length of the apical dendrite at P23

	Zeb2$^{fl/fl}$	*Zeb2*$^{fl/fl}$ *Nex*^{Cre}	p-value
Mean ± SD	279.1 ± 55.29	266.9 ± 52.67	>0.05
Number of values	26	23	

Statistics: Welch's *t* test

Table 41 (refers to Fig. 26b): Zeb2 regulates the orientation of apical dendrite starting from P2 and onwards

Age		*Zeb2*$^{fl/fl}$	*Zeb2*$^{fl/fl}$ *Nex*^{Cre}	p-value
E18.5	Mean ± SD	2.209 ± 3.888	2.622 ± 3.189	>0.05
	Number of values	40	33	
P2	Mean ± SD	2.683 ± 2.801	22.423 ± 39.207	*** <0.001
	Number of values	36	56	
P7	Mean ± SD	6.572 ± 6.936	35.218 ± 33.944	*** <0.001
	Number of values	33	22	

P23	Mean ± SD	9.737 ± 5.863	34.43 ± 26.41	*** <0.001
	Number of values	65	65	

Statistics: Mann-Whitney test

Table 42 (refers to Fig. 27b): Nrp1 regulates radial migration but not the orientation of the apical dendrite

	Zeb2$^{fl/fl}$ + shScr	*Zeb2*$^{fl/fl}$ + Cre + shScr	*Zeb2*$^{fl/fl}$ + Cre + shNrp1	p-value
Mean ±SD	3.040 ± 4.349	15.17± 15.10	13.15± 16.35	WT vs KO *** <0.001 KO vs KO+shNrp1 >0.05 WT vs KO + shNrp1 *** <0.001
Number of values	143	49	64	

Statistics: One-way ANOVA (Kruskal-Wallis) with Dunn´s Multiple Comparison test

Table 43 (refers to Fig. 28b): Nrp1 does not control the apical dendrite orientation

	WT	WT + Nrp1	p-value
Mean ± SD	4.01 ± 4.67	5.61 ± 6.15	>0.05
Number of animals	3	3	
Number of values	22	25	

Statistics: Mann-Whitney test

Table 44 (refers to Fig. 29b): Upregulation and mislocalisation of Cdh6 under loss of Zeb2 at E18.5

	Zeb2$^{fl/fl}$	*Zeb2*$^{fl/fl}$ *Nex*^{Cre}	p-value
Mean ± SD	1.585 ± 0.065	1.259 ± 0.079	** <0.01
Number of values	3	3	

Statistics: Unpaired *t* test

Table 45 (refers to Fig. 29d): Upregulation and mislocalisation of Cdh6 under loss of Zeb2 at P2

	Zeb2$^{fl/fl}$	*Zeb2*$^{fl/fl}$ *Nex*^{Cre}	p-value
Mean ± SD	1.584 ± 0.118	1.173 ± 0.115	* <0.05
Number of values	3	3	

Statistics: Unpaired *t* test

Table 46 (refers to Fig. 30c): Validation of the shRNA against Cdh6

	shScr	Cdh6 + shCdh6	p-value
Mean ± SD	4.81 ± 4.16	8.59 ± 12.2	shScr vs Cdh6 + shCdh6 >0.05
Number of animals	7	3	
Number of values	31	58	

Mean ± SD shown. Statistics: Two-way ANOVA with Bonferroni post-hoc test

Table 47 (refers to Fig. 31c): Cdh6 regulates apical dendrite orientation downstream of Zeb2

	Zeb2$^{fl/fl}$ + shScr	*Zeb2*$^{fl/fl}$ + Cre	*Zeb2*$^{fl/fl}$ + Cre + shCdh6	p-value
Mean ± SD	3.040 ± 4.349	44.68 ± 27.72	13.09 ± 12.47	*Zeb2*$^{fl/fl}$ + shScr vs *Zeb2*$^{fl/fl}$ + Cre + shCdh6 *** <0.001
Number of animals	7	5	4	*Zeb2*$^{fl/fl}$ + shScr vs *Zeb2*$^{fl/fl}$ + Cre *** <0.001
Number of values	143	57	85	*Zeb2*$^{fl/fl}$ + Cre + shCdh6 vs *Zeb2*$^{fl/fl}$ + Cre *** <0.001

Statistics: One-way ANOVA (Kruskal-Wallis test) with Dunn´s multiple comparison test

Table 48 (refers to Fig. 32b): Tight balance of Cdh6 is crucial for the correct apical dendrite orientation

	Zeb2$^{fl/fl}$ + shScr	*Zeb2*$^{fl/fl}$ *Nex*^{Cre} + shScr	*Zeb2*$^{fl/fl}$ *Nex*^{Cre} + shCdh6	p-value
Mean ± SD	9.737 ± 5.863	34.43 ± 26.41	80.11 ± 48.57	*Zeb2*$^{fl/fl}$ + shScr vs *Zeb2*$^{fl/fl}$ *Nex*^{Cre} + shScr *** <0.001
Number of animals	5	5	5	*Zeb2*$^{fl/fl}$ + shScr vs *Zeb2*$^{fl/fl}$ *Nex*^{Cre} + sh Cdh6 *** <0.001
Number of values	65	65	79	*Zeb2*$^{fl/fl}$ *Nex*^{Cre} + shScr vs *Zeb2*$^{fl/fl}$ *Nex*^{Cre} + sh Cdh6 *** <0.001

Statistics: One-way ANOVA (Kruskal-Wallis test) with Dunn´s multiple comparison test

Table 49 (refers to Fig. 33b): Cdh6 does not regulate neuronal radial migration

Cortical bin	Control (WT)	+ Cdh6	p-value
5	13.52 ± 7.994	8.173 ± 5.164	>0.05
4	8.487 ± 4.325	10.43 ± 5.400	>0.05
3	5.532 ± 3.763	9.219 ± 5.981	>0.05
2	13.28 ± 7.558	17.72 ± 6.351	>0.05
1	59.19 ± 7.069	54.45 ± 12.803	>0.05
N. of brains	6	10	
N. of cells counted	1391	3512	

Mean ± SD shown. Statistics: Two-way ANOVA with Bonferroni post-hoc test

Table 50 (refers to Fig. 34b): Cdh6 regulates cell adhesion downstream of Zeb2. Aggregation assay

Time (min)	*Zeb2*$^{fl/fl}$ + shScr		*Zeb2*$^{fl/fl}$ + Cre + shScr		*Zeb2*$^{fl/fl}$ + Cre + shCdh6		p-value
	Mean ± SEM	N. of values	Mean ± SEM	N. of values	Mean ± SEM	N. of values	
0	75.750 ± 8.000	8	63.801 ± 4.000	12	61.832 ± 7	9	*Zeb2*$^{fl/fl}$ + shScr vs *Zeb2*$^{fl/fl}$ + Cre + shScr >0.05 *Zeb2*$^{fl/fl}$ + Cre + shScr vs *Zeb2*$^{fl/fl}$ + Cre + shCdh6 >0.05 *Zeb2*$^{fl/fl}$ + shScr vs *Zeb2*$^{fl/fl}$ +

							Cre + shCdh6 >0.05
30	414.780 ± 41.000	9	1342.184 ± 143.000	3	405.143 ± 103	7	*Zeb2*$^{fl/fl}$ + shScr vs *Zeb2*$^{fl/fl}$ + Cre + shScr ** <0.01 *Zeb2*$^{fl/fl}$ + Cre + shScr vs *Zeb2*$^{fl/fl}$ + Cre + shCdh6 ** <0.01 *Zeb2*$^{fl/fl}$ + shScr vs *Zeb2*$^{fl/fl}$ + Cre + shCdh6 >0.05
60	1055.249 ± 103.000	4	968.816 ± 237.000	3	679.409 ± 112	4	*Zeb2*$^{fl/fl}$ + shScr vs *Zeb2*$^{fl/fl}$ + Cre + shScr >0.05 *Zeb2*$^{fl/fl}$ + Cre + shScr vs *Zeb2*$^{fl/fl}$ + Cre + shCdh6 >0.05 *Zeb2*$^{fl/fl}$ + shScr vs *Zeb2*$^{fl/fl}$ + Cre + shCdh6 >0.05

Statistics: One-way ANOVA (Kruskal-Wallis) with Dunn´s Multiple comparison test

Table 51 (refers to Fig. 34d): Cdh6 regulates adhesion to the extracellular matrix downstream of Zeb2. Adhesion assay

	Zeb2$^{fl/fl}$ + shScr	*Zeb2*$^{fl/fl}$ + Cre + shScr	*Zeb2*$^{fl/fl}$ + Cre + shCdh6	p-value
Mean ± SD	205 ± 74.5	396 ± 175	264 ± 102.8	*Zeb2*$^{fl/fl}$ + shScr vs. *Zeb2*$^{fl/fl}$ + Cre + shScr *** <0.001
Number of values	21	26	41	*Zeb2*$^{fl/fl}$ + shScr vs. *Zeb2*$^{fl/fl}$ + Cre + shCdh6 >0.05 *Zeb2*$^{fl/fl}$ + Cre + shScr vs. *Zeb2*$^{fl/fl}$ + Cre + shCdh6 ** <0.01

Statistics: One-way ANOVA (Kruskal-Wallis test) with Dunn´s multiple comparison test

Table 52 (refers to Fig. 35c): Cdh6 is a novel downstream target of Zeb2. ChIP-qPCR

Fold enrichment	Replicate 1	Replicate 2	Replicate 3
Ntf3	2.991	3.070	3.031
Cdh6-1	2.907	2.752	2.830
Cdh6-2	3.113	2.414	2.764
Cdh6-3	3.546	2.607	3.077
Cdh6-4	3.184	2.716	2.950
Cdh6-5	3.162	2.842	3.002
Cdh6-6	3.201	2.178	2.690

Table 53 (refers to Fig. 36b): Cdh6 regulates the orientation of apical dendrite postnatally

Age		shScr	Cdh6 + shScr	p-value
E18.5	Mean ± SD	2.801 ± 3.765	3.012 ± 2.815	>0.05
	Number of cells	45	47	
	Number of animals	3	5	

P7	Mean ± SD	6.572± 6.936	35.56± 37.37	*** <0.001
	Number of cells	33	70	
	Number of animals	3	5	
P23	Mean ± SD	4.81 ± 4.16	48.7 ± 31.8	*** <0.001
	Number of cells	31	25	
	Number of animals	7	3	

Statistics: One-way ANOVA (Kruskal-Wallis test) with Dunn´s multiple comparison test

Table 54 (refers to Fig. 37c): Cdh6 is essential for the correct establishment of apical dendrite orientation and it regulates apical dendrite orientation through its RGD motif and ItgB1 signalling

	Mean ± SD	Number of animals	Number of values	p-value
shScr	4.81 ± 4.16	7	31	shScr vs Cdh6 + shScr *** <0.001
Cdh6 + shScr	48.7 ± 31.8	3	25	shScr vs shCdh6 *** <0.001
Cdh6 + shCdh6	8.59 ± 12.2	3	58	shScr vs Cdh6 + shCdh6 >0.05
Cdh6-RGDmut + shScr	8.45 ± 13.4	4	53	shScr vs Cdh6-RGDmut + shScr >0.05
shCdh6	28.1 ± 30.2	5	66	Cdh6 + shScr vs shCdh6 >0.05 Cdh6 + shScr vs Cdh6 + shCdh6 *** <0.001 Cdh6 + shScr vs Cdh6-RGDmut + shScr *** <0.001 shCdh6 vs Cdh6 + shCdh6 *** <0.001

				shCdh6 vs Cdh6-RGDmut + shScr *** <0.001 Cdh6 + shCdh6 vs Cdh6-RGDmut + shScr >0.05

Statistics: One-way ANOVA (Kruskal-Wallis test) with Dunn´s multiple comparison test

References

1 Molnar, Z. Evolution of cerebral cortical development. *Brain Behav Evol* **78**, 94-107, doi:10.1159/000327325 (2011).

2 Dan H. Sanes, T. A. R., William A. Harris. *Development of the Nervous System*. Third edn, (2012).

3 Petreanu, L., Mao, T., Sternson, S. M. & Svoboda, K. The subcellular organization of neocortical excitatory connections. *Nature* **457**, 1142-1145, doi:10.1038/nature07709 (2009).

4 Costa, M. R., Kessaris, N., Richardson, W. D., Gotz, M. & Hedin-Pereira, C. The marginal zone/layer I as a novel niche for neurogenesis and gliogenesis in developing cerebral cortex. *J Neurosci* **27**, 11376-11388, doi:10.1523/JNEUROSCI.2418-07.2007 (2007).

5 Ledonne, F. *et al.* Targeted Inactivation of Bax Reveals a Subtype-Specific Mechanism of Cajal-Retzius Neuron Death in the Postnatal Cerebral Cortex. *Cell Rep* **17**, 3133-3141, doi:10.1016/j.celrep.2016.11.074 (2016).

6 Malatesta, P. *et al.* Neuronal or glial progeny: regional differences in radial glia fate. *Neuron* **37**, 751-764, doi:10.1016/s0896-6273(03)00116-8 (2003).

7 Noctor, S. C., Martinez-Cerdeno, V., Ivic, L. & Kriegstein, A. R. Cortical neurons arise in symmetric and asymmetric division zones and migrate through specific phases. *Nat Neurosci* **7**, 136-144, doi:10.1038/nn1172 (2004).

8 Noctor, S. C. *et al.* Dividing precursor cells of the embryonic cortical ventricular zone have morphological and molecular characteristics of radial glia. *J Neurosci* **22**, 3161-3173, doi:20026299 (2002).

9 Nadarajah, B., Alifragis, P., Wong, R. O. & Parnavelas, J. G. Neuronal migration in the developing cerebral cortex: observations based on real-time imaging. *Cereb Cortex* **13**, 607-611, doi:10.1093/cercor/13.6.607 (2003).

10 Tabata, H. & Nakajima, K. Multipolar migration: the third mode of radial neuronal migration in the developing cerebral cortex. *J Neurosci* **23**, 9996-10001 (2003).

11 Barnes, A. P. & Polleux, F. Establishment of axon-dendrite polarity in developing neurons. *Annu Rev Neurosci* **32**, 347-381, doi:10.1146/annurev.neuro.31.060407.125536 (2009).

12 Nadarajah, B. & Parnavelas, J. G. Modes of neuronal migration in the developing cerebral cortex. *Nat Rev Neurosci* **3**, 423-432, doi:10.1038/nrn845 (2002).

13 Nadarajah, B., Brunstrom, J. E., Grutzendler, J., Wong, R. O. & Pearlman, A. L. Two modes of radial migration in early development of the cerebral cortex. *Nat Neurosci* **4**, 143-150, doi:10.1038/83967 (2001).
14 Noctor, S. C., Flint, A. C., Weissman, T. A., Dammerman, R. S. & Kriegstein, A. R. Neurons derived from radial glial cells establish radial units in neocortex. *Nature* **409**, 714-720, doi:10.1038/35055553 (2001).
15 Urbanska, M., Blazejczyk, M. & Jaworski, J. Molecular basis of dendritic arborization. *Acta Neurobiol Exp (Wars)* **68**, 264-288 (2008).
16 Simo, S. & Cooper, J. A. Regulation of dendritic branching by Cdc42 GAPs. *Genes Dev* **26**, 1653-1658, doi:10.1101/gad.199034.112 (2012).
17 Namba, T. *et al.* Extracellular and Intracellular Signaling for Neuronal Polarity. *Physiol Rev* **95**, 995-1024, doi:10.1152/physrev.00025.2014 (2015).
18 Barnes, A. P. *et al.* LKB1 and SAD kinases define a pathway required for the polarization of cortical neurons. *Cell* **129**, 549-563, doi:10.1016/j.cell.2007.03.025 (2007).
19 Polleux, F. & Snider, W. Initiating and growing an axon. *Cold Spring Harb Perspect Biol* **2**, a001925, doi:10.1101/cshperspect.a001925 (2010).
20 Sosa, L. *et al.* IGF-1 receptor is essential for the establishment of hippocampal neuronal polarity. *Nat Neurosci* **9**, 993-995, doi:10.1038/nn1742 (2006).
21 Shelly, M., Cancedda, L., Heilshorn, S., Sumbre, G. & Poo, M. M. LKB1/STRAD promotes axon initiation during neuronal polarization. *Cell* **129**, 565-577, doi:10.1016/j.cell.2007.04.012 (2007).
22 Yi, J. J., Barnes, A. P., Hand, R., Polleux, F. & Ehlers, M. D. TGF-beta signaling specifies axons during brain development. *Cell* **142**, 144-157, doi:10.1016/j.cell.2010.06.010 (2010).
23 Jossin, Y. Polarization of migrating cortical neurons by Rap1 and N-cadherin: Revisiting the model for the Reelin signaling pathway. *Small GTPases* **2**, 322-328, doi:10.4161/sgtp.18283 (2011).
24 Hand, R. *et al.* Phosphorylation of Neurogenin2 specifies the migration properties and the dendritic morphology of pyramidal neurons in the neocortex. *Neuron* **48**, 45-62, doi:10.1016/j.neuron.2005.08.032 (2005).
25 Arikkath, J. Molecular mechanisms of dendrite morphogenesis. *Front Cell Neurosci* **6**, 61, doi:10.3389/fncel.2012.00061 (2012).

26 Jan, Y. N. & Jan, L. Y. Branching out: mechanisms of dendritic arborization. *Nat Rev Neurosci* **11**, 316-328, doi:10.1038/nrn2836 (2010).
27 Lanoue, V. & Cooper, H. M. Branching mechanisms shaping dendrite architecture. *Dev Biol* **451**, 16-24, doi:10.1016/j.ydbio.2018.12.005 (2019).
28 Rosario, M. *et al.* Neocortical dendritic complexity is controlled during development by NOMA-GAP-dependent inhibition of Cdc42 and activation of cofilin. *Genes Dev* **26**, 1743-1757, doi:10.1101/gad.191593.112 (2012).
29 Bourne, J. N. & Harris, K. M. Balancing structure and function at hippocampal dendritic spines. *Annu Rev Neurosci* **31**, 47-67, doi:10.1146/annurev.neuro.31.060407.125646 (2008).
30 Tavosanis, G. Dendritic structural plasticity. *Dev Neurobiol* **72**, 73-86, doi:10.1002/dneu.20951 (2012).
31 Forrest, M. P., Parnell, E. & Penzes, P. Dendritic structural plasticity and neuropsychiatric disease. *Nat Rev Neurosci* **19**, 215-234, doi:10.1038/nrn.2018.16 (2018).
32 Epifanova, E., Babaev, A., Newman, A. G. & Tarabykin, V. Role of Zeb2/Sip1 in neuronal development. *Brain Res* **1705**, 24-31, doi:10.1016/j.brainres.2018.09.034 (2019).
33 Conidi, A. *et al.* Few Smad proteins and many Smad-interacting proteins yield multiple functions and action modes in TGFbeta/BMP signaling in vivo. *Cytokine Growth Factor Rev* **22**, 287-300, doi:10.1016/j.cytogfr.2011.11.006 (2011).
34 Weng, Q. *et al.* Dual-mode modulation of Smad signaling by Smad-interacting protein Sip1 is required for myelination in the central nervous system. *Neuron* **73**, 713-728, doi:10.1016/j.neuron.2011.12.021 (2012).
35 Nelles, L., Van de Putte, T., van Grunsven, L., Huylebroeck, D. & Verschueren, K. Organization of the mouse Zfhx1b gene encoding the two-handed zinc finger repressor Smad-interacting protein-1. *Genomics* **82**, 460-469 (2003).
36 Verschueren, K. *et al.* SIP1, a novel zinc finger/homeodomain repressor, interacts with Smad proteins and binds to 5'-CACCT sequences in candidate target genes. *J Biol Chem* **274**, 20489-20498 (1999).
37 Van de Putte, T. *et al.* Mice lacking ZFHX1B, the gene that codes for Smad-interacting protein-1, reveal a role for multiple neural crest cell defects in the etiology of Hirschsprung disease-mental retardation syndrome. *Am J Hum Genet* **72**, 465-470, doi:10.1086/346092 (2003).

38 Hegarty, S. V., O'Keeffe, G. W. & Sullivan, A. M. BMP-Smad 1/5/8 signalling in the development of the nervous system. *Prog Neurobiol* **109**, 28-41, doi:10.1016/j.pneurobio.2013.07.002 (2013).
39 Rogers, C. D., Saxena, A. & Bronner, M. E. Sip1 mediates an E-cadherin-to-N-cadherin switch during cranial neural crest EMT. *J Cell Biol* **203**, 835-847, doi:10.1083/jcb.201305050 (2013).
40 Miquelajauregui, A. *et al.* Smad-interacting protein-1 (Zfhx1b) acts upstream of Wnt signaling in the mouse hippocampus and controls its formation. *Proc Natl Acad Sci U S A* **104**, 12919-12924, doi:0609863104 [pii]

10.1073/pnas.0609863104 (2007).
41 Seuntjens, E. *et al.* Sip1 regulates sequential fate decisions by feedback signaling from postmitotic neurons to progenitors. *Nat Neurosci* **12**, 1373-1380, doi:10.1038/nn.2409 (2009).
42 van den Berghe, V. *et al.* Directed migration of cortical interneurons depends on the cell-autonomous action of Sip1. *Neuron* **77**, 70-82, doi:10.1016/j.neuron.2012.11.009 (2013).
43 McKinsey, G. L. *et al.* Dlx1&2-dependent expression of Zfhx1b (Sip1, Zeb2) regulates the fate switch between cortical and striatal interneurons. *Neuron* **77**, 83-98, doi:10.1016/j.neuron.2012.11.035 (2013).
44 Hegarty, S. V., Sullivan, A. M. & O'Keeffe, G. W. Targeting transcriptional regulators to regenerate midbrain dopaminergic axons in Parkinson's disease. *Neural Regen Res* **12**, 1814-1815, doi:10.4103/1673-5374.219039 (2017).
45 Srivatsa, S., Parthasarathy, S., Molnar, Z. & Tarabykin, V. Sip1 downstream Effector ninein controls neocortical axonal growth, ipsilateral branching, and microtubule growth and stability. *Neuron* **85**, 998-1012, doi:10.1016/j.neuron.2015.01.018 (2015).
46 Turovskaya, M. V. *et al.* Sip-1 mutations cause disturbances in the activity of NMDA- and AMPA-, but not kainate receptors of neurons in the cerebral cortex. *Neurosci Lett* **650**, 180-186, doi:10.1016/j.neulet.2017.04.048 (2017).
47 Ivanovski, I. *et al.* Phenotype and genotype of 87 patients with Mowat-Wilson syndrome and recommendations for care. *Genet Med* **20**, 965-975, doi:10.1038/gim.2017.221 (2018).

48 Zweier, C. *et al.* Characterisation of deletions of the ZFHX1B region and genotype-phenotype analysis in Mowat-Wilson syndrome. *J Med Genet* **40**, 601-605 (2003).
49 Higashi, Y. *et al.* Generation of the floxed allele of the SIP1 (Smad-interacting protein 1) gene for Cre-mediated conditional knockout in the mouse. *Genesis* **32**, 82-84 (2002).
50 Goebbels, S. *et al.* Genetic targeting of principal neurons in neocortex and hippocampus of NEX-Cre mice. *Genesis* **44**, 611-621, doi:10.1002/dvg.20256 (2006).
51 Ambrozkiewicz, M. C. *et al.* Polarity Acquisition in Cortical Neurons Is Driven by Synergistic Action of Sox9-Regulated Wwp1 and Wwp2 E3 Ubiquitin Ligases and Intronic miR-140. *Neuron* **100**, 1097-1115 e1015, doi:10.1016/j.neuron.2018.10.008 (2018).
52 Epifanova, E. *et al.* Adhesion dynamics in the neocortex determine the start of migration and the post-migratory orientation of neurons. *Sci Adv* **7**, doi:10.1126/sciadv.abf1973 (2021).
53 Polleux, F. & Ghosh, A. The slice overlay assay: a versatile tool to study the influence of extracellular signals on neuronal development. *Sci STKE* **2002**, pl9, doi:10.1126/stke.2002.136.pl9 (2002).
54 Parthasarathy, S., Srivatsa, S., Nityanandam, A. & Tarabykin, V. Ntf3 acts downstream of Sip1 in cortical postmitotic neurons to control progenitor cell fate through feedback signaling. *Development* **141**, 3324-3330, doi:10.1242/dev.114173 (2014).
55 Dyballa, N. & Metzger, S. Fast and sensitive colloidal coomassie G-250 staining for proteins in polyacrylamide gels. *J Vis Exp*, doi:10.3791/1431 (2009).
56 Dimidschstein, J. *et al.* Ephrin-B1 controls the columnar distribution of cortical pyramidal neurons by restricting their tangential migration. *Neuron* **79**, 1123-1135, doi:10.1016/j.neuron.2013.07.015 (2013).
57 Lee, K. K. *et al.* Dominant-negative beta1 integrin mice have region-specific myelin defects accompanied by alterations in MAPK activity. *Glia* **53**, 836-844, doi:10.1002/glia.20343 (2006).
58 Bartolome, R. A. *et al.* VE-cadherin RGD motifs promote metastasis and constitute a potential therapeutic target in melanoma and breast cancers. *Oncotarget* **8**, 215-227, doi:10.18632/oncotarget.13832 (2017).
59 de Anda, F. C. *et al.* Centrosome localization determines neuronal polarity. *Nature* **436**, 704-708, doi:10.1038/nature03811 (2005).

60 Horton, A. C. *et al.* Polarized secretory trafficking directs cargo for asymmetric dendrite growth and morphogenesis. *Neuron* **48**, 757-771, doi:10.1016/j.neuron.2005.11.005 (2005).
61 Kriegstein, A. R. & Dichter, M. A. Morphological classification of rat cortical neurons in cell culture. *J Neurosci* **3**, 1634-1647 (1983).
62 Deaton, A. M. & Bird, A. CpG islands and the regulation of transcription. *Genes Dev* **25**, 1010-1022, doi:10.1101/gad.2037511 (2011).
63 Roadmap Epigenomics, C. *et al.* Integrative analysis of 111 reference human epigenomes. *Nature* **518**, 317-330, doi:10.1038/nature14248 (2015).
64 John, S. *et al.* Genome-scale mapping of DNase I hypersensitivity. *Curr Protoc Mol Biol* **Chapter 27**, Unit 21 27, doi:10.1002/0471142727.mb2127s103 (2013).
65 Niland, S. & Eble, J. A. Neuropilin: Handyman and Power Broker in the Tumor Microenvironment. *Adv Exp Med Biol* **1223**, 31-67, doi:10.1007/978-3-030-35582-1_3 (2020).
66 Valdembri, D. *et al.* Neuropilin-1/GIPC1 signaling regulates alpha5beta1 integrin traffic and function in endothelial cells. *PLoS Biol* **7**, e25, doi:10.1371/journal.pbio.1000025 (2009).
67 Fukasawa, M., Matsushita, A. & Korc, M. Neuropilin-1 interacts with integrin beta1 and modulates pancreatic cancer cell growth, survival and invasion. *Cancer Biol Ther* **6**, 1173-1180, doi:10.4161/cbt.6.8.4363 (2007).
68 Hynes, R. O. Integrins: bidirectional, allosteric signaling machines. *Cell* **110**, 673-687, doi:10.1016/s0092-8674(02)00971-6 (2002).
69 Leone, D. P. *et al.* Regulation of neural progenitor proliferation and survival by beta1 integrins. *J Cell Sci* **118**, 2589-2599, doi:10.1242/jcs.02396 (2005).
70 Semple, B. D., Blomgren, K., Gimlin, K., Ferriero, D. M. & Noble-Haeusslein, L. J. Brain development in rodents and humans: Identifying benchmarks of maturation and vulnerability to injury across species. *Prog Neurobiol* **106-107**, 1-16, doi:10.1016/j.pneurobio.2013.04.001 (2013).
71 Brasch, J. *et al.* Homophilic and Heterophilic Interactions of Type II Cadherins Identify Specificity Groups Underlying Cell-Adhesive Behavior. *Cell Rep* **23**, 1840-1852, doi:10.1016/j.celrep.2018.04.012 (2018).

72 Casal, J. I. & Bartolome, R. A. Beyond N-Cadherin, Relevance of Cadherins 5, 6 and 17 in Cancer Progression and Metastasis. *Int J Mol Sci* **20**, doi:10.3390/ijms20133373 (2019).
73 Nagano, T., Morikubo, S. & Sato, M. Filamin A and FILIP (Filamin A-Interacting Protein) regulate cell polarity and motility in neocortical subventricular and intermediate zones during radial migration. *J Neurosci* **24**, 9648-9657, doi:10.1523/JNEUROSCI.2363-04.2004 (2004).
74 Tsai, J. W., Chen, Y., Kriegstein, A. R. & Vallee, R. B. LIS1 RNA interference blocks neural stem cell division, morphogenesis, and motility at multiple stages. *J Cell Biol* **170**, 935-945, doi:10.1083/jcb.200505166 (2005).
75 Ramos, R. L., Bai, J. & LoTurco, J. J. Heterotopia formation in rat but not mouse neocortex after RNA interference knockdown of DCX. *Cereb Cortex* **16**, 1323-1331, doi:10.1093/cercor/bhj074 (2006).
76 Kriegstein, A. R. & Noctor, S. C. Patterns of neuronal migration in the embryonic cortex. *Trends Neurosci* **27**, 392-399, doi:10.1016/j.tins.2004.05.001 (2004).
77 Inoue, M. *et al.* Prdm8 regulates the morphological transition at multipolar phase during neocortical development. *PLoS One* **9**, e86356, doi:10.1371/journal.pone.0086356 (2014).
78 Inaguma, Y. *et al.* SIL1, a causative cochaperone gene of Marinesco-Sojgren syndrome, plays an essential role in establishing the architecture of the developing cerebral cortex. *EMBO Mol Med* **6**, 414-429, doi:10.1002/emmm.201303069 (2014).
79 Bai, J. *et al.* RNAi reveals doublecortin is required for radial migration in rat neocortex. *Nat Neurosci* **6**, 1277-1283, doi:10.1038/nn1153 (2003).
80 Liu, X., Sun, L., Torii, M. & Rakic, P. Connexin 43 controls the multipolar phase of neuronal migration to the cerebral cortex. *Proc Natl Acad Sci U S A* **109**, 8280-8285, doi:10.1073/pnas.1205880109 (2012).
81 Cortay, V. *et al.* Radial Migration Dynamics Is Modulated in a Laminar and Area-Specific Manner During Primate Corticogenesis. *Front Cell Dev Biol* **8**, 588814, doi:10.3389/fcell.2020.588814 (2020).
82 Betizeau, M. *et al.* Precursor diversity and complexity of lineage relationships in the outer subventricular zone of the primate. *Neuron* **80**, 442-457, doi:10.1016/j.neuron.2013.09.032 (2013).

83 Jossin, Y. & Cooper, J. A. Reelin, Rap1 and N-cadherin orient the migration of multipolar neurons in the developing neocortex. *Nat Neurosci* **14**, 697-703, doi:10.1038/nn.2816 (2011).
84 Kuo, G., Arnaud, L., Kronstad-O'Brien, P. & Cooper, J. A. Absence of Fyn and Src causes a reeler-like phenotype. *J Neurosci* **25**, 8578-8586, doi:10.1523/JNEUROSCI.1656-05.2005 (2005).
85 Hatanaka, Y., Hisanaga, S., Heizmann, C. W. & Murakami, F. Distinct migratory behavior of early- and late-born neurons derived from the cortical ventricular zone. *J Comp Neurol* **479**, 1-14, doi:10.1002/cne.20256 (2004).
86 Mizutani, K. I. Physiological significance of multipolar cells generated from neural stem cells and progenitors for the establishment of neocortical cytoarchitecture. *Genes Cells* **23**, 6-15, doi:10.1111/gtc.12546 (2018).
87 Takahashi, T., Nowakowski, R. S. & Caviness, V. S., Jr. The cell cycle of the pseudostratified ventricular epithelium of the embryonic murine cerebral wall. *J Neurosci* **15**, 6046-6057 (1995).
88 Nakamura, F. & Goshima, Y. Structural and functional relation of neuropilins. *Adv Exp Med Biol* **515**, 55-69, doi:10.1007/978-1-4615-0119-0_5 (2002).
89 Polleux, F., Giger, R. J., Ginty, D. D., Kolodkin, A. L. & Ghosh, A. Patterning of cortical efferent projections by semaphorin-neuropilin interactions. *Science* **282**, 1904-1906, doi:10.1126/science.282.5395.1904 (1998).
90 Chen, G. *et al.* Semaphorin-3A guides radial migration of cortical neurons during development. *Nat Neurosci* **11**, 36-44, doi:10.1038/nn2018 (2008).
91 Polleux, F., Morrow, T. & Ghosh, A. Semaphorin 3A is a chemoattractant for cortical apical dendrites. *Nature* **404**, 567-573, doi:10.1038/35007001 (2000).
92 Yaqoob, U. *et al.* Neuropilin-1 stimulates tumor growth by increasing fibronectin fibril assembly in the tumor microenvironment. *Cancer Res* **72**, 4047-4059, doi:10.1158/0008-5472.CAN-11-3907 (2012).
93 Schmid, R. S. & Anton, E. S. Role of integrins in the development of the cerebral cortex. *Cereb Cortex* **13**, 219-224, doi:10.1093/cercor/13.3.219 (2003).
94 Graus-Porta, D. *et al.* Beta1-class integrins regulate the development of laminae and folia in the cerebral and cerebellar cortex. *Neuron* **31**, 367-379, doi:10.1016/s0896-6273(01)00374-9 (2001).

95 Belvindrah, R., Graus-Porta, D., Goebbels, S., Nave, K. A. & Muller, U. Beta1 integrins in radial glia but not in migrating neurons are essential for the formation of cell layers in the cerebral cortex. *J Neurosci* **27**, 13854-13865, doi:10.1523/JNEUROSCI.4494-07.2007 (2007).
96 Anton, E. S., Kreidberg, J. A. & Rakic, P. Distinct functions of alpha3 and alpha(v) integrin receptors in neuronal migration and laminar organization of the cerebral cortex. *Neuron* **22**, 277-289, doi:10.1016/s0896-6273(00)81089-2 (1999).
97 Hatanaka, Y. & Murakami, F. In vitro analysis of the origin, migratory behavior, and maturation of cortical pyramidal cells. *J Comp Neurol* **454**, 1-14, doi:10.1002/cne.10421 (2002).
98 Rakic, P. Mode of cell migration to the superficial layers of fetal monkey neocortex. *J Comp Neurol* **145**, 61-83, doi:10.1002/cne.901450105 (1972).
99 Hartfuss, E. *et al.* Reelin signaling directly affects radial glia morphology and biochemical maturation. *Development* **130**, 4597-4609, doi:10.1242/dev.00654 (2003).
100 Nishikawa, S., Goto, S., Hamasaki, T., Yamada, K. & Ushio, Y. Involvement of reelin and Cajal-Retzius cells in the developmental formation of vertical columnar structures in the cerebral cortex: evidence from the study of mouse presubicular cortex. *Cereb Cortex* **12**, 1024-1030, doi:10.1093/cercor/12.10.1024 (2002).
101 Britto, J. M. *et al.* Exogenous Reelin modifies the migratory behavior of neurons depending on cortical location. *Cereb Cortex* **24**, 2835-2847, doi:10.1093/cercor/bht123 (2014).
102 Franco, S. J., Martinez-Garay, I., Gil-Sanz, C., Harkins-Perry, S. R. & Muller, U. Reelin regulates cadherin function via Dab1/Rap1 to control neuronal migration and lamination in the neocortex. *Neuron* **69**, 482-497, doi:10.1016/j.neuron.2011.01.003 (2011).
103 Landrieu, P. & Goffinet, A. Inverted pyramidal neurons and their axons in the neocortex of reeler mutant mice. *Cell Tissue Res* **218**, 293-301, doi:10.1007/BF00210345 (1981).
104 Sasaki, Y. *et al.* Fyn and Cdk5 mediate semaphorin-3A signaling, which is involved in regulation of dendrite orientation in cerebral cortex. *Neuron* **35**, 907-920, doi:10.1016/s0896-6273(02)00857-7 (2002).
105 Colognato, H., Ramachandrappa, S., Olsen, I. M. & ffrench-Constant, C. Integrins direct Src family kinases to regulate distinct phases of oligodendrocyte development. *J Cell Biol* **167**, 365-375, doi:10.1083/jcb.200404076 (2004).

106 Francou, A. & Anderson, K. V. The Epithelial-to-Mesenchymal Transition (EMT) in Development and Cancer. *Annu Rev Cancer Biol* **4**, 197-220, doi:10.1146/annurev-cancerbio-030518-055425 (2020).
107 Inoue, T., Chisaka, O., Matsunami, H. & Takeichi, M. Cadherin-6 expression transiently delineates specific rhombomeres, other neural tube subdivisions, and neural crest subpopulations in mouse embryos. *Dev Biol* **183**, 183-194, doi:10.1006/dbio.1996.8501 (1997).
108 Osterhout, J. A. *et al.* Cadherin-6 mediates axon-target matching in a non-image-forming visual circuit. *Neuron* **71**, 632-639, doi:10.1016/j.neuron.2011.07.006 (2011).
109 Ishino, Y. *et al.* Regional Cellular Environment Shapes Phenotypic Variations of Hippocampal and Neocortical Chandelier Cells. *J Neurosci* **37**, 9901-9916, doi:10.1523/JNEUROSCI.0047-17.2017 (2017).
110 Dunne, E. *et al.* Cadherin 6 has a functional role in platelet aggregation and thrombus formation. *Arterioscler Thromb Vasc Biol* **32**, 1724-1731, doi:10.1161/ATVBAHA.112.250464 (2012).
111 Shimazui, T., Giroldi, L. A., Bringuier, P. P., Oosterwijk, E. & Schalken, J. A. Complex cadherin expression in renal cell carcinoma. *Cancer Res* **56**, 3234-3237 (1996).
112 Casal, J. I. & Bartolome, R. A. RGD cadherins and alpha2beta1 integrin in cancer metastasis: A dangerous liaison. *Biochim Biophys Acta Rev Cancer* **1869**, 321-332, doi:10.1016/j.bbcan.2018.04.005 (2018).
113 Halfter, W., Dong, S., Yip, Y. P., Willem, M. & Mayer, U. A critical function of the pial basement membrane in cortical histogenesis. *J Neurosci* **22**, 6029-6040, doi:20026580 (2002).
114 Terakawa, Y. W., Inoue, Y. U., Asami, J., Hoshino, M. & Inoue, T. A sharp cadherin-6 gene expression boundary in the developing mouse cortical plate demarcates the future functional areal border. *Cereb Cortex* **23**, 2293-2308, doi:10.1093/cercor/bhs221 (2013).
115 Lodato, S. & Arlotta, P. Generating neuronal diversity in the mammalian cerebral cortex. *Annu Rev Cell Dev Biol* **31**, 699-720, doi:10.1146/annurev-cellbio-100814-125353 (2015).
116 Murray, S. B., Spangler, B. B., Helm, B. M. & Vergano, S. S. Polymicrogyria in a 10-month-old boy with Mowat-Wilson syndrome. *Am J Med Genet A* **167A**, 2402-2405, doi:10.1002/ajmg.a.37171 (2015).

117 Silengo, M., Ferrero, G. B. & Wakamatsu, N. Pachygyria and cerebellar hypoplasia in a patient with a 2q22-q23 deletion that includes the ZFHX1B gene. *Am J Med Genet A* **127A**, 109, doi:10.1002/ajmg.a.20607 (2004).
118 Long, K. R. *et al.* Extracellular Matrix Components HAPLN1, Lumican, and Collagen I Cause Hyaluronic Acid-Dependent Folding of the Developing Human Neocortex. *Neuron* **99**, 702-719 e706, doi:10.1016/j.neuron.2018.07.013 (2018).

Publication list

1. **Epifanova, E.**, Salina, V., Lajkó, D., Textoris-Taube, K., Naumann, T., Bormuth, O., Bormuth, I., Horan, S., Borisova, E., Schaub, T., Hernandez-Miranda, L.R., Ambrozkiewicz, M., Tarabykin V., Rosário M. Adhesion dynamics in the neocortex determine the start of migration and the post-migratory organization of neurons. *Sci. Adv.*, 7, 27: eabf1973, doi: 10.1126/sciadv.abf1973 (**2021**).
2. Lowenstein, E.D., Rusanova, A., Stelzer, J., Hernaiz-Llorens, M., Schroer, A.E., **Epifanova, E.**, Bladt, F., Isik, E.G., Jia, S., Tarabykin, V., Hernandez-Miranda, L.R. Olig3 acts as a master regulator of cerebellar development. *eLife,* 10:e64684 doi:10.7554/eLife.64684 (**2021**).
3. Mitroshina, E., Yarkov, R.S., Mishchenko, T.A., Krut, V.G., Gavrish, M.S., **Epifanova, E.A.**, Babaev, A.A., Vedunova, M.V. Brain-Derived Neurotrophic Factor (BDNF) Preserves the Functional Integrity of Neural Networks in the β-Amyloidopathy Model in vitro. *Front. Cell Dev. Biol.,* 8, 582. doi:10.3389/fcell.2020.00582 (**2020**).
4. Turovskaya, M.V., **Epifanova, E.A.**, Tarabykin, V.S., Babaev A.A., Turovsky, E.A. Interleukin-10 restores glutamate receptor-mediated Ca2+-signaling in brain circuits under loss of Sip1 transcription factor. *International Journal of Neuroscience*, 1-12, doi:10.1080/00207454.2020.1803305 (**2020**).
5. **Epifanova, E**., Babaev, A., Newman, A.G. & Tarabykin, V. Role of Zeb2/Sip1 in neuronal development. *Brain Res* 1705, 24-31, doi:10.1016/j.brainres.2018.09.034 (**2019**).
6. Mitroshina, E., Mishchenko, T.A., Shirokova, O.M., Astrakhanova, T.A., Loginova, M.M., **Epifanova, E. A.**, Babaev, A.A., Tarabykin, V.S., Vedunova, M. V. Intracellular Neuroprotective Mechanisms in Neuron-Glial Networks Mediated by Glial Cell Line-Derived Neurotrophic Factor. *Oxid Med Cell Longev* 2019, 1036907, doi:10.1155/2019/1036907 (**2019**).
7. Turovskaya, M.V., Zinchenko, V.P., Babaev, A.A., **Epifanova, E.A.**, Tarabykin, V.S., Turovsky, E.A. Mutation in the Sip1 transcription factor leads to a disturbance of the preconditioning of AMPA receptors by episodes of hypoxia in neurons of the cerebral cortex due to changes in their activity and subunit composition. The protective effects of interleukin-10. *Arch Biochem Biophys* 654, 126-135, doi:10.1016/j.abb.2018.07.019 (**2018**).
8. Mitroshina, E., Mishchenko, T.A., Usenko, A. V., **Epifanova, E. A.**, Yarkov, R.S., Gavrish, M.S., Babaev, A.A., Vedunova, M.V. AAV-

Syn-BDNF-EGFP Virus Construct Exerts Neuroprotective Action on the Hippocampal Neural Network during Hypoxia In Vitro. *Int J Mol Sci* 19, doi:10.3390/ijms19082295 (**2018**).

9. Mitroshina E.V., **Epifanova E.A.**, Mishchenko T.A., Yarkov R.S., Babaev A.A., Vedunova M.V. Application of the AAV-Syn-BDNF-EGFP Virus Vector as a Neuroprotective Agent in Modeling Hypoxia in vitro. *Modern Technologies in Medicine* 10, 2, doi: 10.3390/ijms19082295 (**2018**).

10. Belousova I.I., Zhidkova N.M., Borisova E.V., **Epifanova E.A.**, Salina V.A., Tutukova S.A., Lapshin R.D., Babaev A.A., Mukhina I.V., Tarabykin V.S. Phenotypic Variations in the Behavior of Sip1 Knockout Mice. *Modern Technologies in Medicine* 10, 2, doi: 10.17691/stm2018.10.2.02 (**2018**).

11. Borisova E.V., **Epifanova E.A.**, Tutukova S.A., Belousova I.I., Zhidkova N.M., Rusanova A.M., Salina V.A., Turovsky E.A., Turovskaya M.V., Tarabykin V.S., Babaev A.A. Identification of novel mutations controlling cerebral cortex malformations caused by ENU-induced mutagenesis in the mouse. *Modern Technologies in Medicine* 10, 3, doi: 10.17691/stm2018.10.3.8 (**2018**).

12. Turovskaya, M.V., Babaev, A.A., Zinchenko, V.P., **Epifanova, E.A.**, Borisova, E.V., Tarabykin, V.S., Turovsky, E.A. Sip-1 mutations cause disturbances in the activity of NMDA- and AMPA-, but not kainate receptors of neurons in the cerebral cortex. *Neurosci Lett* 650, 180-186, doi:10.1016/j.neulet.2017.04.048 (**2017**).

13. **Epifanova, E.A.,** Salina, V., Naumann, T., Sriwatsa, S., Rosario, M., Tarabykin V. Sip1 controls dendritic arbor formation in the mammalian neocortex. *Journal of Neurochemistry*, 2017, 142(1):139 (**2017**).

14. **Epifanova E.A.**, Borisova E.V., Salina V.A., Babaev A.A. Viral Vectors for Delivering Gene Material into Cells and Their Application in Neurobiology. *Modern Technologies in Medicine* 9, 1, doi:10.17691/stm2017.9.1.21 (**2017**).

15. Borisova E.V., **Epifanova E.A.**, Tutukova S.A., Salina V.A., Babaev A.A. Optogenetic approaches in neurobiology. *Molecular Genetics, Microbiology and Virology*, 31, 4, doi:10.3103/S0891416816040029 (**2016)**.

Acknowledgements

Rational human beings should be treated as an end in themselves and not as means to something else

Immanuel Kant

I would like to say thanks to all the people who have surrounded me during my PhD. PhD is not an aim it is a path that I have come with amazing people around me. I have learnt many important life lessons but the most important one is that people matter. It was a great pleasure to work with all of you, guys!

Firstly, I would like to thank my supervisors Marta and Victor.

Marta, you are the best supervisor I could have ever dreamed of. The amount of work, time and patience you invested in me throughout all these years is invaluable! Your drive and passion for science are infectious! I am extremely lucky that you have guided me into the world of science.

Victor, I am very grateful that you gave me a chance to challenge myself through doing a PhD. You have taught me how to be pragmatical, never give up, be persistent and defend what I believe.

I would like to express special thanks to my Russian mafia: Katya, Alexandra (Sascha, I know you would love it), Valya, Sveta and Tanya. All of you guys was the greatest support and partners in crime which I could ever wish for.

My dearest friend Katya, я не знаю, чтобы я без тебя делала 😊.

My dear friend Alexandra, thank you for always being there for me.

My dearest friend Denis, you always cheered me up in moments of sadness.

My officemate and friend Diana, I am grateful for all these days we have spent side by side fighting through PhD.

My lovely friend Lara, I found a soulmate in you, I am endlessly happy to meet you!

I would like to especially thank my dear friend Simon, who has supported me through the darkest moments of my dissertation!

Thank you for all the help, support and scientific advice throughout my PhD life: Olya and Ingo, Andrew, Ioana, Mateusz, Theres, Stephen, Luis, Kamilla, Kuo, Rike, Ulrike and Jutta.

Last but not least I would like to express my special gratitude to my Mom for her unconditional love, patience, support and faith in me. You were by my side despite the distance. To my Dad and Granny who believed in me till the very last day.

I am blessed to be surrounded by such people!